論文 / 著書情報
Article / Book Information

題目(和文)	エポキシ樹脂硬化物の構造と接着特性に関する研究
Title(English)	Studies on Structure and Adhesion Property of Epoxy Thermosetting Resin Composite
著者(和文)	市川功
Author(English)	Isao Ichikawa
出典(和文)	学位:博士（工学）, 学位授与機関:東京工業大学, 報告番号:甲第9963号, 授与年月日:2015年9月25日, 学位の種別:課程博士, 審査員:淺井　茂雄,扇澤　敏明,安藤　慎治,佐藤　満,塩谷　正俊
Citation(English)	Degree:, Conferring organization: Tokyo Institute of Technology, Report number:甲第9963号, Conferred date:2015/9/25, Degree Type:Course doctor, Examiner:,,,,
学位種別(和文)	博士論文
Type(English)	Doctoral Thesis

Studies on Structure and Adhesion Property of Epoxy Thermosetting Resin Composite

Isao Ichikawa

Department of Chemistry and Materials Science

Graduate School of Science and Engineering

Tokyo Institute of Technology

2015

Contents

Chapter 1

General introduction.

1-1. Development process of organic polymer products in current industry

To understand the significance of this study in academic and industrial fields, the concept for the organic polymer product development is describing firstly.

Product designing starts with the recognition the difference between customer demand and current products in terms of functions, properties, and prices, then elucidating a policy of material design and assuming an appropriate formulation. Next, several evaluations are performed using the trial sample based on the assumption, and new products that satisfy the requirements can be created. At this time, there are two main evaluation processes as shown in Figure 1. The first evaluation process involves the reproductive experiment performed in the same way as the customer performs, as shown in "Process I" in the Figure. The repetition of this evaluation provides extensive phenomenological results, and the recipe including the process condition can be chosen among the trial sample exhibiting the better results after each evaluation and combined with them. Thus, the material development in this process is the development with the "induction" approach based on the mathematical statistics theory. Material design using this process is appropriate for radically new product families and offers the advantage of enabling rapid short-term progress.

However, the results that differ from the primary supposition are recognized as irregular events and are not closely analyzed, even if these results are important essentially. Improper adoption of the base material for the design can cause partial optimization in the semi-stable field.

Additionally, the material designing method on this process is often applied as a means

of achieving small improvement, though it takes huge effort and expense to conduct a round-robin experiment. When the demanded properties could not be provided via this process, it became difficult to obtain the solution methodology and idea of the appropriate formulation for next evaluation. Consequently, the development is not accomplished and the project itself sometimes must be abandoned. The result, which makes the researchers and engineers engaged in the project discouraged, is an extremely negative outcome for company organization.

Contrary to this, another process shown as upper flow "Process II" in Figure 1 also starts by assuming the appropriate formulation from difference between development products and customer demands, but the evaluation results are considered by the primary structure information, such as the functional group species, molecular configuration and chemical states of composition, in addition to the higher order structure information such as the phase separation state.

This deep consideration clarifies the mechanisms governing mechanical properties, and the results are then fed back into the formulation for the next evaluation. This evaluation cycle are repeated. That is, its conclusion is persuasive, because the credibility of the assumptions made in the analysis is verified at every evaluation for all trial production. This evaluation process thus could be called the 'deductive' approach. Material development through this process can steadily increase the share in the current market in which strong sales are expected. Even if the resulting products represent only incremental improvement on existing products, this will sufficiently motivate customers to adopt them. The technology developed by this evaluation process is also useful and can be used for other products in different fields as well as in next generation products. Therefore, the technology generated on this process is the property of the organization.

In the development of polymeric material at the manufacturing stage, the material designs are often evaluated following sample changes in the amount rate of components or substitutions of the components previously used or the components used in other products. Such evaluation initially relies on the intuition and experience through the former evaluation process (Process I), because the structural analysis of polymeric materials is difficult and time consuming.

1-2. Analytical method development for organic polymer products

Figure 2 shows a technological trend of material designing and analysis for polymeric product. Since the 1980s, not only the synthesis technique, which is controlled by the primary structure, but also the compounding and manufacturing technique, which affect their higher-order structure, have been utilized for product design. This technique initially was applied to film material, membrane material and thermoplastic products [1, 2, and 3]. These products have simple components and their structure was relatively easy to control accurately.

Thermosetting or photo cross-linkable composite material with a complex composition are then developed using these higher-order structural control techniques [4, 5, and 6]. This became possible owing to the appearance of acrylic block copolymer, functional gel and nm size filler on the market at the 1990s.

Additionally, quantitative analysis of the molecular configuration and conformation in polymeric products has recently been required to ensure the stability of product functions and properties via a blending and dispersing technique.

In response to this, as shown on the right side of the figure, the morphological

observation and scattering analysis methods become essential. The former can provide the structural information of nm size by high spatial resolution devices like transmission electron microscopy (TEM) [7] and scanning probe microscopy (SPM), while the latter can provide structural periodicity information by the light scattering and the small angle X-ray scattering (SAXS) [8, 9]. These additional methods complement the chemical analysis for the functional group and intra-molecular structure using the traditional method represented by NMR, IR, GPC and GC-MS.

Additionally, in-situ measurement using a high bright synchrotron radiation source such as Spring-8 and Photon Factory recently has been actively carried out in research on soft matter materials on the same time scale with manufacturing or service condition as a reproducible experiment on fabrication [10].

1-3. Background and purpose of the present study and contents of the thesis.

Based on the technical background of designing the organic polymer products detailed above, the present study aims to investigate the effects of the primary molecular structure and the higher order structure of composite polymer material on the mechanical properties and to evaluate the mechanism governing these properties with the polymer material using the epoxy thermosetting resin system.

1-3-1. Background of the present study

Epoxy thermosetting resins have found application as adhesives in many industrial products and have enabled technological advances in organic-inorganic hybrid devices.

For example, in assembly process for semiconductor devices, parts composed of many components are used and bonded through various adhesive techniques. Adhesion durability is important for device reliability.

Additionally, epoxy thermosetting resin systems are easily functionalized because they have many kinds of industrial products and highly compounding technique. However epoxy thermosetting resin system suffers from brittleness due to the numerous covalent bonds formed in thermal curing. To improve the mechanical strength, epoxy resin, which has a flexible framework, is synthesized and the composites with several elastomer materials are evaluated. Among these, biphenyl type epoxy compounds, which lack the carbon bridge between aromatic rings and have the planar structure, provide high adhesive reliability and are applied to many materials used in the electronic industry, such as semiconductor IC packaging and printed circuit board [11 –15].

On the other hand, the conductive, dielectric, and magnetic properties of crystalline organic materials, which were composed of planar molecular and had stacking structure of them, were evaluated using the electron state calculated by several molecular orbital methods [16 –19]. Among organic conductors, bis (ethylenedithio)-tetrathiafulvalene (BEDT-TTF) charge transfer complexes, which have a planar structure, have been extensively investigated from the perspectives of their low-dimensionality and novel superconductivity. In these complexes, the lattice of organic donors tends to be arranged in two dimensional structure due to the face to face and the side by side intermolecular atomic contacts, resulting in the formation of two-dimensional electronic systems, as shown in Figure 3 [20, 21, and 22]. Some of these complexes undergo metal-insulator transition at low temperature assosiated with the change of the molecular interaction drived from structual comformtion shift [23, 24]. Figure 4 shows the temperature

dependence of the in-plane and inter-plane resistivity of the complex. The resistivities are different between in-plane direction and inter-plane direction, and the cooling rate alteres resistivity behavior to temperature along with molecular stacking structure.

Additionally, optical and mechanical properties of the polyimaide material has a liquid crystallinity framework due to the molecular planarity were investigated using molecular orbital caluculation. For example, aromatic polyimides hybridized with metal oxides were evaluated in terms of their electron excitation process using the optical spectroscopy and density functional theory (DFT) calculation of fundamental structure. These material created a new area of active research due to the unique combination of advantageous properties from each component [25, 26].

In this way, poperties of materials which formed crystall structure or had liquid crystallinty have been evaluated with the consideration for molecules and moleclar interactions.

Meanwhile, epoxy thermosetting systems are immiscible with the thermoplastic resin components and the mixture of these materials forms the phase separated structure of micrometers size, and this high-order structure is known to be important.

K. Yamanaka and T. Inoue et al. evaluated the phase separation of the epoxy thermosetting resin mixture consisting of the diglycidyl ether of bisphenol A-type epoxy resin, diaminodiphenylmethane as a curing agent, and poly(ether sulphone) [27]. The compound was single-phase mixture in the early stage of curing. As the cure reaction progressed, phase separation occurred with the increase in the molecular weight of epoxy thermo setting resin. At this stage, the composite phase diagram presented a lower critical solution temperature (LCST) and a two-phase region should prevail in the phase diagram

with the increase in the molecular weight at curing. Cured composites exhibited an interconnected globule structure and higher adhesive strength compared with neat epoxy resin.

T. Inada et al. evaluated the relation between the phase separated structure and physical properties of the composites containing epoxy thermosetting resin and acrylic polymer [28, 29]. Such composites also exhibit reaction-induced phase separated structure which was composed of acrylic element rich sea phase and epoxy resin rich island phase. The adhesive film sample based on this material mixture was also prepared by adding silica filler with a diameter of nm order size. The addition of this filler decreased the phase separated structure size and increased the elastic modulus and tearing strength at high temperature. These composite systems were applied to the adhesive film for semiconductor packaging.

1-3-2. Purpose of the present study and contents of the thesis

In **Chapter 2**, the effects of introducing the mesogenic framework, which is planar structure and easily arranged, into the epoxy thermosetting resin system on the mechanical properties was evaluated. The structure and mechanical properties of the cured neat epoxy thermosetting resin sample which has mesogenic framework were examined. The molding compound based on the neat epoxy thermosetting resin was prepared by adding silica filler and its adhesive properties were investigated. And finally the intermolecular interaction between mesogen moieties were evaluated using DFT calculation, to consider the source of characteristic structure and properties.

Additionally, the morphological features and adhesive properties of epoxy resin compositions with a mesogenic framework were investigated in **Chapter 3**. Neat epoxy thermosetting resins employing the [1,1′-Biphenyl]-4,4′-diol, which has mesogenic framework, were prepared in the several mixing conditions. This epoxy resin system has poly-domain phase structure comprising liquid crystalline domains and its size changes according to the mixing conditions. To consider the effects of phase structure on the adhesive properties, epoxy molding compounds based on these neat resin system were also prepared. The inflence of phase separated aspects on the mechanical properties were investigated and its importance were discussed.

In **Chapter 4**, to discuss the effects of phase structure on mechanical properties, quantitative analysis of phase separated structure was conducted and the mechanical properties were investigated for the acrylic copolymer/epoxy thermosetting resin composite. Specifically, the influence of resin reactivity on the phase structure was determined. In addition, the effects of material composition on the phase structure and the mechanical strength were investigated. And then the relation between them was considered. Morphologies were mainly detected by SPM, which provides only local structural information. Therefore, the statistically processing of observed SPM image is necessary to discuss about bulk structure. The phase separated structure of composites was then examined using two analyzing techniques with SPM images. Firstly, the distribution of the diameter and the nearest neighbor distance between the centers of island domains were derived by particle size analysis. Secondly, the periodicity and correlation length of the phase structure were evaluated by two-dimensional fast-Fourier

transform (2D-FFT) analysis. These quantitative analyses of the phase structure provided insight into the phase separation process and physical strength development.

In **Chapter 5**, these acrylic copolymer/epoxy thermosetting resin composites were applied for adhesive material, and the influence of phase-separated aspects on the adhesion properties was investigated.

Previous studies have recognized the importance of morphology aspects for fracture toughness and adhesive properties [30 –33]. However, few studies have adopted a quantitative approach. To propose a fracture mechanism and investigate the parameters that contribute to mechanical properties, the effects of phase-separated structure and the destruction mode on mechanical strength were evaluated for adhesives employed in semiconductor assembly. The phase structures for a variety of cured adhesive samples with different acrylic copolymer and epoxy resin systems were examined by 2D-FFT analysis of SPM images, providing quantitatively structural information. The adhesive properties and fracture surface aspects were then compared and considered together with the structural correlation length. The ultimate goal of this study is to enhance the adhesive strength and the product reliability under the manufacturing process and the usage environment.

As described above, the influence of primary molecular structure and higher order structure on the adhesive properties for epoxy composite adhesion materials are most interest in present study, which aims to propose a fracture mechanism of adhesive state and further enhance the adhesive strength.

References

1) H. Marubayashi, S. Asai, and M. Sumita, *Polymer*, **53**, 4262 (2012).

2) T. Shirahase, Y. Komatsu, H. Marubayashi, Y. Tominaga, S. Asai, and M. Sumita, *Polymer Degradation and Stability*, **92**, 1626 (2007).

3) S. P. Nunes and T. Inoue, *Journal of Membrane Science*, 111, **93** (1996).

4) Y. Tominaga, G. H. Kwak, S. Hirahara, S. Asai, and M. Sumita, *Polymer*, **44**, 4769 (2003).

5) M. A. Ortenzi, L. Basilissi, H. Farina, G. D. Silvestro, L. Piergiovanni, and E. Mascheroni, *European Polymer Journal*, **66**, 478 (2015).

6) W. Fan and S. Zheng, *Polymer*, **49**, 3157 (2008).

7) Y.Liao, S. Horiuchi, J. Nunoshige, H. Akahoshi, and M. Ueda, *Polymer*, **48**, 3749 (2007).

8) G. Jimenez, S. Asai, A. Shishido, and M. Sumita, *European Polymer Journal*, **36**, 2039 (2000).

9) Y. Tominaga, S. Igawa, S. Asai, and M. Sumita, *Electrochimica Acta*, **50**, 3949 (2005).

10) SPring-8 Section A: Scientific Research Report

11) M. Shimbo, M. Ochi, and N. Ohoyama, *Wear*, **91**, 89 (1983).

12) M. Ochi, H. Iesako and M. Shimbo, *Polymer*, **26**, 45(1985).

13) M. Ochi, T. Shiba, H. Takeuchi, M. Yoshizumi, and M. Shimbo, *Polymer*, **30**, 1079 (1989).

14) M. Ochi, K. Onishi, and S. Ueda, *Polymer*, **33**, 4550 (1992).

15) T. Okamatsu and M. Ochi, *Polymer*, **43**, 721 (2002).

16) T. Enoki, Y. Komatsu, K. Suzuki, A. Sekine, Y. Ohashi, and G. Saito, *Synthetic Metals*, **70**, 785 (1995).

17) M. Kobayashi, T. Enoki, K. Imaeda, H. Inokuchi, and G. Saito, *Physica B+C*, **143**, 550 (1986).

18) A. Kobayashi, R. Kato, H. Kobayashi, T. Mori, and H. Inokuchi, *Physica B+C*, **143**,

562 (1986).

19) K. Enomoto, A. Miyazaki, and T. Enoki, *Synthetic Metals*, **120**, 977 (2001).

20) T. Mori, A. Kobayashi, Y. Sasaki, H. Kobayashi, and G. Saito, *Bull. Chem. Soc. Jpn.*, **57**, 627 (1984).

21) T. Enoki, I. Ichikawa, A. Miyazaki, and G. Saito, *Synthetic Metals*, **86**, 1971 (1997).

22) A. Miyazaki, I. Ichikawa, T. Enoki, and G. Saito, *Bull. Chem. Soc. Jpn.*, **70**, 2647 (1997).

23) Y. Komatsu, Master Thesis, Tokyo Institute of Technology.

24) I. Ichikawa, Master Thesis, Tokyo Institute of Technology.

25) H. Gao, D. Yorifuji, J. Wakita, Z. H. Jiang, and S. Ando, *Polymer*, **51**, 3173 (2010).

26) N. H. You, Y. Suzuki, T. Higashihara, S. Ando, M. Ueda, *Polymer*, **50**, 789 (2009).

27) K.Yamanaka and T. Inoue, *Polymer*, **30**, 662 (1989).

28) S. Inada, K. Hatakeyama and T. Matsuzaki, *J. Network Polym. Japan*, **25**, 13 (2004).

29) S. Inada, T. Iwakura, K. Hatakeyama and T. Matsuzaki, *J. Network Polym. Japan*, **26**, 18 (2005).

30) Y. Nakamura, M. Yamaguchi, A. Tanaka, and M. Okubo, *Polymer*, **34**, 3220 (1993).

31) Y. Nakamura, M. Yamaguchi, A. Kitayama, M. Okubo, and T. Matsumoto, *Polymer*, **32**, 2221 (1991).

32) Y. Nakamura, M. Yamaguchi, M. Okubo, and T. Matsumoto, *Polymer*, **32**, 2976 (1991).

33) H. Kishi, A. Ozaki, N. Odagiri, A. Yamamoto, K. Yoshimura, *Japan Thermosetting Plastic Industry Association*, **13**, 135 (1992).

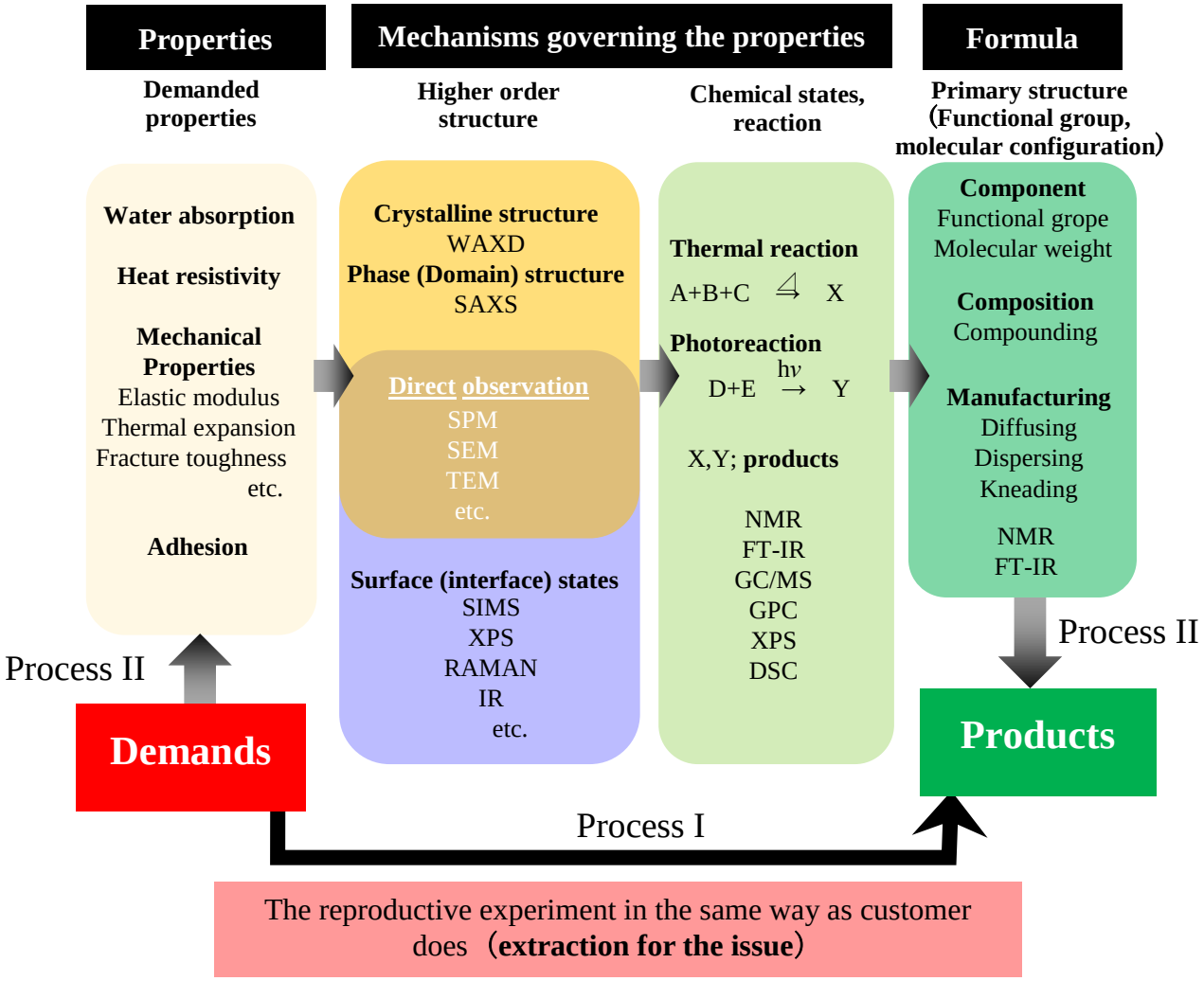

Figure 1. Conceptual diagram of designing process of organic polymer products in the industry

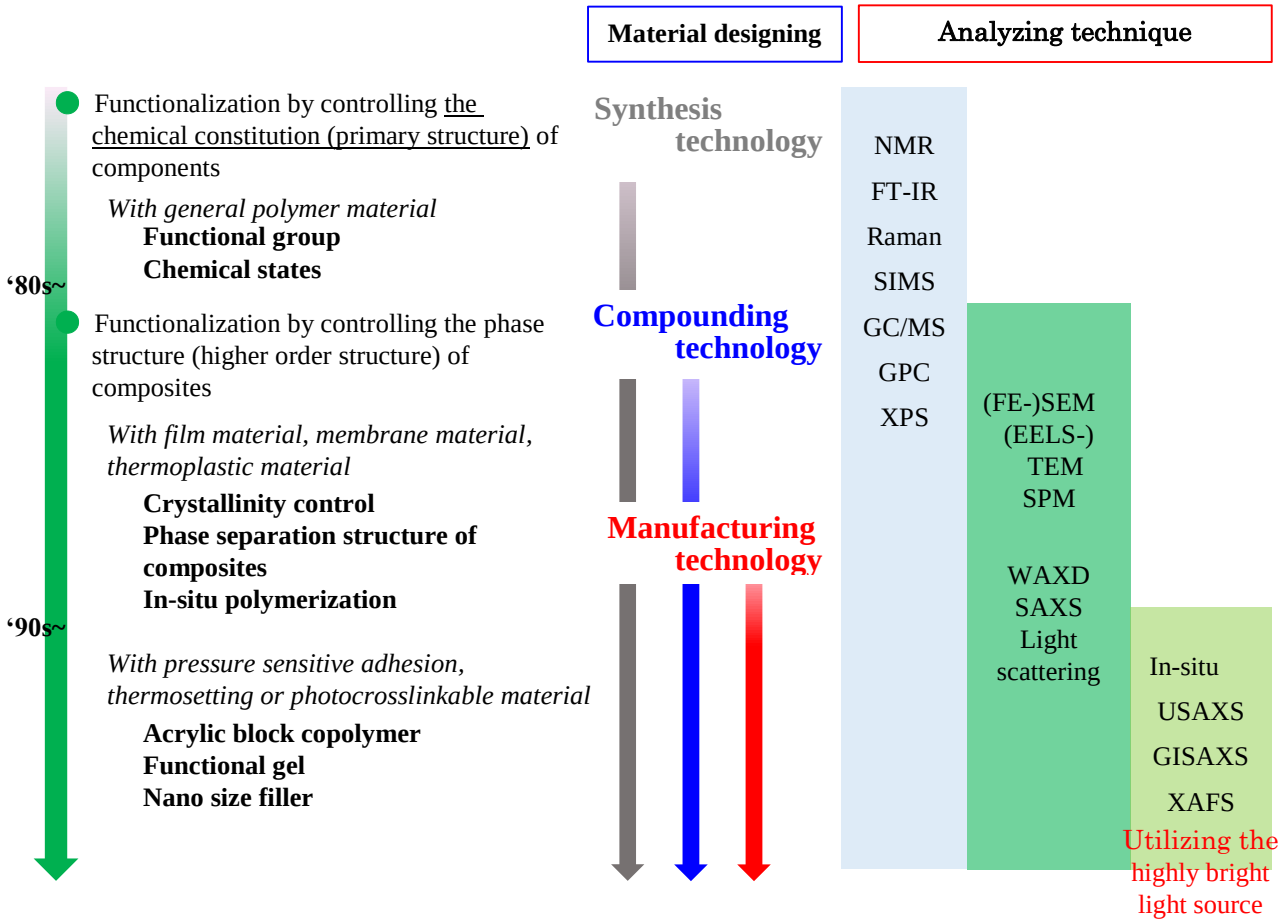

Figure 2. Technology trend for designing and analysis for polymer material

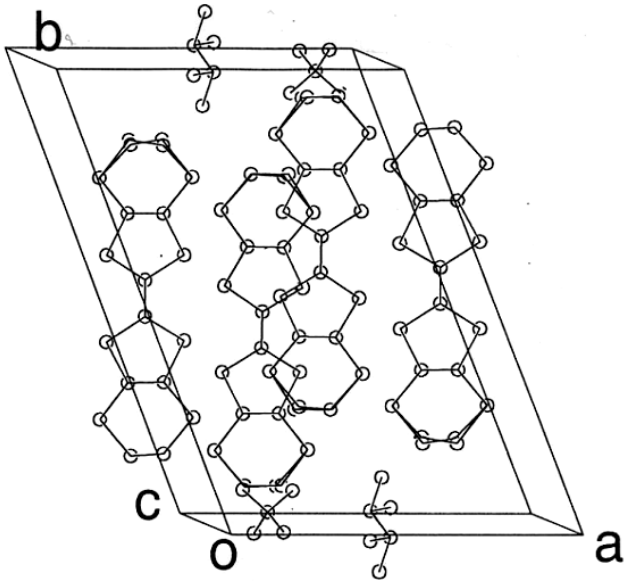

Figure 3. The unit cell of $(BEDT\text{-}TTF)_2BF_4(TCE)_{0.5}$
BEDT-TTF; bis (ethylenedithio)-tetrathiafulvalene
TCE; 1,1,2-trichloroethane [22]

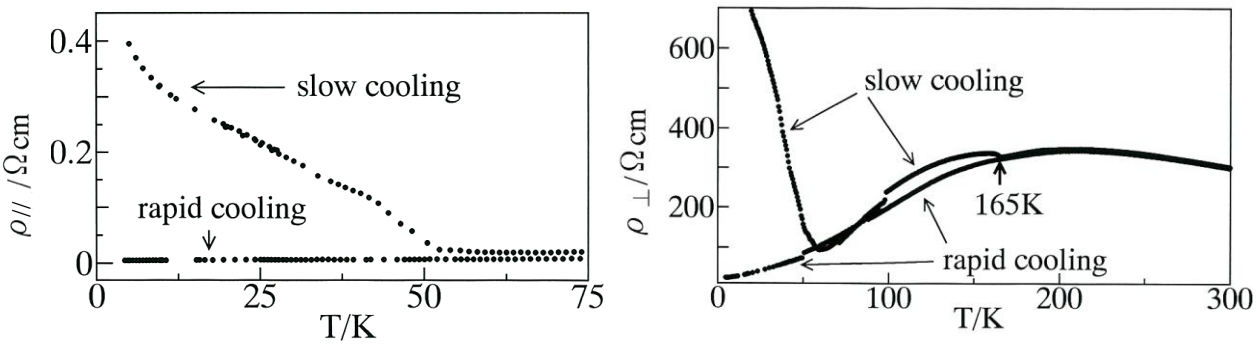

Figure 4. Temperature dependence of the in-plane electrical resistivity $\rho_{//}$ (left) and inter-plane resistivity $\rho_{\perp}$ (right) of the TCE salt in the cooling runs under the slow (-5Kh^{-1}) and rapid (-1Kmin^{-1}) processes. [24]

Chapter 2

Structure and mechanical properties of epoxy resin composite introducing mesogenic framework.

2-1. Introduction

For the semiconductor package device, it is necessary to protect the elements, which composed of a metal silicon and have electrical function, from an electric and dynamic external stimulation [1, 2]. Therefore these are generally sealed and adhered by the molding compound mainly comprising epoxy thermosetting resin with the phenolic resin hardening agent [3, 4, and 5]. Thus, the semiconductor package device has the adhesion interface interiorly between the components of different mechanical properties [6, 7].

The surface mounting method is performed on the connection process of electronic parts, and the whole semiconductor package is exposed under the high temperatures over the solder melting point. At this high temperature, an internal stress is generated on the adhesive interface, because thermal linear expansions of each component material are different from each other. In addition to this, the solder alloy composed of tin, copper and silver is recently employed instead of the tin-lead alloy formerly used. Thus the temperature for the connection process rises to 260 °C from 240 °C. When an internal stress exceeds the adhesive strength, a bonding state is broken [8]. As a result, metal lead frame and elements are corroded by invasion of the water molecules in adhesive failure area. This might remarkably reduce the electrical reliability of semiconductor package devices. Thus, keeping up the adhesive state is important for devices.

At the present day, the biphenyl type epoxy resin categorized as mesogenic framework compound are used as the matrix of molding compound material for the semiconductor package which requires the high reliability in usage environment. It is known to be that the internal stress generated on the adhesive interface can be decreased by introducing the biphenyl framework into the network.

Most of the mesogenic compounds represented by biphenol derivatives exhibit the liquid crystallinity. They have the conjugated electron and induce the structural orientation attributed to competition between the molecular packing and the multipole interaction. Utilizing these structural aspects, many liquid crystal material were developed and applied to the products. The epoxy thermosetting resins which have the mesogenic skeleton exhibit the characteristic mechanical, optical and electric properties due to the higher-order structure formed by self-organization at curing process.

Ochi and Harada et al. evaluated the network chain orientation in the toughening process of the elastomer modified epoxy thermosetting resin by polarized microscopic FT-IR technique quantitatively. The high toughening effects were observed with the mesogenic epoxy resin system modified by the elastomer, in which the network chains were easily arranged against the external force. At the fracture test, the network chains were arranged in the parallel to the direction of the crack propagation near the crack-tip before staring the destruction. When the maximum stress was loaded, a large deformation occurred in the vicinity of the crack-tip, and thus the network chains were rearranged in the perpendicular to the crack propagation.

They concluded that this toughening was attributed to the introduction of twisted planar and rigid mesogenic moieties which have the high deformability in the mixture with the elastomer [9].

Shiota et al. evaluated the structure formation of the liquid crystallinity with rigid rod thermosetting resins, such as the biphenyl, phenyl, benzoate, methyl stilbene and naphthyl type [10]. Most of them showed a nematic-like phase even if they were densely crosslinked. Howeve, when a rigid rod epoxy compound reacted with a curing agents having two groups with different reactivities, a smetic like structure was exhibited. This

resulting smetic like structure indicated the occasion of stepwise thermal reaction. At first linear chain propagated, next the branch structure and network structure finally formed by crosslinking.

This self-organization of rigid rod molecules at the polymerization process suggested the existence of the interaction between rigid rod molecules. Therefore, the composite material which has biphenyl framework easily provides the molecular arrangement structure, and resulting the characteristic bulk mechanical properties.

For the evaluation of the optical and electrical properties of polymer materials, the electron state of molecules is very important, and the molecular orbital calculation technique has been utilized and developing [11, 12]. The intermolecular interaction has been also discussed with the results of the molecular orbital calculation for several simple molecules, quantitatively [13, 14].

Tsuduki et al. investigated the intermolecular interaction energy of the cluster with simple benzene and ammonia molecular, water molecular and methane molecular as a model of NH/π, OH/π and CH/π interaction with high revel ab initio calculation. The calculation was conducted by the Hartree–Fock (HF) method, the second order Moller-Plesset perturbation method (MP2) and the coupled cluster calculation using single and double substitutions with noniterative triple excitations method (CCSD(T)) using the large basis sets [15, 16]. The intermolecular interaction was divided into the four elements with the physicochemical factor by the energy decomposition analysis (EDA), in order to evaluate the source of the interaction. The total energy calculated by HF method (E_{HF}) was mainly composed of the electrostatic energy ($\boldsymbol{E}_{\mathbf{es}}$) and the exchange repulsion energy ($\boldsymbol{E}_{\mathbf{rep}}$). The E_{es} was calculated as an interaction between the distributed multipoles, such as the dipole and the quadrupole of isolated molecules. The E_{rep}, which is mainly the

exchange repulsion energy but also contains some other energy component, was derived as the difference between E_{HF} and E_{es}. The attractive dispersion energy ($\boldsymbol{E}_{\mathbf{dis}}$), which mainly constitutes the electron correlation energy (E_{corr}), was derived by subtracting the E_{HF} from the total energy calculated by MP2 or CCSD(T) method. The charge transfer interaction energy ($\boldsymbol{E}_{\mathbf{CT}}$) which develop in short range order derived from the resonance integral. As a result of calculation, the value of total energy consisted largely of E_{dis}. It indicated that the dispersion interaction was important for the attraction in the XH/π interactions. Contrary to this, the absolute values of E_{es} were not large in the NH/π, OH/π and CH/π, but were different from each other and have orientation dependence. The charge transfer was not essential for attraction, because the total interaction was also effected in long-range order.

Tsuduki also reported the intermolecular interaction between benzene molecules as a prototype for the π-π interaction [17]. The calculated total interaction energies of the parallel (θ = 0°), T-shape (θ = 90°), and slipped-parallel benzene dimers were -1.48, -2.46, and -2.48 kcal/mol, respectively. The θ is the angle of normal vectors for molecular plane. Thus the slipped-parallel benzene dimers was most stable among them. The major source of attraction was long-range interactions such as the electrostatic and dispersion interaction. Although the absolute value of E_{es} was considerably smaller than E_{dis}, it was highly orientation dependent. Thus the electrostatic and the dispersion interactions were both important for the directionality of the benzene dimer interaction.

From these results of previous works, the molecular orbital calculation technique with dimer of simple molecules has provided the valuable information for intermolecular interaction. However for the real polymer material, the complicated combination should be considered for accurate analysis, but the calculation for the cluster composed of several

molecules at one time is very difficult and takes a lot of time.

In this chapter, in order to discuss about the effects of mesogenic moiety in the epoxy thermosetting resin matrix on the structure and properties, the several reactants were used for epoxy thermosetting resin system and the stepwise evaluation was conducted. Firstly, the structure and mechanical properties were examined for cured neat epoxy thermosetting resin samples. And next, the epoxy molding compound based on the neat epoxy thermosetting resin were prepared and their adhesive strength to the metal frames were evaluated by the actual semiconductor test method. Ultimately, in order to investigate the source of the mesogenic framework effects, the capability of the molecular interaction between flat aromatic conjugated compounds was evaluated by the electron states of component molecules.

2-2. Experiment

2-2-1. Sample preparation

Neat epoxy thermosetting resin

The composition of the neat epoxy thermosetting resin samples are shown in Table 1. Polyglycidyl ether of *o*-cresol formaldehyde novolac (OCNGE) epoxy resin (EOCN-102S-65, Nippon Kayaku Co., Ltd., Tokyo Japan, n= 4~5, epoxy equivalent: 218 g/eq, M_w: c.a. 870, mp.: 65 °C),

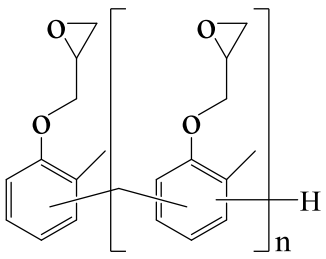

and phenol formaldehyde novolac (PN) curing agents (H-4, Meiwa Plastic Industries, Ltd., Yamaguchi Japan, n= 2~3, hydroxyl equivalent: 104 g/eq, mp.: 71 °C),

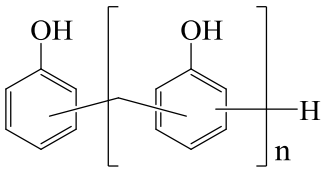

were adopted as the fundamental combination. And triphenyl phosphine (TPP, Hokko Chemical Industry Co., Ltd., Tokyo Japan, M_w: 265.3, mp.: 80 °C),

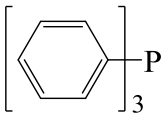

organophosphorus compound was used as an accelerator. Equivalent ratio of hydroxyl group in curing agents to epoxied group was adjusted to stoichiometric ratio and the accelerator was involved 1phr. They were melted and mixing at 80 °C and milled into the powder at room temperature. Then, a plate specimen with the size of 50 mm ×30 mm ×0.5 mm was prepared by molding the powder at 175 °C for 120 s under 10 MPa and the post mold curing was conducted at 175 °C for 8 h to react fully the epoxy thermosetting systems (Sample name; p-OCNGE).

To evaluate the effects of molecular structure on the properties, other three samples were prepared. The neat epoxy thermosetting resin sample which has [1,1′-biphenyl]-4,4′-diol (BP) curing agents (Biphenol, Honshu Chemical Industry Co., Ltd., Tokyo Japan, hydroxyl equivalent: 93 g/eq, M_w: 186, mp.: 281 °C (sublimation)),

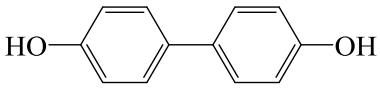

as the curing agent of half amount (p-BP) was prepared.

The samples used the mixture of biphenol diglycidyl ether (BPDGE)

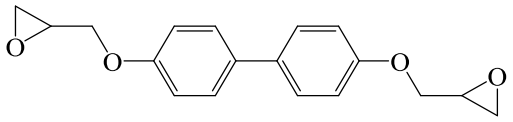

and tetramethyl biphennol diglycidyl ether (TMBPDGE)

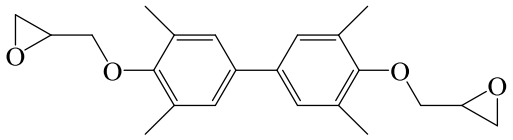

in the ratio of 1:1 (YL6121H, Mitsubishi Chemical Corporation, Tokyo Japan, epoxy equivalent: 175 g/eq, M_w:298/ 354, mp.: 158 °C / 108 °C) and polyglycidyl ether of bis-phenol A (BADGE, 1001, Mitsubishi Chemical Corporation, Tokyo Japan, n= 2~3 epoxy equivalent: 475 g/eq, M_w: c.a. 900, mp.: 64 °C)

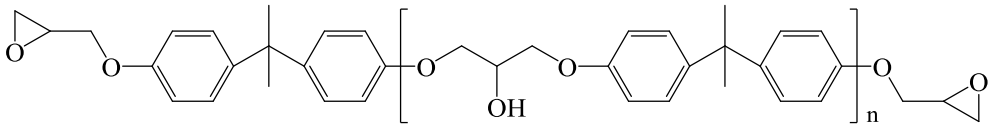

as a part of epoxy resin (p- BPDGE/TMBPDGE and p- BADGE) were prepared. The skeleton density of each was adjusted to 8.85×10^{-4} mol/g in the neat epoxy thermosetting samples.

Epoxy molding compound

The epoxy molding compound were prepared by adding silica filler with 24 μm median diameter, a dollop of silane coupling agent, and others to each neat epoxy thermosetting resin system at melt mixing process (m-OCNGE, m-BP, m- BPDGE/TMBPDGE, and m-BADGE). Mixing was conducted with open roll equipment (10 inch diameter; Nippon Roll MFG. Co., Ltd., Tokyo Japan) at 80 °C. The filler content was 87.5 wt% and the skeleton density was 6.19×10^{-5} mol/g. They were molded and annealed as a post mold curing process under the same condition as the preparation for neat epoxy thermosetting resin samples.

2-2-2. Measurement and analysis

In order to investigate the structure of the neat epoxy thermosetting resin sample in sub nm size, wide angle X-ray diffraction (WAXD) measurements were performed at 23 °C by X'Pert Pro X-ray diffractometer (PANalytical B.V., Almelo Netherlands), using nickel-filtered Cu Kα radiation (λ= 1.5418 Å) in the angle range of 2θ= 5 º –60 º on reflection mode at intervals of 0.033°. The center angle of the amorphous halo peak was determined by fitting the Gaussian function to the every scattering patterns.

In addition to this, the measurement was conducted up to 170 °C by RINT-Ultima III (Rigaku Corporation, Tokyo Japan) with parallel beam method using nickel-filtered Cu Kα radiation in the angle range of 2θ= 5 º –40 º on reflection mode and also the center angle of halo was derived.

As the mechanical properties, the temperature dependence of storage modulus and tanδ were measured by DMA EXSTRA6000 system (Seiko Instruments Inc., Chiba Japan). For the cured neat epoxy thermosetting resin, the specimens formed in the size of 30 mm ×5 mm ×0.5 mm were prepared and measured at the heating rate of 5 °C /min in a temperature range of -150 °C –270 °C on the tension mode of 10Hz. For the epoxy molding compound, the specimens were formed in the size of 20 mm ×4.3 mm ×2.9 mm and the measurement was conducted at the heating rate of 5 °C /min in a range of 25 °C –300 °C on the bending mode of 10 Hz.

The linear expansion was measured by TMA EXSTRA6000 system (Seiko Instruments Inc., Chiba Japan). For the cured neat epoxy thermosetting resin, the thermal strain based

on the length at -100 °C was derived in a range of -100 °C –300 °C at the heating rate of 5 °C /min on the tension mode of 5 kgf. The specimens were formed in the size of 20 mm ×4mm ×0.5 mm. For the cured epoxy molding compound, the linear expansion coefficient and glass transition temperature were derived. Measurement was conducted at the heating rate of 5 °C /min in a range of 30 °C –300 °C on the compression mode of 5 kgf with the specimens formed in the size of 16 mm ×4.3 mm ×2.9 mm.

The water absorption property of neat epoxy thermosetting resin sample was measured, because the adhesion strength generally declines with moisture absorption. The water absorption rate for the cured neat epoxy thermosetting resin was obtained as the rate of the weight increment under 85 °C, 60 %RH environment for 168 h, which is one of the standard condition prescribed by Joint Electron Device Engineering Council (JEDEC) [18]. The specimens had the size of 50 mm ×30 mm ×0.5 mm.

As the adhesive properties of epoxy molding compound sample, the strength at break of the bonding state against shear force was measured at room temperature. As shown in Figure 1, test piece for measurement was made by transfer molding at 180 °C for 60 s under 7.8 MPa in quadrangular prism 2 mm× 2 mm× 2 mm shape on the metal adherend plate. At this time, the adhesive state between molding compound sample and metal plate was generated. The moldings were annealed at 175 °C for 8 h as the post mold curing. The strength at break of the bonding state was measured at the shear rate of 5 mm/min [19]. The measurement was also conducted with the specimen after moisture absorption treatment at 85 °C, 60 %RH for 168 h. As the adherend, four types of metal plates were selected. First one was composed of KLF125 which is Cu alloy (Ni; 3.2 wt%, Si; 0.7 wt%,

Zn; 0.3 wt%, Sn; 1.25 wt%, Cu; 94.6 wt%). Second one was Ag plated Cu alloy. Third one was Cu alloy wholly plated by Ni, Pd and Au in this order. And last one consisted of Ni 42 % Fe alloy. They had mainly Cu, Ag, Au, Fe elements on the surface, and are versatilely utilized for composition of metal lead frame of semiconductor package. The thermal expansion coefficients of the parent metal of Cu and Ni-Fe alloy are 17 ppm K^{-1} and 4.4 ppm K^{-1}, respectively.

The strength on the three point bending mode was conducted at 23 °C with Universal / Tensile Testing Machine AG-Xpuls series (SHIMADZU, Kyoto Japan) at a 2.0 mm/min pushing rate, and the strain at break was derived for each epoxy molding compound, in order to evaluate the relaxivity of cured sample for the external force. The specimen was prepared by molding with each compound in the size of 10 mm ×4.0 mm ×80 mm and annealed under the same condition as making process of shear test specimen, and was placed on the two clamps with the distance of 64mm.

To evaluate the adhesive property of epoxy molding compound sample at high temperature, the quad flat type semiconductor package (QFP) molded with each molding compound sample was prepared as the test specimen (Figure 2). The Si elements were bonded to metal lead frame located at center of package with silver paste adhesives and sealed by molding with each compound in the size of 28 mm ×28 mm ×3.2 mm under the same condition as with making process of share test specimen. Then the QFP specimens were also processed with the post mold curing. Three types of lead frames were used for package specimen. First one consists of Cu alloy and have Ag plated area on the inner lead parts for electrically bonding with Au wire around element bonding area as shown

in Figure 2a. And second one consists of Cu alloy wholly plated by Ni, Pd and Au in this order. Last one consists of Ni 42 % Fe alloy and also have Ag plated area on the inner lead parts. There were the adhesive interface between each molding compound and Si element (α in Figure 2), metal lead frame (β), and Ag plated metal lead frame (γ) in the package specimen.

The packages were heated to 260 °C three times by infrared rays (IR) irradiation after moisture absorption treatment at 85 °C under 60 %RH for 168 h. The fraction of adhesion failure area to each bonding interface area were derived from the scanning acoustic tomogram (SAT) after IR heating test.

As the evaluation for the capability of the molecular interaction as a monomolecule, the molecular orbital calculation method was used for the biphenyl type molecules. The structure was optimized and the electron state was calculated by DFT method "the three-parameter Becke-style hybrid functional (B3LYP)" with 6-311G^{++} (d, p) basis set. The dipole moments and the quadrupole moments of BP, BPDGE, and TMBPDGE were calculated to evaluate the effect of the electrostatic interaction on the intermolecular interaction. Calculation was conducted using the Gaussian-09 software package installed at the Global Scientific Information and Computing Center, Tokyo Institute of Technology.

2-3. **Results and Discussion**

2-3-1. Structure and mechanical properties of neat epoxy thermosetting resins

The WAXD patterns of neat epoxy thermosetting resin samples are shown in Figure 3.

The broad diffraction halo from the amorphous was observed and its center angle positions was slightly shifted with sample composition. The figures shows the center angle of the amorphous halo peak determined by fitting with the Gaussian function, and the value for p-OCNGE and p-BADGE were lower than others.

Considering the results of previous works, the biphenyl moieties which has twisted plane structure are easily oriented in parallel with each other [9, 10]. And this orientation structure seems to decrease the intermolecular distance and affect the amorphous halo [12]. In fact, the mean intermolecular distance estimated from the center angle values with Bragg equation were 4.63 Å and 4.67 Å for the p-OCNGE and p-BADGE, respectively, shown in the last column of Table 1. They were longer than that of p-Bp (4.55 Å) and p-BPDGE/TMBPDGE (4.58 Å). Thus the large mean intermolecular distances of p-OCNGE and p-BADGE seem to indicate that the intermolecular interaction is hardly developed and it will be caused by their complex structure and low mobility of OCNGE, BADGE, and PN molecules at the curing.

Among the samples which have biphenyl skeleton in components, the mean intermolecular distances of p- BPDGE/TMBPDGE was longer than that of p-BP. The BP molecule has more simple structure and less steric hindrance than BPDGE and TMBPDGE molecules. In addition to this, the WAXD profile of p-BP exhibits the small peaks at the 23.02 ° and 28.60 ° which are attributed to the diffraction from the BP crystal, indicating that the small amount of BP crystal remains in the cured neat epoxy thermosetting resin due to the intermolecular interaction between BP molecules. Therefore, the decrease of intermolecular distances with the sample has biphenyl skeleton should be attributable to the densification of segments owing to the intermolecular interaction.

Temperature dependence of mean intermolecular distance derived from WAXD profile are shown in Figure 4. The mean intermolecular distance of each epoxy thermosetting resin are gradually increase with temperature and has inflection point around 120 °C – 150 °C. The slopes at high temperature above inflection point are larger than that at low temperature, and are different from each other. Those of p-OCNGE and p-BP are smaller than that of others.

The temperature dependences of storage modulus and tanδ of neat epoxy thermosetting resin are shown in Figure 5 and the tanδ peak temperature are listed in Table 2. The storage moduli of p-BP, p-BPDGE/TMBPDGE, and p-BADGE in the temperature range above 150 °C are smaller than that of p-OCNGE. The BP, BPDGE, TMBPDGE, and BADGE molecules are the bifunctional reactants, whereas the OCNGE and PN are the multifunctional compounds. The molecular chain formed by thermal reaction with BP, BPDGE, TMBPDGE, and BADGE have lower dimensional cross link structure than that formed with OCNGE and PN. The flexible structures are formed and their molecular mobility are enhanced by using bifunctional molecules.

The peak temperatures on tanδ profile for p-BPDGE/TMBPDGE and p-BADGE become lower than that for p-OCNGE. This lower tanδ peak temperatures appears to be attributed to the lower dimensional cross link structure of molecular chain as with the modulus at high temperature. On the other hand, p-BP has a higher tanδ peak temperature than others, indicating that the molecular mobility are suppressed by the densification of segments.

The temperature dependence of the linear expansion of neat epoxy thermosetting resin

is shown in Figure 6. The linear expansions at low temperature region are increasing with temperature in the same way for all. Above glass transition temperature (T_g), which is inflection point of the linear expansion, the slope of expansion toward temperature is larger for p-BPDGE/TMBPDGE and p-BADGE than that for p-OCNGE. However, p-BP exhibits the same temperature dependence of liner expansion as that of p-OCNGE even above T_g.

The increase tendency of thermal expansion is similar to that of the mean intermolecular distance derived from WAXD profile shown in Figure 4. The thermal expansion behavior corresponds approximately to the increment of the mean intermolecular distance. Ochi et al. reported the effects of the formation of the active hydrogens in curing agent molecule on the mechanical properties of biphenol-type epoxy resins cured with several phenolic curing compounds such as phenol novolac and catechol novolac types [20]. The biphenol type epoxy resin cured with catechol novolac which has two active hydrogens in a benzene ring had a high modulus and mechanical strength at high temperature region as compared with the phenol novolac cured system. And this catechol cured system does not have a clear glass transition in thermal expansion. It was concluded that the network chain motion was strongly suppressed in the biphenol resin/ catechol novolac system and this suppression of the chain motion was due to the orientation of mesogenic group in the networks. Because the epoxy molecules, which has mesogenic framework and react with the neighboring hydrogens, should be close to each other in the cured network system and resulted in the characteristic thermal expansion behavior.

In our experiment, the similarity of the temperature dependence of the thermal expansion and the mean intermolecular distance appears to indicate that the expanding of

free volume in the cured epoxy thermosetting resin is detected as the increment of mean intermolecular distance. Thus, the molecular arrangements seems to influence the bulk property as the thermal expansion.

Above results are summarized as follows, when the compound with two functional groups in molecule is used instead of multifunctional OCNGE or PN partly, the storage moduli become lower and the linear expansions become higher in the rubber region because the dimensionality of covalent bonds network is decreased. However for the sample p-BP, which uses the mesogenic compound BP, the storage modulus also becomes lower but the linear expansions is not easily enhanced. This phenomenon seems to be caused by the molecular densification with the orientation structure.

The weight increment under the environment at high temperature (85 °C) under high humidity (60 %RH and 85 %RH; **Condition 1** and **2**, respectively) of neat epoxy thermosetting resin was measured and the results were listed in Table 2. The increase of weigh exhibits the water absorption amount. Generally the water absorption for epoxy thermosetting resin materials is enhanced by the amount of epoxy group. Because the hydroxyl group generated by thermal reaction of the epoxy resin and curing agent has the dipole moment. The amount of epoxy group for unite volume increases with the smaller epoxy and hydroxyl equivalent compounds. Therefore the water absorption rate of p-BADGE is smaller than that of p-OCNGE.

However, p-BPDGE/TMBPDGE exhibits the slightly lower absorption rate and p-BP exhibits a little higher absorption than p-OCNGE, despites the smaller epoxy equivalent of BPDGE and TMBPDGE and hydroxyl equivalent of BP. It should be attributable to the density of the hydrophobic benzene ring, which are 6.96×10^{-3} mol/g, 7.06×10^{-3}

mol/g, 7.03 × 10^{-3} mol/g, and 7.00 × 10^{-3} mol/g for p-OCNGE, p-BP, p-BPDGE/TMBPDGE and p-BADGE, respectively.

2-3-2. Mechanical properties and adhesion properties of epoxy molding compounds

The storage modulus, the coefficient of thermal expansion, and T_g of cured epoxy molding compounds are listed in Table 3. T_g was derived from bending point of temperature dependence of liner expansion.

It is noteworthy that the effects of introducing the each framework on mechanical properties for the neat epoxy thermosetting resin are reproduce with the epoxy molding compounds. The value of storage modulus for m-BP, m-BPDGE/TMBPDGE, and m-BADGE are lower than that of m-OCNGE at high temperature. The coefficient of thermal expansion below and above T_g (β_1, β_2) of m-BPDGE/TMBPDGE and m-BADGE are higher than that of m-OCNGE, but the m-BP shows the same β_1 and β_2 values as the m-OCNGE.

The strength at break of the adhesive state to metal plates against shear force was measured as the adhesivity of molding compound. The measurement was carried out with the moldings after post mold curing and after additional moisture absorption treatment. The moisture absorption treatment were conducted on the condition of 85 °C, 60 %RH for 168 h. All specimens were broken at the adhesive interface between molding compound and metal adherend, which are Cu alloy, Ag plated Cu alloy, Ni/ Pd/ Au plated Cu alloy and Ni 42 % Fe alloy plate. The results are listed in Table 4.The adhesive strengths to Cu alloy are rather smaller than that to others, but the moisture absorption

treatment process have a low impact on the adhesive strength of each molding compound. It seems to be caused by little difference of moisture absorption rates between base materials as shown Table 2.

However the adhesive strength are significantly different with each molding component. For m-BPDGE/TMBPDGE and m-BADGE, the shear strength is larger than that for m-OCNGE and the adhesive strength for m-BP is largest of all. This result seems to be caused by the relaxivity for the internal stress generates on the adhesion surface. Because the strains at break of m-BPDGE/TMBPDGE, m-BADGE, and m-BP are 0.63 %, 0.71 %, and 0.80 %, and they are larger than that of m-OCNGE (0.59 %) due to the bifunctional molecular structure. In addition to this, for m-BP the internal stress seems to be smaller than that for others. Because the internal stress is generated due to the difference of thermal expansion rate with metal adherend and the temperature difference between the curing and the measuring condition. The smaller thermal expansion of m-BP seems to decreases the internal stress and enhance the adhesive strength.

The adhesion property at high temperature after moisture absorption was evaluated with QFP semiconductor package specimen. The SAT image of QFP packages after IR heating test with moisture absorption treatment were shown in Figure 7. These SAT images are the results of QFP packages using the Cu lead frame and molding with m-OCNGE (Figure 7a) and m-BP (Figure 7b). The left figure is the top-view image and the right one shows the bottom-view image. In other words the left shows the adhesion state of epoxy molding compound with Si element surface and partly plated metal lead frame, and the right shows that with metal lead frame.

The white region in the SAT image of Figure 7a shows the adhesive failure area at the

inner lead Ag plated region in top-view and at the four terminal region of square shape of Cu lead frame in the bottom view. This white region is not found with the result for m-BP shown in Figure 7b.

The fractions of adhesion failure area at each adhesive interface was quantified with SAT image as shown in Figure 7c. It is found that the fractions of adhesion failure area on each surface of Ni 42 % Fe alloy based frame is larger than that of Cu alloy based frame with each molding compound. The larger internal stress seems to be generated on the adhesive interface because of the smaller thermal expansion coefficient of 42 alloy frame than that of Cu based lead frame.

At the each adhesive interface of each metal lead frame, the fraction of adhesion failure area of the specimen molded with m-OCNGE is largest of all, and becomes smaller with m-BADGE, m-BPDGE/TMBPDGE, and m-BP in order. For m-BP, the little failure area is shown at every interface. These facts indicate that the relaxivity for the internal stress is enhanced by using the bifunctional reactants. In fact, the strain at brake at 260 °C are 1.64 %, 1.89 %, 1.89 %, and 1.78% for m-OCNGE, m-BADGE, m-BPDGE/TMBPDGE, and m-BP, respectively. In addition to this, the internal stress generated at the high temperature on the adhesive interface is decreased for m-BP by the lower elastic modulus and the smaller difference of thermal expansion with metal lead frame. Generally the polymer material which has lower modulus exhibits the higher thermal expansion. However for the m-BP, both low modulus and thermal expansion are accomplished resulting in the good adhesive property. This phenomenon appears to be caused by introducing the mesogenic skeleton and their molecular orientation structure.

From these results, the using the mesogenic molecule as the component of molding compound is useful and provide the high adhesive reliability for the semiconductor

package.

2-3-3. Electron states of components

The mean intermolecular distances of the neat epoxy thermosetting samples with biphenyl framework were shorter than those of others, and among them the thermal expansion of the epoxy thermosetting sample using the BP reactant was suppressed at high temperature.

Considering these fact, the intermolecular interaction which develops between the biphenyl moieties is presumed to be effective on the molecular orientation.

From this assumption, the electron states of the BP, BPDGE, and TMBPDGE were calculated in order to evaluate the source of the intermolecular interaction based on the EDA concept.

The dipole moments and the quadrupole moments of BP, BPDGE, and TMBPDGE were calculated to examine the electrostatic energy (E_{es}) qualitatively as shown in Table 5. Each molecules has the small dipole moments in a transverse direction of molecule (y in the Table 5) but does not have in a longitudinal (x) and perpendicular direction to the molecular plane (z) due to their symmetry. On the other hand, the values of quadrupole moments are relatively large in a longitudinal direction and in a perpendicular direction. The dipole moment of BP is largest of all but quite small. However the quadrupole moments of BP molecule is smaller than that of BPDGE and TMBPDGE. Thus the electrostatic interaction does not seem to be effective for intermolecular interaction for BP. However, this result could not explain the highest melting point 281 °C of BP shown in Table 1 and shortest mean atomic distance of p-BP. Because the melting temperature (T_m) is described as the ratio of the enthalpy change (ΔH) to the entropy change (ΔS)

thermodynamically as equation below.

$$T_m = \Delta H / \Delta S \qquad (1)$$

And ΔS of BP at T_m is much larger than that of others because BP is sublimated at T_m. The T_m of BP is supposed to be lowest of all due to small ΔH and large ΔS.

Thus, the dispersion interaction which are effects in long range order seems to affects for molecular arrangements as with above-quoted evaluation, and enhance the ΔH. In addition, the probability of the CT interaction effect which acts in short range order via CT electron excitation is also indicated from the shorter intermolecular distance.

But this argument about the source of the molecular interaction requires the experimental confirmation.

2-4. Conclusion

In this chapter we evaluated the effects of the mesogenic molecular skeleton in the cured epoxy thermosetting resin on the mechanical and adhesive properties. And the possibility of the molding compound using the mesogenic molecules for semiconductor packaging material was verified. When the mesogenic molecules were used as the epoxy thermosetting resin component, the strain at break became larger, and the elastic modulus became smaller and the difference of liner expansion with metal lead frame were decreased. Therefore, the relaxivity for the internal stress was enhanced and the internal stress generated at the high temperature on the adhesive interface was decreased. As a results, the good adhesivity was provided.

The mesogenic molecule is useful as the component of molding compound for providing

the high adhesive reliability. These good adhesive property seems to be caused by the densification of molecular chain due to the simple planer shape and the high mobility of biphenyl moieties.

In addition, the effects of the mesogenic framework were investigated with the molecular orbital calculation technique. The quadrupole moments of BP molecule is smaller than that of BPDGE and TMBPDGE. Thus the electrostatic interaction does not seem to be effective for intermolecular interaction. Considering the decreases of the mean intermolecular distance of the cured neat resin sample with the mesogenic skeleton molecule, the CT interaction appears to be considered as one of the possibility of the source of the mesogenic framework effects.

References

1) Chien-Pan Liu, Yen-Fu Liu, Chang-Hung Li, Hung-Chieh Cheng, Yi-Chun Kung and Jeng-Yu Lin, *Microelectronics Reliability*, **52**, 725 (2012).

2) J.H. Kang, K. Cho and C.E. Park, *Polymer* **42**, 2513 (2001).

3) Mingzhi Ni, Ming Li and Dali Mao, *Microelectronics Reliability*, **52**, 206 (2012).

4) I. Ichikawa, K. Enomoto and K. Uchida, *J. Adhesion Soc. Japan*, **40**, 51 (2004).

5) Y. Nakamura, M. Yamaguchi, M. Okubo and T. Matsumoto, *Polymer*, **33**, 3415 (1992).

6) Y. Nakamura, M. Yamaguchi, K. Iko, M. Okubo and T. Matsumoto, *Polymer*, **31**, 2066 (1990).

7) Y. Nakamura, M. Yamaguchi, A. Tanaka and M. Okubo, *Polymer*, **34**, 3220 (1993).

8) I. Ichikawa, K. Yanagimoto, M. Furudate, M. Kashio and T. Sugizaki, *J. Adhesion Soc. Japan*, **47**, 335 (2011).

9) M. Ochi, T. Morishita, S. Kokufu and M. Harada, *Polymer*, **42**, 9687 (2001).

10) A.Shiota and C.K.Ober, *Prog. Polym. Sci.*, **22**, 975 (1997).

11) S. L. Deng, S. Y. Xie, X. Lu, Y. B. Jiang, X. L. Fang, R. B. Huang and L. S. Zheng, *Journal of Molecular Structure*, **829**, 51 (2007).

12) H. Gao, D. Yorifuji, J. Wakita, Z. H. Jiang and S. Ando, *Polymer*, **51**, 3173 (2010).

13) S. Grimm, *Angew. Chem. Int. Ed.*, **47**, 3430 (2008).

14) S. Grimm, J. Antony, T.Schwabe and C. Muck-Lichtenfeld, *Org. Biomol. Chem.*, **5**, 741 (2007).

15) S. Tsuzuki, K. Honda, T. Uchimaru, M. Mikami and K. Tanabe, *J. Am. Chem. Soc.*, **122**, 3746 (2000).

16) S. Tsuzuki, K. Honda, T. Uchimaru, M. Mikami and K. Tanabe, *J. Am. Chem. Soc.*, **122**, 11450 (2000).

17) S. Tsuzuki, K. Honda, T. Uchimaru, M. Mikami and K. Tanabe, *J. Am. Chem. Soc.*, **124**, 104 (2002).

18) JEDEC Standard 22, Method A113F, “PRECONDITIONING OF PLASTIC SURFACE MOUNT DEVICES PRIOR TO RELIABILITY TESTING.

19) MIL-STD (Military Standard) -883G, METHOD 2019.7

20) M. Ochi, N. Tsuyuno, K. Sakaga, Y. Nakanishi and Y. Murata, *J. Appl. Polym. Sci.*, **56**, 1161 (1995).

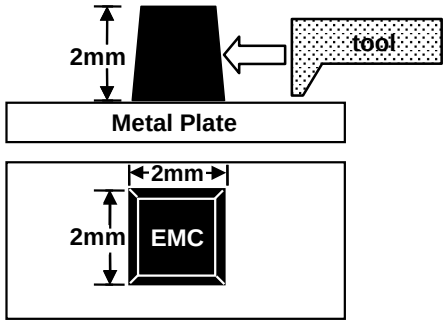

Figure 1. Adhesion strength measurement method
EMC: epoxy molding compound

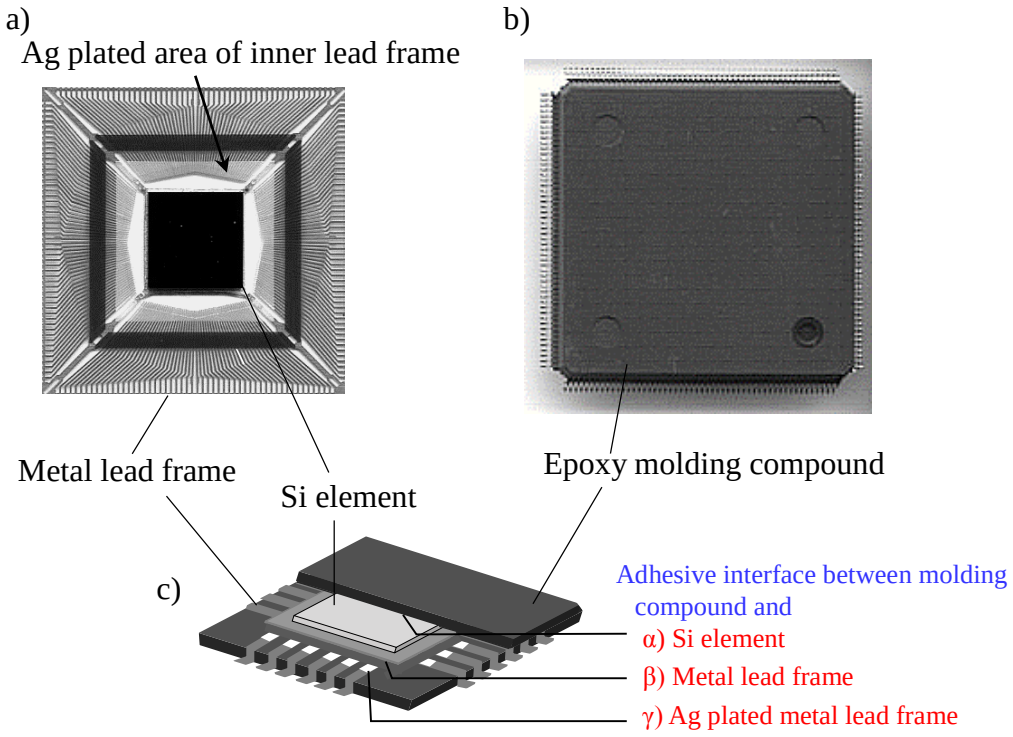

Figure 2. QFP semiconductor package specimen a) Cu alloy lead frame bonded Si element before molding and b) after molding with m-OCNGE and c) Schematic view of the internal package structure. α)~ γ) shows the each adhesive interface in the package specimen

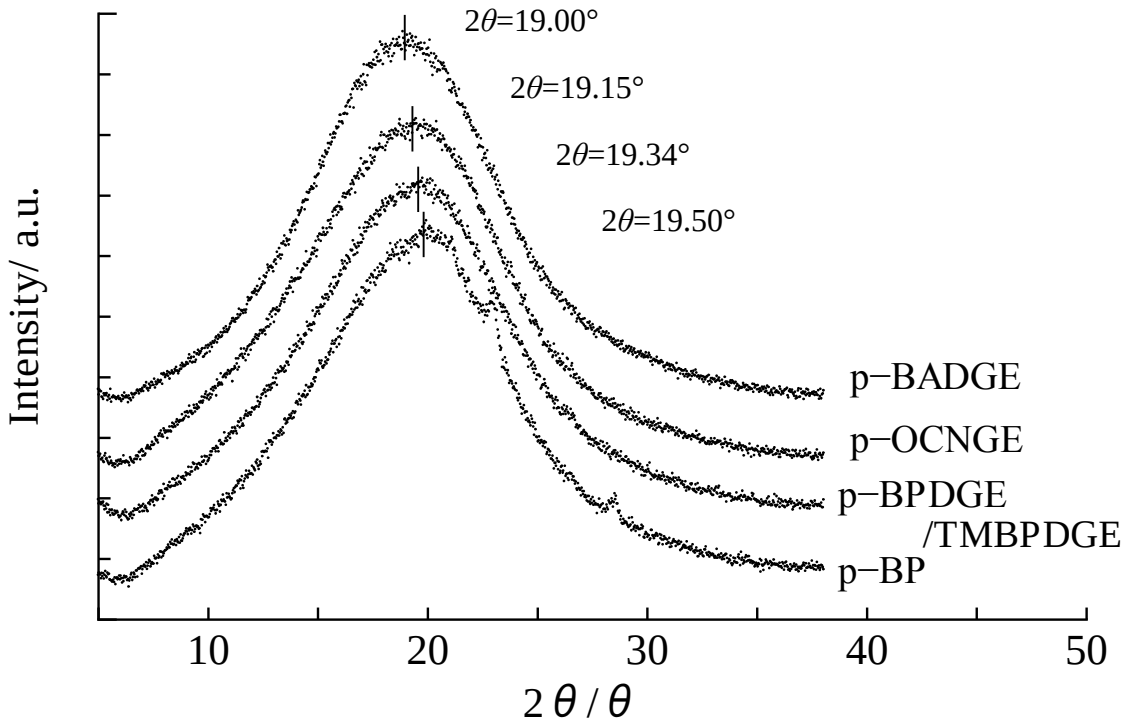

Figure 3. WAXD patterns of each neat epoxy thermo setting resin sample at room temperature. The figures shows the center angle of the amorphous halo determined by fitting with the Gaussian function.

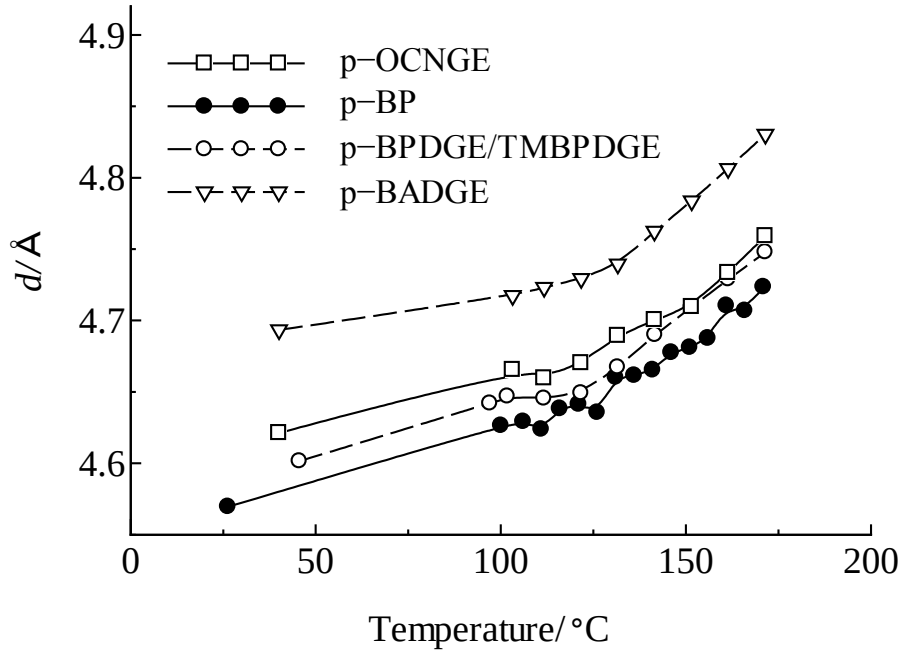

Figure 4. Temperature dependence of mean intermolecular distance derived from WAXD profile.

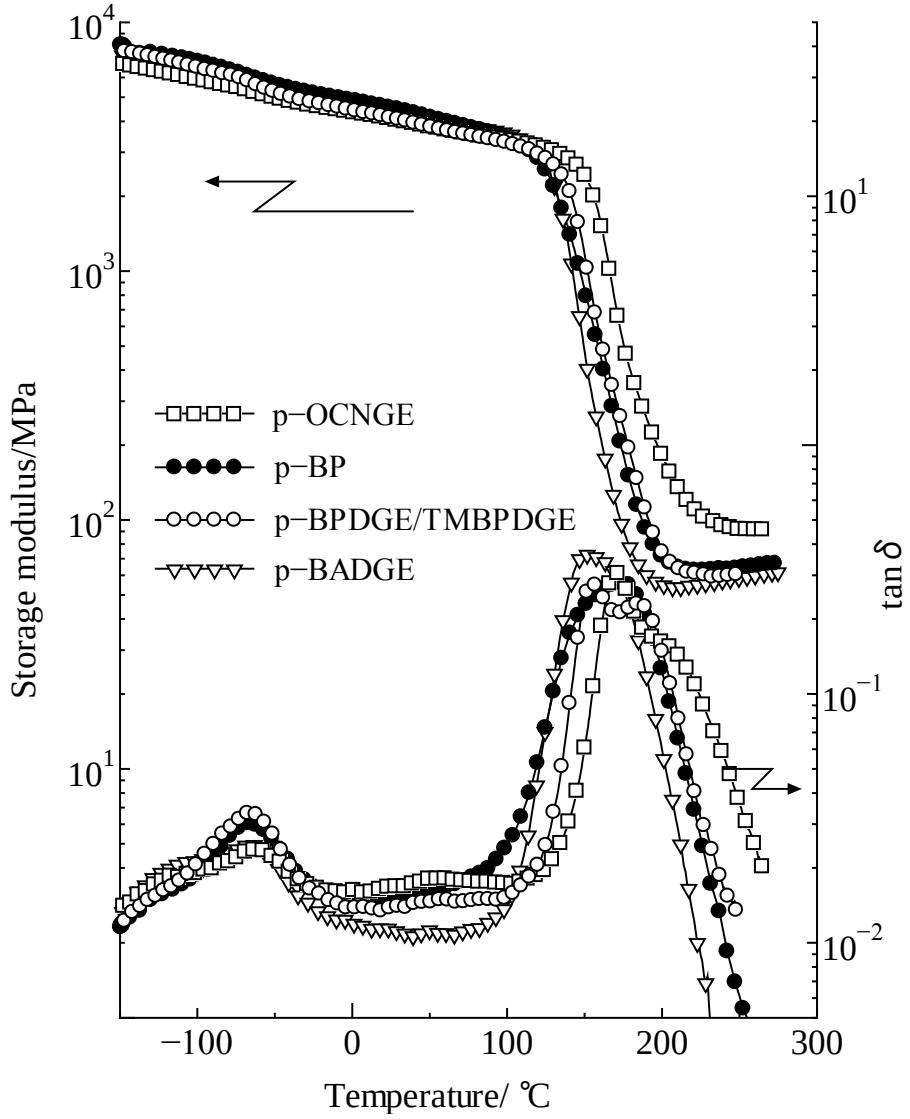

Figure 5.Temperature dependence of storage modulus and tanδ of neat epoxy thermo setting resin samples measured by DMA.

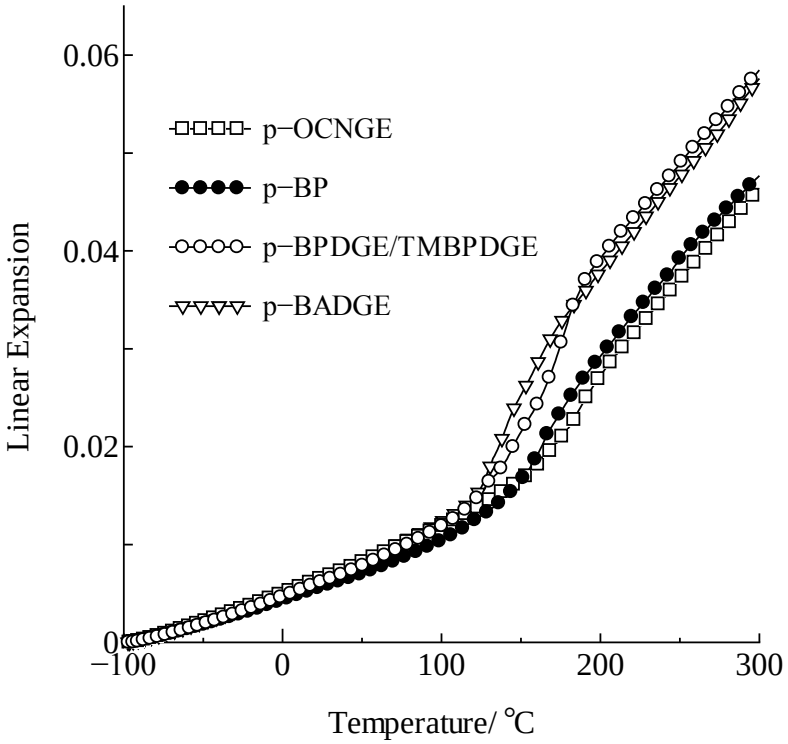

Figure 6. The temperature dependence of thermal strain of neat epoxy thermosetting resin samples measured by TMA.

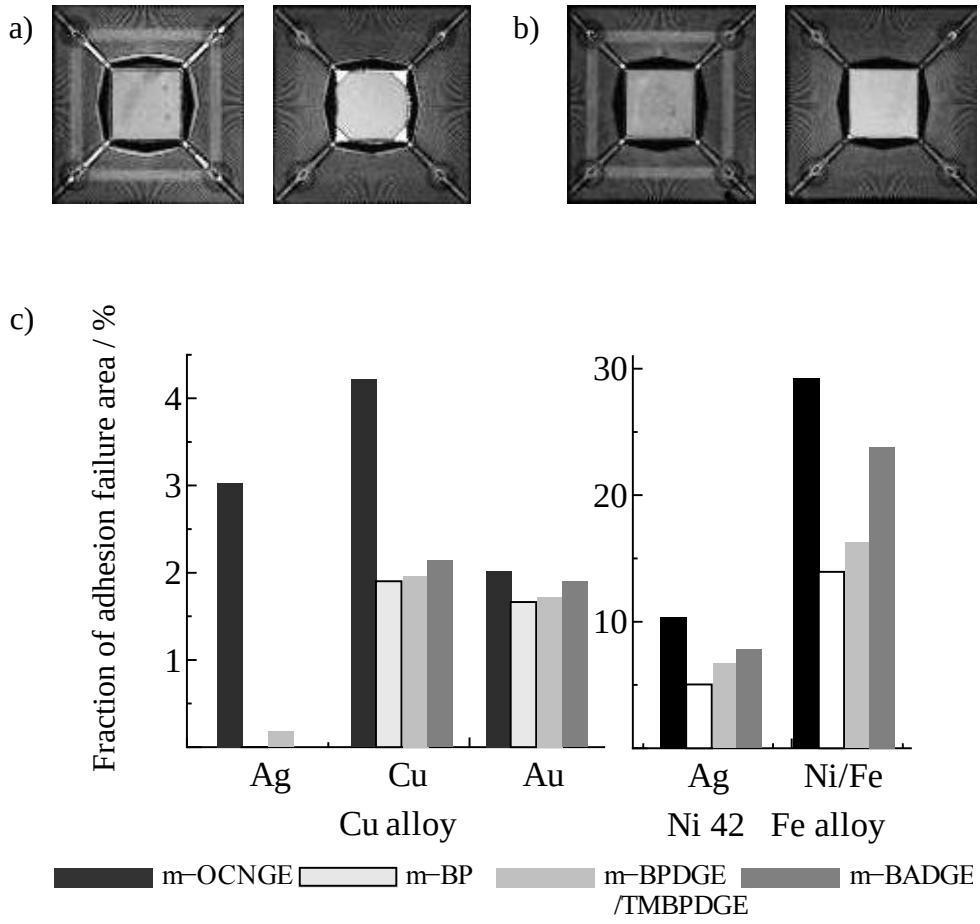

Figure 7. Scanning acoustic tomogram of QFP208 IC package molded with a) m-OCNGE and b) m-BP after 85 °C /60 %RH/168 h moisture soaking treatment and 260 °C IR reflow heating (left: upper side, right: bottom side) and c) the fraction of adhesion failure area to all bonding interface.

Table 1 Sample components and compositions.

The weight-average molecular weight (M_w), the melting point (m.p.) and the equivalent weight of epoxide group or hydroxyl group of each component.

	Composition for neat epoxy thermosetting resin (wt%)					
	OCNGE	BP	BPDGE /TMBPDGE	BADGE	PN	TPP
M_w	869.1	186.2	270.3 /326.4	909.1	479.4	265
m.p. / °C	65	281 (sublimation)	158 /108	44	71	80
Equivalent / g/eq	218	93	175	475	104	-
p-OCNGE	65.1	-	-	-	33.9	1.0
p-BP	66.4	16.3	-	-	16.3	1.0
p-BPDGE /TMBPDGE	33.3	-	30.1	-	35.6	1.0
p-BADGE	43.9	-	-	26.4	28.6	1.0

Table 2 Properties of **neat epoxy thermosetting resin**
Mean intermolecular distance (*d*) estimated with the center angle of halo value and Bragg diffraction qualification, storage modulus at high temperature, tanδ peak temperature, and water absorption rate.

	WAXD*	**DMA**		**Water absorption / %**	
	d/ Å	Storage modulus at 260 °C/ MPa	tanδ peak temperature/ °C	Condition Level 2**	Condition level 1***
p-OCNGE	4.63	91.3	173	1.06	1.68
p-BP	4.55	65.8	175	1.10	1.73
p-BPDGE /TMBPDGE	4.58	63.8	155	1.01	1.60
p-BADGE	4.67	59.6	151	0.82	1.50

*measured at room temperature, **85°C, 60%RH, for 168h (JEDEC Moisture soak Level 2), ***85°C, 85%RH, for 168h (JEDEC Moisture soak Level 1)

Table 3 Mechanical properties of **molding compound**
Storage modulus (*E'*) at 23 °C and 260 °C measured by DMA, T_g and the coefficient of thermal expansion below and above T_g (β_1, β_2) derived from TMA measurement.

	DMA		**TMA**		
	E' / GPa at 23 °C	*E'* / GPa at 260 °C	T_g / °C	β_1 /ppm K^{-1}	β_2 /ppm K^{-1}
m-OCNGE	13.5	1.23	134	8.5	34
m-BP	13	0.98	136	8.7	34
m-BPDGE /TMBPDGE	12.1	0.96	129	10.0	36
m-BADGE	13.4	0.92	126	9.8	36

Table 4 Shear strength of epoxy molding compound sample to every adherent plate after PMC and water absorption treatment. (standard deviations (SD) are in parentheses)

		Shear strength / MPa			
	adherent	Cu alloy	Ag plated Cu alloy	Au (Ni/Pd) plated Cu alloy	Ni 42 % Fe alloy
m-OCNGE	PMC*	3.45 (0.63)	4.12 (2.44)	4.92 (2.06)	-
	Moisture treatment**	**3.50 (1.68)**	**4.34 (1.90)**	**5.30 (1.37)**	**4.93 (1.04)**
m-BP	PMC	3.59 (1.76)	5.63 (1.10)	6.65 (0.89)	-
	Moisture treatment	**5.06 (1.82)**	**6.01 (1.72)**	**6.13 (0.87)**	**5.65 (1.07)**
m-BPGGE/ TMBPDGE	PMC	4.14 (2.00)	5.84 (0.50)	6.42 (1.69)	-
	Moisture treatment	**4.83 (0.84)**	**4.95 (0.89**	**6.00 (1.49)**	**5.47 (1.27)**
m-BP_mix3	PMC	4.39 (2.26)	4.40 (1.06)	6.62 (0.90))	-
	Moisture treatment	**4.72 (1.65)**	**4.68 (1.00)**	**5.48 (1.54)**	**5.39 (1.15)**

*175 ℃ for 8hours, **85 ℃, 60 %RH for 168 hours

Table 5 Dipole and quadrupole moments of BP, BODGE and TMBPDGE calculated at B3LYP/6-311G^{++} (d, p) level.

	|Dipole moment| / Debye			**|Quadrupole moment| / Debye**					
axis*	x	y	z	xx	yy	zz	xy	xz	yz
BP	0.0	2.5	0.0	75.3	73.1	85.2	0.0	6.3	0.0
BPDGE	0.0	1.5	0.0	144.2	126.5	128.6	0.0	1.3	0.0
TMBPDGE	0.0	0.1	0.0	174.6	144.9	160.7	0.0	21.6	0.0

* the definition of Cartesian axes

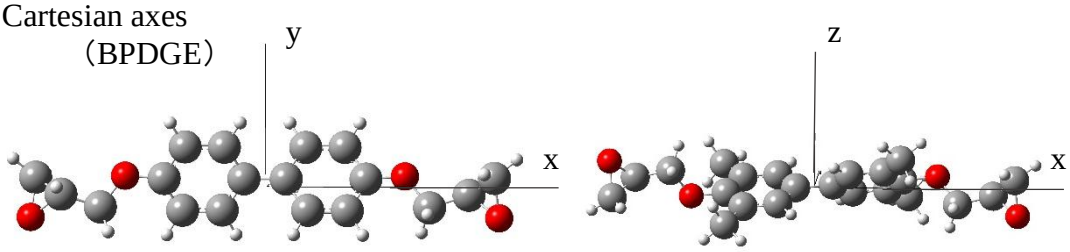

Chapter 3

Phase structure and adhesive property of epoxy resin composite introducing mesogenic framework.

3-1. Introduction

Recently, the composite parts constituted with several materials are widely used as the functional device, e.g. semiconductor IC package and printed circuit board, and their stability for long term is demanded. Device reliability is influenced by many factors such as an external force, a change of temperature, and a high pressure and humidity during both manufacturing and usage environment. Especially, the mechanical impact from the outside and the rusting of metal components are serious problem to functional stability. Thus, the fixing the parts is effective to protect the functional components from external force, and the inhibiting the water intrusion is important to prevent metal component from rusting. In order to accomplish the functional reliability for long term, adhesive technology is employed for bonding the different materials and sealing the metal parts. Additionally, the internal stress which derived from thermal stimulus and generates at the week mechanical strength point, such as metal eutectic bonding spot, could be also relaxed by surrounding with adhesive material.

In semiconductor package, epoxy thermosetting resin is applied to the composition of adhesives such as die bonding film and transfer molding compound [1-6]. The epoxy thermosetting resin with mesogenic skeleton is employed to the matrix compound of adhesives which are required to provide the high bonding reliability on the product stage [7, 8]. In chapter 2, by introducing the mesogenic framework to the epoxy compound, the intermolecular distance of the cured epoxy thermosetting systems becomes shorter and elastic modulus becomes lower maintaining the low linear expansion at high temperature. Thus the internal stress developed by an external thermal stimulus on the adhesive interface is decreased, because the inorganic metal adherend

has low coefficient of thermal expansion [9, 10]. These phenomena appears to be caused by the molecular arrangement of mesogenic moieties [11, 12].

In this chapter, to evaluate the effects of introducing the mesogenic skeleton into the epoxy network on the phase structure and the mechanical properties, neat epoxy thermosetting resins system using the biphenol type curing agent were prepared on the several mixing and kneading condition. The resin system had poly-domain structure consists of liquid crystalline phase and domain size altered with the mixing condition.

In addition, to consider the effects of the phase structure on the adhesive properties, molding compounds based on the neat resin system were prepared and their adhesive properties were evaluated. This study ultimately intended to propose a fracture mechanism of adhesive state and enhance the adhesive strength.

3-2. Experiment

3-2-1. Sample preparation

OCN type epoxy resin, polyglycidyl ether of *o*-cresol formaldehyde novolac (**OCNGE**), (EOCN-102S-65, n= 4~5, Nippon Kayaku Co., Ltd., Tokyo Japan, epoxy equivalent: 218 g/eq, M_w: c.a. 870, mp.: 65 °C)

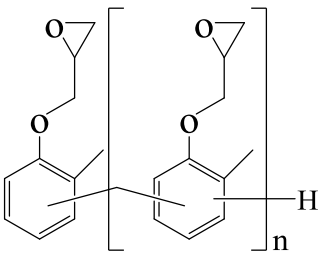

and phenol formaldehyde novolac (**PN**) (H-4, n= 2~3, Meiwa Plastic Industries, Ltd., Yamaguchi Japan, hydroxyl equivalent: 104 g/eq, mp.: 71 °C)

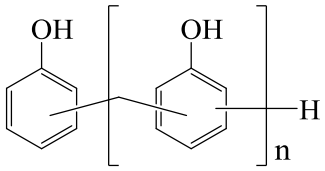

were adopted as fundamental components for thermosetting resin system.

Triphenyl phosphine (**TPP**, Hokko Chemical Industry Co., Ltd., Tokyo Japan, M_w: 265.3, mp.: 80 °C), organophosphorus compound

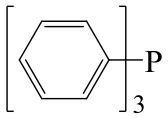

was used as an accelerator.

The compositions of neat epoxy thermosetting resins are shown in Table 1. Equivalent ratio of hydroxyl group in curing agents to epoxied group was adjusted to stoichiometric ratio and the accelerator was involved 1 phr. They were melted and mixed at 80 °C and milled at room temperature (**p-OCNGE**).

In order to evaluate the effects of molecular structure of biphenyl skeleton on the phase structure and properties, the neat epoxy thermosetting resin sample which has [1,1′-Biphenyl]-4,4′-diol (**BP**) (Biphenol, Honshu Chemical Industry Co., Ltd., Tokyo Japan, hydroxyl equivalent: 93 g/eq, M_w: 186, mp.: 281 °C (sublimation))

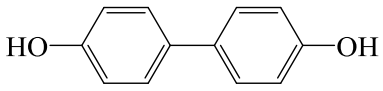

as the curing agent of half amount was prepared (**p-BP_mix1**). In addition, other three samples were prepared on the several mixing condition. For the well- blending of the BP molecule, the pre-melt mixing processes were conducted before mixing epoxy thermosetting composition shown as Figure 1, and the pre-melt mixing condition are also listed in Table 1. On a pre-mixing process, the same amount of PN and BP were melt at 160 °C dispersing at 128 rpm in the reactor vessel of versatile mixer (Dalton Co.,

Ltd., Tokyo Japan). On the other pre-mixing process, the same compositions were melt at 100 °C and blended with shear force by passing through the narrow clearance between two rotating screws revolving at 200 rpm or 440 rpm with the twin screw extruder TEM-35BS (Toshiba Machine Co., Ltd., Shizuoka Japan). The curing agents with the pre-melt mixing treatment were used as component for the epoxy thermosetting composition, and melted and mixing with other components of OCNEG and TPP at 80 °C and milled into the powder at room temperature. The sample with the pre-mixing process in the reactor vessel was named **p-BP_mix2**. And the samples with the pre-mixing process by the twin screw extruder were named **p-BP_mix3** and **p-BP_mix4** in order of lower screw rotation speed at kneading.

Next, plate specimens with the size of 50 mm× 30 mm× 0.5 mm were prepared by molding the powder sample at 175 °C for 120 s under 10 MPa and the post mold curing was conducted with plate specimens at 175 °C for 8 h to react the epoxy thermosetting systems completely.

To evaluate the adhesive properties, epoxy molding compound was manufactured by adding silica filler which has 24 μm median diameter, a dollop of silane coupling agent, and others to above neat epoxy thermosetting resins and blending by open mixing roll equipment (10 inch diameter; Nippon Roll MFG. Co., Ltd., Tokyo Japan) at 80 °C (**m-OCNGE, m-BP_mix1~4**). The filler content was 87.5 wt% and the biphenyl skeleton density was 6.19×10^{-5} mol/g. The pre-mixing process was same as that of neat epoxy thermosetting resins.

3-2-2. Measurement and analysis

The morphology of the neat epoxy thermosetting resin sample was observed by polarization microscope equipment E600POL (Nikon Instech Co., Ltd., Tokyo Japan) on transparent mode at room temperature. The specimen was set between a polarizer and an analyzer of crossed nicols arrangement.

Raman mapping measurement was conducted with Microscopic laser Raman Nicolet Almega XR (Thermo Fisher Scientific K.K., Kanagawa Japan) using the 750 nm wavelength laser. The Raman spectrum of p-BP_mix2 was measured in 15×15 μm^2 area at intervals of 1 μm. The area fraction of two peaks in spectra around 1610 cm^{-1} and 1430 cm^{-1}, which were assigned to C=C stretching vibration in benzene ring and bending vibration of methylene group, were calculated. BP had a benzene ring in high concentration in the molecule. In contrast to this, PN had a methylene group within the molecule. The region displays high area fraction of 1610 cm^{-1} peak could be attributed to the BP curing agent rich phase and that of 1430 cm^{-1} peak could be attributed to the PN curing agent rich phase. Therefore, the mapping images of these area fraction of two peaks displayed the dispersion state of the BP and PN.

The distribution of the area fraction value of C=C stretching vibration peak on every measuring spectrum was also derived in order to confirm the existence of the different composition phase.

For the evaluation of the structure in nm order scale of the neat epoxy thermosetting resin samples, wide angle X-ray diffraction (WAXD) was measured at room temperature by X'Pert Pro X-ray diffractometer (PANalytical B.V.), using nickel-filtered Cu Kα radiation (λ=1.5418 Å) on the scattering angle range of 2θ= 5 °–

60 °. The center angle of the amorphous halo peak detected at around 2θ= 19 ° was determined by fitting the Gaussian function to the diffraction pattern. Then mean intermolecular distances was estimated from the center angle value with a Bragg's equation.

As the mechanical properties, the temperature dependence of the storage modulus and tanδ of neat epoxy thermosetting resins were measured by DMA EXSTRA6000 system (Seiko Instruments Inc., Chiba Japan). The specimens formed in the plate shape of 30 mm× 5 mm× 0.5 mm were measured in a temperature range of -150 °C –270 °C at the heating rate of 5 °C /min on the tension mode of 10 Hz.

The linear expansion was also measured by TMA EXSTRA6000 system (Seiko Instruments Inc., Chiba Japan) with the specimens of 20 mm× 4 mm× 0.5 mm size. The thermal strain based on the length at -100 °C was derived in a temperature range of -100 °C –300 °C at the heating rate of 5 °C /min on the tension mode of 5 gf.

As the adhesive properties of epoxy molding compound sample, the strength at break of the bonding state to shear force was measured at room temperature. Test piece for measurement was made by transfer molding in quadrangular prism 2 mm× 2 mm× 2 mm shape on the metal adherend plate as shown in Figure 2 at 180 °C for 60 s under 7.8 MPa. The moldings are annealed at 175 °C for 8 h as the post mold curing. The strength at break of the bonding state was measured at the shear rate of 5 mm/min [13]. The measurement was also conducted for the specimen after water absorption treatment at 85 °C, 60 %RH for 168 h, which is one of the standard condition prescribed by Joint Electron Device Engineering Council (JEDEC) [14]. As the adherend, four types of

metal plates were selected. First one was composed of KLF125 which is Cu alloy (Ni; 3.2 wt%, Si; 0.7 wt%, Zn; 0.3 wt%, Sn; 1.25 wt%, Cu; 94.6 wt%). Second one was Ag plated Cu alloy. Third one was Cu alloy wholly plated by Ni, Pd and Au in this order. And last one consisted of Ni 42 % Fe alloy. They had mainly Cu, Ag, Au, Fe elements on the surface, and are versatilely utilized for composition of metal lead frame of semiconductor package. The thermal expansion coefficients of the parent metal of Cu and Ni-Fe alloy are 17 ppm K^{-1} and 4.4 ppm K^{-1}, respectively.

To evaluate the adhesive property of epoxy molding compound sample at high temperature, the quad flat type semiconductor package (QFP) specimen molded with each molding compound was prepared. The configuration and making process of specimen and the evaluation method in detail were same as that described in Chapter 2 (below the middle on page 28 and Figure. 2).

3-3. Results and Discussion

3-3-1. Structure of neat epoxy thermosetting resins

The morphology of the neat epoxy thermosetting resin sample was observed by polarized microscope as shown in Figure 3. Polarized image for p-OCNGE has no characteristic pattern exhibiting isotropic nature of structure. Though, for p-BP_mix1~4, small liquid crystalline domains, which exhibit the interference pattern of polarized light, are distributed in whole of images. The domain size ranges from several μm to a dozen μm and alters with pre-kneading process. It becomes smaller with moderate mixing (p-BP_mix2, 3) but larger by more strongly kneading with the higher rotation

speed of the twin screw (p-BP_mix4).

The Raman mapping images of p-BP_mix2 in the range of 15×15 μm^2 are shown with polarized image in the same magnification in Figure 4. The left image shows the dispersion state of BP rich phase derived from the area fraction of C=C stretching vibration peak in the spectrum and the right image shows the dispersion state of PN rich phase derived from that of CH_2 bending vibration peak. Red area in the figure indicates the region where the each component exists in the high concentration. Both peak were observed in the spectra all over the measured area. However in the region where the area fraction of C=C stretching vibration peak is high, the area fraction of CH_2 bending vibration peak is low. This indicates the existence of the BP rich phase and the PN rich phase.

Both images display the poly-domain structure in which a few domains are connected. This structure is observed in the polarized micrograph image, but its size is rather smaller. The difference of the domain size of Raman mapping images and the polarized micrographs image seems to be caused by the difference of observation depth of each measurement method. The former observes only a few μm surface layer and the latter observes through the thickness of 500 μm.

The distribution of the value of area fraction of C=C stretching vibration peak in every measured spectrum is also shown in Figure 4. It is well fitted with combination of two Gaussian curves. This indicates that there are two phases with different mean fraction of the BP component, and the existence of the BP rich phase and poor phase was confirmed chemically.

The WAXD patterns of each neat epoxy thermosetting resin are shown in Figure 5. No diffraction peak is exhibited, though the broad halo from the amorphous is observed.

The figures shows the center angle of the amorphous halo peak of each determined by fitting with the Gaussian function. The center angle of p-OCNGE is lower than others, however the scattering patterns for p-BP_mix1~4 accord with each other. Thus, the mean intermolecular distance of 4.63 Å for p-OCNGE, which is estimated from the center angle values with Bragg equation, is longer than that for p-BP_mix2~4 (4.55 Å) [15].

Considering this fact, for p-BP_mix2~4 used planer and high mobility molecule of BP, the molecular arranged structure appears to develop, resulting in the shorter mean intermolecular distance of p-BP series. However the mean intermolecular distance is not changed by pre-melt mixing condition of BP. The structure in domains is not different, but the domain size alters with pre-mixing condition as observed by polarized microscope (Figure 3) for the neat epoxy thermosetting resins using BP reactant.

3-3-2. Mechanical properties of neat epoxy thermosetting resins

The temperature dependence of storage modulus and linear expansion of neat epoxy thermosetting resin are shown in Figure 6 and 7, respectively. The storage moduli of p-BP series above the tanδ peak temperature are smaller than that of p-OCNGE. Considering the fact that BP is the bifunctional reactant, the molecular chain formed by thermal reaction between OCNGE and BP has lower dimensional cross link structure than that between OCNGE and PN. The flexible structure is formed and its molecular mobility is enhanced by using BP molecule. Thus, for the p-BP series the modulus of

rubber state at high temperature seems to be decreased. However there is no significant difference in the storage modulus with the pre-mixing condition.

The linear expansions at low temperature are increasing along with temperature in the same way with every sample. However, for p-BP_mix1 and p-BP_mix4 the temperature dependence of linear expansion at high temperature around and above the glass transition temperature (T_g), which is inflection point of the linear expansion, is larger than others. This large temperature dependence of linear expansion appears to be attributed to the lower dimensional cross link structure of molecular chain as with the decrease of storage modulus at high temperature. Contrary to this, for p-BP_mix2 and p-BP_mix3 the slope of linear expansion toward temperature are smaller than those for p-BP_mix1 and p-BP_mix4 around and above T_g. It suggests that the thermal expansions for p-BP_mix2 and p-BP_mix3 at high temperature are suppressed similarly to p-OCNGE.

From the observation results of polarized microscope, the specific surface area of domains composed of BP rich and poor phases are larger for p-BP_mix2 and p-BP_mix3 with their smaller domain size than that for p-BP_mix1 and p-BP_mix4.

J. Gonzales-Benito et al. evaluated the effect of uniformly dispersed TiO_2 nanoparticles on the coefficient of thermal expansion (CTE) of poly (ethylene-co-vinyl acetate) (EVA) composites film by atomic force microscope technique [16]. Not only amount of the inorganic TiO_2 particle, which had quite smaller CTE than that of EVA, but also the size of particle had an impact on the composites CTE. Smaller CTE was provided by the composites had smaller TiO_2 particle. An interphase, in which the expansion was suppressed by particles, was created in boundary area of EVA and bulk

composite CTE was decreased with large specific surface area of TiO_2 with small particles.

In this study, the same effect seems to be exhibited in the linear expansions phenomenon for p-BP series. In particular, thermal expansion of BP rich phase will be smaller than that of BP poor phase, and the interphase, which shows relatively small expansion, may be formed in boundary. The amount of interphase are increased with smaller domain particles. As a results, the linear expansions for p-BP_mix2 and p-BP_mix3 appear to be suppressed at high temperature by the good deal of interphase.

3-3-3. Adhesion properties of epoxy molding compounds

The strength at break of the adhesive state to metal plates against shear force was measured as the adhesivity of molding compound. The measurement was conducted with the moldings after post mold curing and after additional moisture absorption treatment at 85 °C, 60 %RH for 168 h as listed in Table 2. All specimens were broken at the adhesive interface between molding compound and metal adherend, which are Cu alloy, Ag plated Cu alloy, Ni/ Pd/ Au plated Cu alloy and Ni 42 % Fe alloy plate. The adhesive strengths to Cu alloy are rather smaller than that to others, but the adherend species and the water absorption treatment process have a low impact on the adhesive strength of each molding compound. However the adhesive strengths are significantly different with each molding component. The adhesive strengths of m-BP_mix1~4 using the BP molecule are larger than that of m-OCNGE owing to the lower storage modulus as discuss in chapter 2. Among the m-BP series, the adhesive strength of m-BP_mix4, m-BP_mix1, m-BP_mix3, and m-BP_mix2 become larger in this order, and this

tendency correspond to the domain particle size shown in Figure 3. Thus the adhesive strength becomes larger with smaller domain, and m-BP_mix2 which has the smallest domain particles provides the largest adhesive strengths to each adherend.

Considering the fact that the linear expansion was suppressed for the sample had smaller domain, an internal stress, which generates at the adhesive interface by the thermal stimulus, decreases with the smaller expansion of mold compound. Because the coefficient of thermal expansion of metal adherend (Cu alloy: 17 ppm K^{-1}, Ni-Fe alloy: 4.4 ppm K^{-1} as describe above) is smaller than that of molding compound (e.g. 34 ppm K^{-1} for m-BP_mix2) and the temperature of 180 °C on curing condition is quite higher than the measuring temperature of 23 °C.

The adhesion property at high temperature after moisture absorption was evaluated with QFP semiconductor package specimen. The fractions of adhesion failure area at each adhesive interface after the absorption treatment and heating up to 260 °C by IR was quantified with SAT image as shown in Figure 7. It is found that the fractions of adhesion failure area on Ni 42 % Fe alloy based frame are larger than those of Cu alloy based frame with each molding compound. The larger internal stress seems to be generated on the adhesive interface because of the smaller thermal expansion of Ni 42 % Fe alloy frame.

At the each adhesive interface of each metal lead frame, the fraction of adhesion failure area of specimen molded with m-OCNGE is largest, and becomes smaller by introducing the biphenyl skeleton in the epoxy network with BP. Among the m-BP series, the fraction of adhesion failure area of m-BP_mix4, m-BP_mix1, m-BP_mix3,

and m-BP_mix2 became smaller in this order. This tendency is generally consistent with the domain particle size shown in Figure 3 as with the adhesive strength of them at 23 °C.

These facts indicate that the inner stress generated at the high temperature on the adhesive interface is decreased for the molding compound sample has lower elastic modulus and thermal expansion, and the good adhesive properties are derived, as a result. And the thermal expansion is depended on the domain particle size for m-BP series. This characteristic mechanical properties seems to be caused by introducing the mesogenic skeleton and the resulting molecular oriented structure in epoxy network.

3-4. Conclusion

The neat epoxy thermosetting resin using BP molecule showed poly-domain phase structure which consists of BP rich and poor phases. This domain size was altered with pre-melt mixing condition of BP, but the structure in each domain was not change. When the specific surface area of domains was larger with pre-mixing process under moderate mixing condition, the linear expansion was suppressed at high temperature. It would be caused by the interphase, which was formed in boundary and showed relatively smaller expansion than that of BP poor phase. This low expansion effect developed for adhesive strength, because the internal stress decreased and bonding state could be maintained. From these fact, the phase structure aspect was very important and effective to enhance the adhesive strength. Controlling of dispersion states of BP rich phase with great accuracy would be provide the good adhesive properties.

The thermosetting resin which is composed of mesogenic molecules and exhibits the liquid crystallinity has mostly isotropic structure on the molten state at high temperature

before thermal reaction, then transfer to liquid crystal phase during the curing process. However the reaction-induced phase structure sometimes does not develop fully because of the rapid thermal reaction rate of thermosetting system. The high reactivity of the thermosetting composites is demanded for high productivity on the manufacturing process. Therefore, the initial state of reactants formed by kneading and dispersing is important and dominant factor for the phase structure development.

Hence, the manufacturing technique of these initial states of reactants is important for the controlling the phase structure, and will derive the full potential of industrial products.

References

1) Y. Ebe, H. Senoo, T. Sugino and O. Yamazaki, *J. Adhesion Soc. Japan*, **40**, 379 (2004).

2) Y. Ebe, H. Senoo, T. Sugino and O. Yamazaki, *J. Adhesion Soc. Japan*, **41**, 289 (2005).

3) I. Ichikawa, K. Yanagimoto, M. Furudate, M. Kashio and T. Sugizaki, *J. Adhesion Soc. Japan*, **47**, 335 (2011).

4) Mingzhi Ni, Ming Li and Dali Mao, *Microelectronics Reliability*, **52**, 206 (2012).

5) Chien-Pan Liu, Yen-Fu Liu, Chang-Hung Li, Hung-Chieh Cheng, Yi-Chun Kung and Jeng-Yu Lin, *Microelectronics Reliability*, **52**, 725 (2012).

6) J.H. Kang, K. Cho and C.E. Park, *Polymer* **42**, 2513 (2001).

7) T. Shiraishi, H. Motobe, M. Ochi, Y. Nakanishi and I. Konishi, *Polymer*, **33**, 2975, (1992).

8) M. Ochi, T. Morishita, S. Kokufu and M. Harada, *Polymer*, **42**, 9687 (2001).

9) I. Ichikawa, K. Enomoto and K. Uchida, *J. Adhesion Soc. Japan*, **40**, 51 (2004).

10) I. Ichikawa, T. Sugizaki, S. Akasaka and S. Asai, *Polym. J.*, (2015) [in press].

11) A.Shiota, C.K.Ober, *J. Polym. Sci.: Part A : Polym. Chem.*, **34**, 1291(1996).

12) H. J. Sue, J. D. Earls, et al., J. Mater. Sci., 1997, 32, 4039-4046.

13) MIL-STD (Military Standard) -883G, METHOD 2019.7

14) JEDEC Standard 22, Method A113F, "PRECONDITIONING OF PLASTIC SURFACE MOUNT DEVICES PRIOR TO RELIABILITY TESTING.

15) H. Gao, D. Yorifuji, J. Wakita, Z. H. Jiang, and S. Ando, *Polymer*, **51**, 3173 (2010).

16) J. Gonzales-Benito, E. Castillo, J.F. Caldito, *European Polymer Journal*, **49**, 1747 (2013).

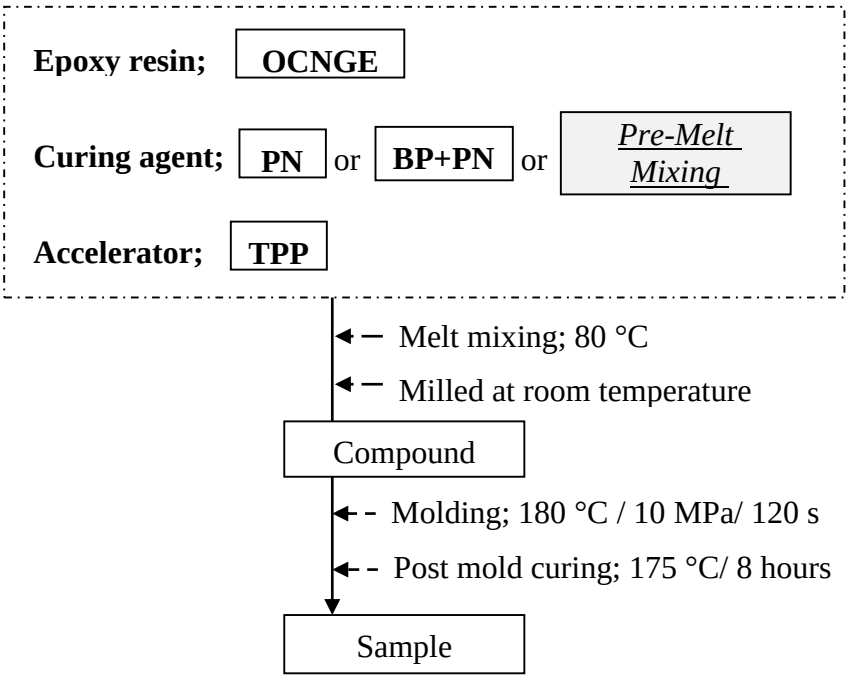

Figure 1. Sample preparing process flow chart.

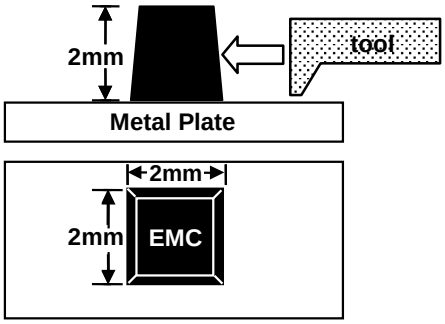

Figure 2. Adhesion strength measurement method
EMC: epoxy molding compound

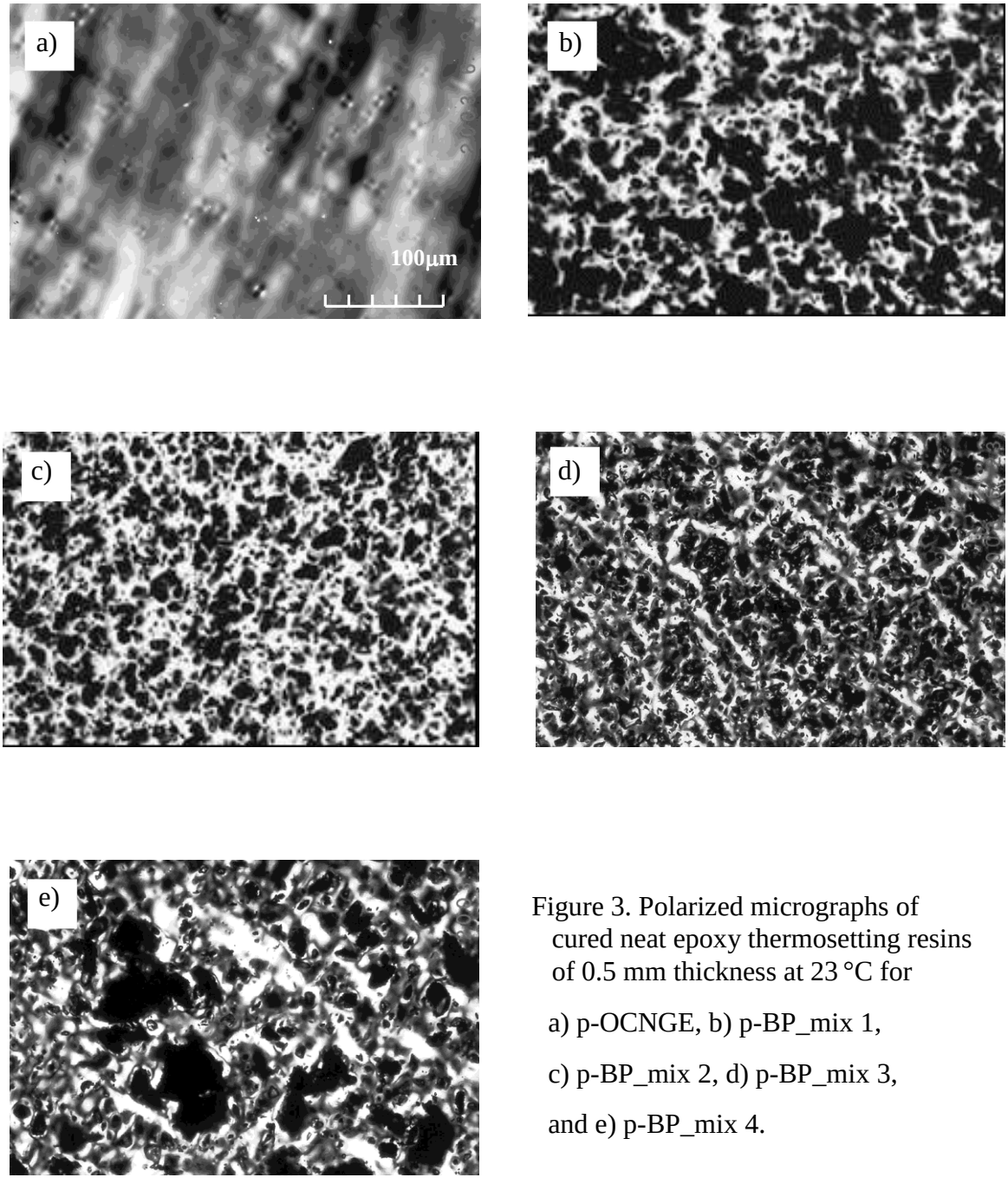

Figure 3. Polarized micrographs of cured neat epoxy thermosetting resins of 0.5 mm thickness at 23 °C for

a) p-OCNGE, b) p-BP_mix 1,

c) p-BP_mix 2, d) p-BP_mix 3,

and e) p-BP_mix 4.

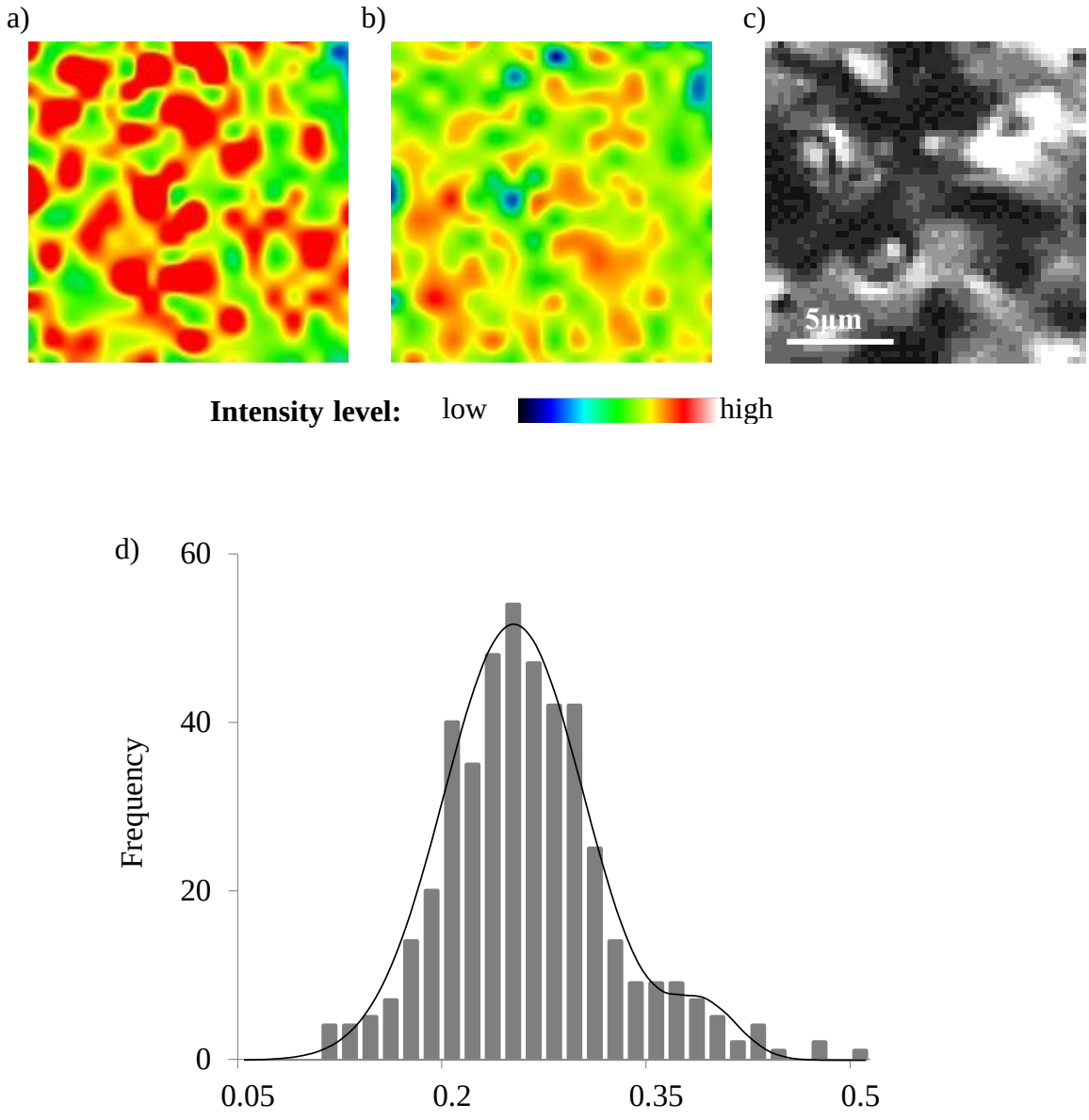

Figure 4. Raman mapping image and spectrum analysis of p-BP_mix 2.

a) Dispersion state of BP derived from the area fraction of the peak around 1610 cm^{-1} assigned to C=C stretching vibration in benzene ring.

b) Dispersion state of PN derived from the area fraction of the peak around 1430 cm^{-1} assigned to CH_2 bending vibration of methylene group.

c) Polarized micrographs image of cured sample shown in Figure 3 in the same magnification.

d) Distribution of the area fraction of C=C stretching vibration peak in every measured spectrum.

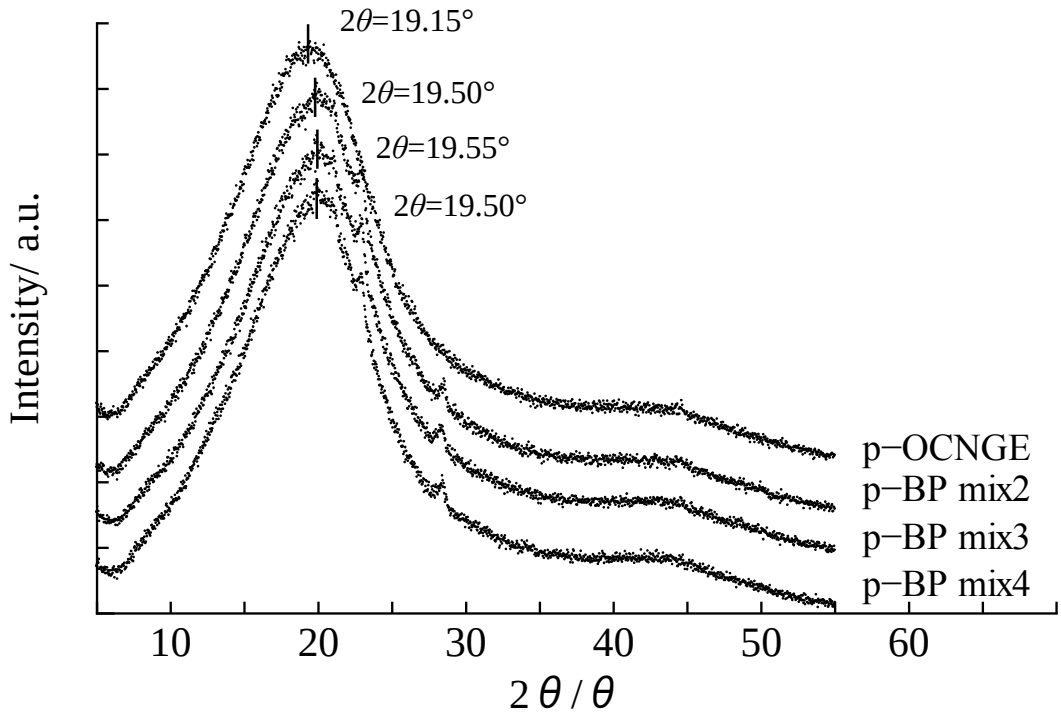

Figure 5. WAXD profile of neat epoxy thermosetting resin.

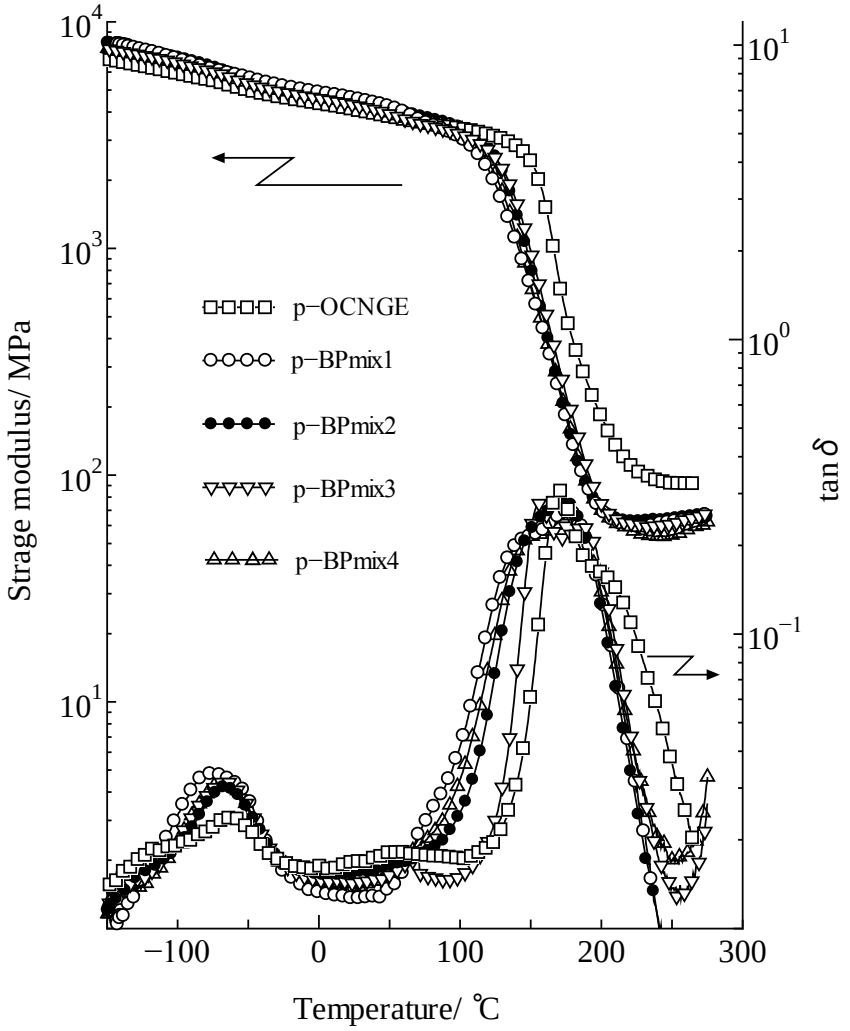

Figure 6. Temperature dependence of storage modulus and tanδ of neat epoxy thermo setting resin sample measured by DMA.

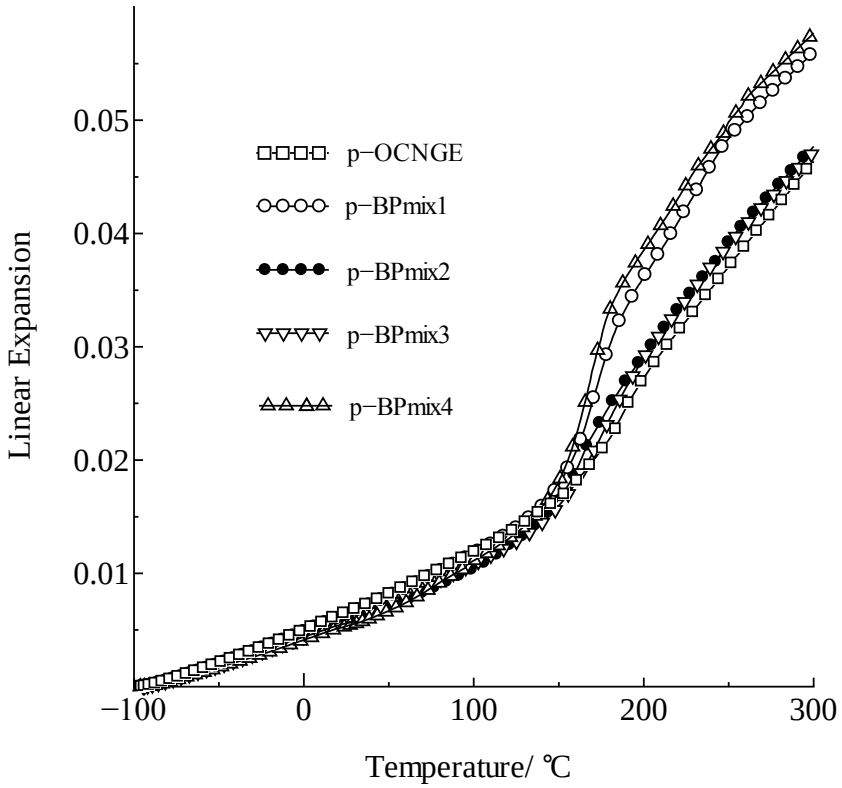

Figure 7. The thermal strain based on the length at -100 °C of neat epoxy thermosetting resin sample measured by TMA.

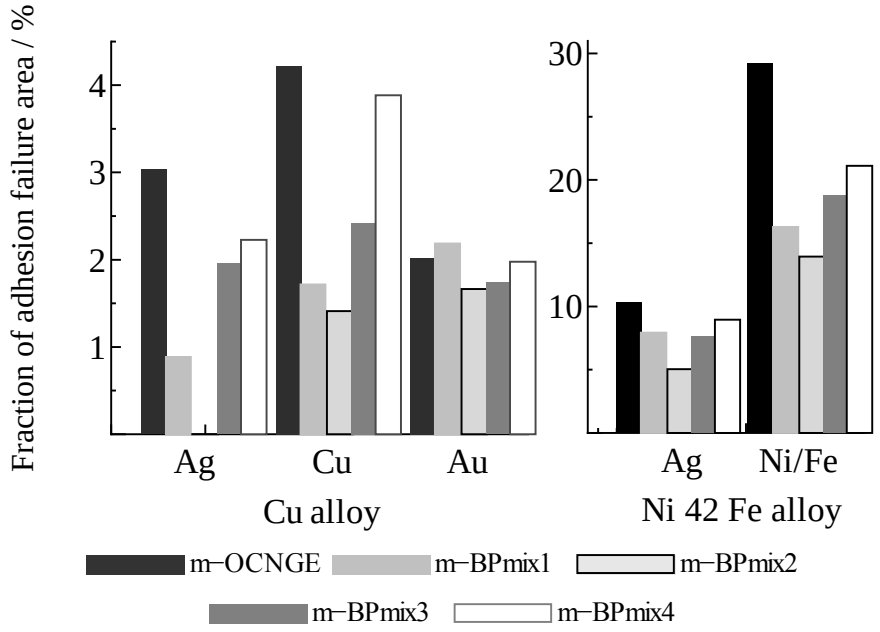

Figure 7. The fraction of adhesion failure area to all adhesive interface.

Table 1 Sample composition and pre-melt mixing condition.

sample	**Composition/ wt%**				**Pre-melt mixing condition**		
	OCNGE	BP	PN	TPP	Machine	Temperature /°C	Rotation speed /rpm
p-OCNGE	65.0	-	34.0	1.0	-	-	-
p-BP_mix1	67.0	16.0	16.0	1.0	-	-	-
p-BP_mix2	67.0	16.0	16.0	1.0	**universal mixer**	160	128
p-BP_mix3	67.0	16.0	16.0	1.0	**twin screw extruder**	100	**200**
p-BP_mix4	67.0	16.0	16.0	1.0	**twin screw extruder**	100	**440**

Table 2 Shear strength to every adherent plate of epoxy molding compound sample after PMC and water absorption treatment. (standard deviations (SD) are in parentheses)

		Shear strength / MPa			
	adherent	Cu alloy	Ag plated Cu alloy	Au (Ni/Pd) plated Cu alloy	Ni 42 % Fe alloy
m-OCNGE	PMC*	3.45 (0.63)	4.12 (2.44)	4.92 (2.06)	-
	Moisture treatment**	**3.50 (1.68)**	**4.34 (1.90)**	**5.30 (1.37)**	**4.93 (1.04)**
m-BP_mix1	PMC	-	-	-	-
	Moisture treatment	**4.35 (1.61)**	**5.56 (0.95)**	**5.76 (1.30)**	**5.61 (1.46)**
m-BP_mix2	PMC	3.59 (1.76)	5.63 (1.10)	6.65 (0.89)	-
	Moisture treatment	**5.06 (1.82)**	**6.01 (1.72)**	**6.13 (0.87)**	**5.65 (1.07)**
m-BP_mix3	PMC	3.69 (1.69)	5.46 (1.24)	5.89 (1.07)	-
	Moisture treatment	**4.19 (1.22)**	**5.68 (1.64)**	**5.80 (1.11)**	**5.31 (1.11)**
m-BP_mix4	PMC	3.76 (1.54)	5.20 (1.87)	6.44 (1.65)	-
	Moisture treatment	**4.99 (2.12)**	**5.36 (1.07)**	**5.88 (1.13)**	**5.40 (1.16)**

*175 °C for 8hours, **85 °C, 60 %RH for 168 hours

Chapter 4

Quantitative analysis of phase-separated structure and mechanical properties of acrylic copolymer/epoxy thermosetting resin composite.

4-1 Introduction

Epoxy thermosetting resins are used as adhesives in many industrial applications and enabled technological advances in organic-inorganic hybrid devices. In the assembly of semiconductor components, many compounds have been used in the devices and bonded with various techniques. For example, metal silicon dies adhere to printed circuit boards due to organic polymer-based die bond materials. Adhesion durability is important for device reliability. In particular, their manufacturing processes require high adhesive strength at temperatures exceeding 250 °C [1]. Therefore, epoxy thermosetting systems have been applied to adhesive matrix resins to satisfy such requirements [2, 3]. These epoxy thermosetting systems are immiscible with other components, such as thermoplastic resins, and generate phase-separated structures of micrometer sizes [4, 5, and 6]. Several studies regarding the phase separation phenomena of epoxy composites using a light scattering method have been reported. Yamanaka and Inoue et al. evaluated the phase separation of an epoxy thermosetting resin mixture consisting of the diglycidyl ether of bisphenol A epoxy resin, diaminodiphenylmethane as a curing agent, and poly(ether sulfone). The compound was a single-phase mixture in the early stage of curing. As the curing reaction progressed, phase separation occurred along with an increase in the molecular weight of the epoxy thermosetting resin. At this stage, the composite phase diagram contained a lower critical solution temperature (LCST), and a two-phase region should prevail in the phase diagram as the molecular weight increases during curing. The thermodynamic change in the phase diagram with epoxy chain extension results in a phase-separated structure with a change in the quench depth, which is the difference in

temperature between the LCST and the reaction temperature. The cured composites exhibited an interconnected globule structure and higher adhesive strength than that of neat epoxy resin. These structures, which play an essential role in their mechanical strength, form via spinodal decomposition as the phase diagram changes [7, 8].

Therefore, physical phenomena, such as phase separation exhibited by composite materials containing an epoxy component, are required to account for many factors, which have thermodynamic and kinetic aspects [9]. In addition, the adhesion mechanism is due to the chemical interaction with the adherend and the strength of the adhesive itself. The latter is very important for thick adhesives and affected by phase-separated structure. Therefore, the evaluation of the phase structure of epoxy thermosetting systems is important for advanced material design.

In this chapter, the phase structure and mechanical properties of composites that are primarily composed of epoxy thermosetting resins and undergo phase separation were investigated. Specifically, the influence of resin reactivity on the phase structure was evaluated for acrylic copolymer/epoxy thermosetting resin composites. In addition, the effects of material composition on the phase structure and mechanical strength were investigated. Then, the phase-separated structure of the composites was examined using two analytical techniques with scanning probe microscopy (SPM) images. First, the distribution of the diameter and the nearest neighbor distance between the centers of island domains were derived by particle size analysis. Second, the periodicity and correlation length of the phase structure were evaluated by two-dimensional fast-Fourier transform (2D-FFT) analysis [10]. These quantitative analyses of the phase structure provided insight into the phase separation process and physical strength development of acrylic copolymer/epoxy thermosetting resin composites.

4-2 Experiment

4-2-1 Sample preparation

The epoxy thermosetting resin and acrylic copolymer molecular structures are shown in Figure 1 and their compositions are shown in Table 1. The epoxy thermosetting system was prepared by mixing four types of epoxide compounds: the diglycidyl ether of bisphenol A epoxy resin (JER-828, Mitsubishi Chemical Corporation, Tokyo Japan, epoxy equivalent: 184 g/eq ~ 194 g/eq, viscosity: 12 Pa·s ~ 15 Pa·s (25 °C)), a multifunctional epoxy resin (a in Figure 1, EPPN-502H, Nippon Kayaku Co., Ltd., Tokyo Japan, epoxy equivalent: 158 g/eq ~ 178 g/eq, mp.: 60 °C ~ 72 °C), a dicyclopentadiene epoxy resin (b, HP-7200H, DIC Corporation, Tokyo Japan, epoxy equivalent: 274 g/eq ~ 286 g/eq, mp.: 88 °C ~ 98 °C), and an *o*-cresol novolac epoxy resin (c, EOCN-104S, Nippon Kayaku Co., Ltd., Tokyo Japan, epoxy equivalent: 218 g/eq, mp.: 92 °C). Phenol novolac (d, PAPS-PN4, Asahi Organic Chemicals Industry Co., Ltd., Tokyo Japan, hydroxyl equivalent: 104 g/eq, mp.: 111 °C) was used as a curing agent. 4,5-Dihydroxymethyl-2-phenylimidazole (e, 2PHZ-PW, Shikoku Chemicals Corp., Kagawa Japan, M_w = 188, mp.: 190 °C ~ 202 °C) was used as an accelerator. The four types of epoxide compounds were mixed in a 4:4:2:1 ratio in an epoxy equivalent amount. The equivalent ratio of hydroxyl groups in the curing agent to the epoxide groups was adjusted to 0.85, and 5.1 mmol of accelerator was added for 1 mol of hydroxyl groups in the curing agent.

The epoxy system was mixed with poly(methyl acrylate) (f, MA, M_w = 280,000, M_w / M_n = 2.9) in 2-butanone. The resulting mixture (i.e., a 70 wt % solution) was cast and dried on a polyethylene terephthalate (PET) film has a release layer. The 40 μm thick

prepared film was cured at 120 °C for 1 h and 175 °C for 2 h (standard conditions) to prepare the MA/E4_1.0 sample. Samples containing one-quarter and four times the accelerator amount were also prepared to investigate the effects of the reactivity of thermal curing on the phase separation (MA/E4_0.25, MA/E4_4.0). In the sample names, the first two characters correspond to the acrylic copolymer component, the next two characters indicate the number of epoxide types in the resin, and the last characters indicate the relative amount of accelerator.

In addition, three samples consisting of different acrylic copolymers and epoxy resin mixtures were prepared to investigate the effects of material composition on phase structure and mechanical strength. The first composite (MH/E4_1.0) consisted of 85:15 (mol/mol) methyl acrylate/2-hydroxyethyle acrylate acrylic copolymer (g, poly[(methyl acrylate)-co-(2-hydroxyethyle acrylate)], MH, M_w = 370,000, M_w / M_n = 4.2) and the original epoxy system (E4_1.0). The second sample (MG/E4_1.0) consisted of 85:15 methyl acrylate/glycidyl methacrylate acrylate copolymer (h, poly[(methyl acrylate) -co-(glycidyl methacrylate)], MG, M_w = 270,000, M_w / M_n = 4.4) and the E4_1.0 epoxy system. The third composite (MH/E2_1.0) combined the MH acrylate copolymer and two types of epoxide compounds as a thermosetting resin (E2_1.0). The E2_1.0 epoxy system is composed of the diglycidyl ether of bisphenol A epoxy resin and *o*-cresol novolac epoxy resin in a 3:8 ratio in an epoxy equivalent amount, and the curing agent and accelerator were added in the same manner as with the original epoxy system (E4_1.0). The last sample had a glycidyl group density of 2.30×10^{-3} mol/g, which is slightly less than that of MH/E4_1.0 (2.41×10^{-3} mol/g).

All of the acrylic polymers were provided by the Nippon Synthetic Chemical Industry Co., Ltd. (Osaka Japan).

4-2-2 Measurements and analysis

The phase structures of the sample surfaces were investigated using SPM images in the 1.2 × 1.2 μm^2 and 20 × 20μm^2 ranges. The scanning was conducted in tapping mode using a SPA-300HV (Hitachi High-Tech Science Corporation, Tokyo Japan) and a SI-DF40 cantilever at a resonance frequency of ca. 320 kHz.

The phase structures of the cross section for the samples which has different acrylic copolymers and epoxy resin mixtures were observed using transmission electron microscopy (TEM) in the 1.2 × 1.2 μm^2 area using H-7650 (Hitachi High-Technologies Corporation, Tokyo Japan) at Center for Advanced Materials Analysis, Tokyo Institute of Technology. The specimen for observation was prepared by ultra microtoming resulting in the 70 nm thickness. The specimens of MG/E4_1.0 and MH/E2_1.0 were stained by RuO_4, but the specimens of MA/E4_1.0 and MH/E4_1.0 were used without staining.

The SPM images were analyzed using two methods. In the first approach, the particle size distribution was evaluated using the topological image. To prepare the specimens for this analysis, the acrylic polymer component (or acrylic polymer-rich phase) that was isolated on the surface was dissolved by immersion in excess 2-butanone for 60 h. The height distribution of the sample surface after immersion exhibited one minimum surrounded by two peaks as shown in Figure 2. Therefore, the SPM topological images could be converted into binary images with a height distribution profile wherein the minimum served as the threshold dividing the two phase areas. The distribution of the particle diameter and the nearest neighbor distance between the centers of island domains

were determined from these binary images using our original software.

In the second method, the structural periodicity was assessed using the SPM phase images. These images were processed by 2D-FFT using the Image-J software (NIH open source) [11, 12].

The light-scattering measurements were performed using a DYNA3000 instrument (Otsuka Electronics Co. Ltd., Osaka Japan) to investigate the phase separation progress with the bulk structural periodicity. The optical system of light scattering apparatus is shown in Figure 3. The measurement chamber was set horizontally on the light scattering stage, and the specimen was irradiated vertically with a He–Ne gas laser ($\lambda = 632.8$ nm). The goniometer was positioned at $2\theta = 60°$, which corresponded to the light beam center scattered from the film under a parallel polarized (Vv) optical alignment. The scattering pattern was acquired using a charge-coupled device (CCD) camera from 48° to 72°, resulting in a 1D light scattering profile. The angles were accurately corrected using sample refractive indices.

The specimens were prepared by curing a MA/E4_1.0 film under various conditions as shown in Figure 4. The films were cured on an $8 \times 8 \times 0.15$ mm^3 glass slide at 125 °C for 30 min (Condition 1) or 1 h (Condition 2) and heated to 175 °C beyond condition 2 (Condition 3) and maintained for 2 h (Condition 4, standard condition). The heating rate was 3 °C/min for each temperature process.

The heat of reaction, molecular mobility (before and after curing), and local surface elastic modulus were measured to characterize the network state formed during curing.

To estimate the number of covalent bonds formed by the epoxy thermosetting resins, the heats of reaction were measured with the samples prior to curing. The measurements were performed using a Pyris 1 heat-compensation differential scanning calorimetry

(DSC) apparatus (Perkin Elmer, Inc., Massachusetts, U.S.) under nitrogen atmosphere at a heating rate of 10 °C/min. The onset temperatures and heats were derived and compared [13].

The storage moduli on the shear mode at 1.0 Hz with the MA/E4_1.0 and MH/E4_1.0 samples prior to curing were measured at 125 °C to compare the molecular mobility at the curing temperature using an ARES-G2 (TA instrument, New Castle U.S.).

The spin–spin relaxation time (T_2) was evaluated by pulse ^{1}H nuclear magnetic resonance (NMR) using a Minispec mq20 instrument (Bruker BioSpin K.K., Kanagawa, Japan) at 20 MHz to assess the molecular mobility after curing. The pulse [$90°_x$ -τ- $90°_y$; solid echo method] [14] and spin echo pulse [$90°_x$ -τ- $(180°_y$ -2τ-$)_n$; Carr–Purcell–Meiboom–Gill (CPMG) method] [15] sequences were adopted. The former pulse sequence has the advantage of avoiding the dead time effect after the pulse, and the latter spin echo pulse can eliminate the effect from the inhomogeneity of the magnetic field. Therefore, the fast decay of magnetization with low mobility proton components was measured by the solid echo method, and the slow decay of magnetization with high mobility components was measured using the CPMG method.

The free induction decay (FID) signal obtained by the solid echo method was split into one Gaussian and two exponential components [16, 17, and 18]:

$$M(\mathrm{t}) = M_1 \exp\{-1/2[t/T_2(1)]^2\} + M_2 \exp[-t/T_2(2)] + M_{3'} \exp[-t/T_2(3')] \quad (1)$$

where M_i and T_2(i) are the initial magnetization intensity and relaxation time of the i$^{\mathrm{th}}$ component, respectively. The dashed number in the third term represents a ‘provisional value’ for a proton component exhibiting a longer relaxation time because it is divided

by the CPMG method.

Similarly, the FID signal measured by the CPMG method was decomposed into three exponential terms as follows:

$$M(\mathrm{t}) = M_3 \exp[-t/T_2(3)] + M_4 \exp[-t/T_2(4)] + M_5 \exp[-t/T_2(5)] \qquad (2)$$

Each component fraction (F_i) was calculated using:

$$\begin{cases} F_\mathrm{i} = \dfrac{M_\mathrm{i}}{\sum_{\mathrm{j}=1}^{3'} M_\mathrm{j}} & (\text{for i = 1, 2}) \\ F_\mathrm{i} = \dfrac{M_{3'}}{\sum_{\mathrm{j}=1}^{3'} M_\mathrm{j}} \cdot \dfrac{M_\mathrm{i}}{\sum_{\mathrm{k}=3}^{5} M_\mathrm{k}} & (\text{for i = 3, 4, 5}). \end{cases} \qquad (3)$$

The measurements were conducted at 95 °C, which is intermediate between the glass transition temperatures of the simple epoxy thermosetting resin after curing under standard conditions (ca. 150 °C) and that of the simple acrylic copolymer (ca. 35 °C) used in this study.

The local surface elastic modulus was estimated according to the Hertz theory using the SPM force curve [19, 20]. The force curves were measured with the same equipment and cantilever as that employed for the morphology observations. The indentation depth and rate were set to 50 nm and 10 nm/s, respectively. The elastic moduli were calculated by fitting Eq. (4) to the force curves for the sea and island areas.

$$F = \frac{4E}{3(1-\nu^2)} R^{1/2} \delta^{3/2} \qquad (4)$$

where δ and F are the sample deformation and exerted force derived from the piezo scanner displacement, cantilever deflection, and spring constant (k = 53 N/m). R is the cantilever tip diameter (10 nm), E is the elastic modulus, and v is Poisson's ratio with values of 0.43, 0.47, 0.38, and 0.48 for MA/E4_1.0, MH/E4_1.0, MG/E4_1.0, and MA/E2_1.0, respectively. These value were derived from the ratio of the strain between the longitudinal and transverse direction observed using an advanced video extensometer at the tensile test on a pulling rate of 1.0 mm/min using a 5567 series Universal testing machine (Instron, Massachusetts, U.S.) at 23 °C.

The tensile strengths were measured at 250 °C at a 5.0 mm/min pulling rate using a 5581 series Universal testing machine (Instron, Massachusetts, U.S.) equipped with a thermostatic chamber. After breaking, the fracture surfaces were observed by scanning electron microscopy (SEM) (VE-9800, KEYENCE, Osaka Japan), and their degree of roughness (R_a) in the 2 × 2 μm^2 areas was measured by SPM, as previously mentioned.

4-3 Results and Discussion

4-3-1 Influence of curing accelerator amount on morphology

The morphologies of the acrylic copolymer/epoxy thermosetting resin composite were examined by SPM phase imaging (Figure 5a). The top and bottom images in Figure 5 correspond to 10 × 10 μm^2 area micrographs and their magnifications, respectively. All of the samples exhibited sea-island structures wherein the island domains were within the submicron range.

The distribution of the particle diameter and the nearest neighbor distance between the

centers of island domains were obtained from the binarized SPM image (Figure 6). The lines in each figure represent fitting results to the lognormal distribution:

$$f(x) = \frac{1}{x\sigma\sqrt{2\pi}} \exp\left[-\frac{(\ln x - \mu)^2}{2\sigma^2}\right] \qquad (5)$$

where μ and σ are the mean and standard deviation of the normal distribution for ln x. All of the frequency data matched the lognormal distribution curve. In addition, the domain particle diameter and the nearest neighbor distance between particles decreased with increasing curing accelerator amount.

The mean (m) and mode (p) values were derived from fitting to Eq. (5) and

$$m = \exp\left[\mu + {\sigma^2}/{2}\right] \qquad (6)$$

Their difference normalized by p ((m-p)/p) was also calculated (Table 2).

An (m-p)/p value of 0 signifies a normal distribution. For the nearest neighbor distance between particles, the m and p values were very close, which indicates a normal distribution. However, for the domain particle diameter, (m-p)/p increased with decreasing amount of accelerator. Therefore, the domain size distribution of composites containing smaller amounts of accelerator significantly deviated from the normal distribution. When the phenomenon occurs spontaneously, the physical quantity that represents this phenomenon has a normal distribution and is an independent variable. By contrast, when a physical quantity displays the lognormal distribution, a physical behavior may obey the law of proportionate effect, wherein the physical quantity proportionally changes in response to a stimulus with the physical quantity of the previous

stage. In this experiment, fine island domains were generated prior to growing and coalescing according to this law [21].

The 2D-FFT images (Figures 7a –c) were obtained from the SPM micrographs. The distance from the image center represents the wavenumber absolute value (q), which is inversely proportional to the periodic length. Each image shows a white concentric annular area around its center, indicating the presence of structural periodicity that extends to the peripheral portion of the image for the accelerator-rich sample (MA/E4_4.0).

These 2D-FFT images were radially averaged to yield 1D intensity profiles (Figure 7d) and correlation lengths (l_m). The 1D profiles were derived from more than six 2D-FFT images for each sample and averaged. These profiles exhibit a peak with an intensity that increased for samples with a smaller accelerator content. The structural periodicity increased when the island domain was larger.

The l_m values (Table 3) were calculated using the q_{peak} values as follows:

$$l_m = 2\pi / q_{peak} \qquad (7)$$

These l_m values correspond to the nearest neighbor distance between particles (Table 2) and follow the same tendency toward reactivity. Specifically, l_m increased as the accelerator content decreased. This behavior indicates that the structural periodicity results from the island's spatial position. In addition, the thermal reaction of the epoxy thermosetting resin acts as a driving force for the phase separation, and the thermal reaction could suppress the phase separation, leading to fixing the structure at the early

stage of decomposition. Therefore, the phase structure of MA/E4_4.0, which has a high accelerator content and exhibits high reactivity, represents "the pseudo in-progress state of phase formation" of MA/E4_0.25.

The light scattering patterns in the 2θ range between 48° and 72° (q = 6.8μm^{-1} –13 μm^{-1}) and the 1D scattering intensity profiles are shown in Figure 8. A high-intensity region in the scattering patterns was observed from approximately 10.5 μm^{-1} to 11.0 μm^{-1} for the samples cured under conditions 3 and 4, corresponding to the peaks exhibited by these samples in their 1D profiles. This peak became clearer, and q_{peak} decreased as the heat curing progresses, suggesting that higher periodicity and longer periodic structures accompany the development of the curing process. Ohnaga et al. evaluated the phase separation phenomena via spinodal decomposition with an epoxy composite using kinetic diffusion equation presented by Cahn–Hilliard, whereby the diffusion coefficient is defined as the product of the molecule mobility and second order differential of the free energy function [8]. The Flory–Huggins equation was employed as the free energy function to represent the thermodynamic steady state. When the quench depth increased at isothermal demixing, the diffusion coefficient increased, and the structural coarsening was suppressed. Therefore, the peak angle of the scattering profile remains constant during the light scattering measurement. However, when the quench depth changing rate (quench rate) is very small, the coarsening process is observed.

In our experiment, the phase separation phenomenon with a small quench rate will occur, and the two-phase region should gradually prevail with the low reactivity and low molecule mobility of the epoxy thermosetting system.

It is also important to note that the noises in the profiles are large due to a low scattering

intensity, and this low intensity indicates the deficient decomposition of each component.

The correlation lengths were estimated using q_{peak} in the same manner as that employed in the 2D-FFT image analysis. The sample cured under condition 4 exhibited an l_m value of 0.60 μm, which is in agreement with the result from 2D-FFT image analysis. Based on light scattering, which provides bulk structure information, the enhanced periodicity with the thermal reaction is also consistent with these image analysis results. Therefore, the surface structure observed by SPM also formed throughout the bulk.

4-3-2 Influence of composition on phase-separated structures and mechanical properties

The SPM phase images (Figures 5b –d) indicate that all of the samples exhibit phase-separated structures but with different morphologies, especially for sample MG/E4_1.0, for which the phase-separated structure has an ambiguous border.

TEM image for the phase structures of the cross section were observed as shown in Figure 9. The morphologies are quite similar to their surface morphologies observed by SPM in Figure 5. It also indicates that the surface structure also formed throughout the bulk as mentioned above with the light scattering results.

The *m*, *p*, and *(m-p)/p* values were derived in the same manner as the evaluation for the effects of reactivity on the composite morphologies (Table 2). The *(m-p)/p* values of the nearest neighbor distance between particles were determined to be approximately zero. However, these values of the domain particle diameters were large, indicating that the distribution deviates significantly from the normal distribution.

The island area fractions decreased well below 69 volume %, which was derived from the design value (wt %) and the densities of the simple acrylic and epoxy elements. These values changed according to the components even though the epoxy thermosetting resin content is the same. This result suggests that the epoxy component could also exist in a high quantity in the sea phase depending on the sample composition.

The DSC thermograms of the curing process (Figure 10) were acquired at a constant heating rate of 10 °C/min. These thermograms exhibit exothermal behaviors for the heat reaction, and the onset temperature and amount of heat vary with the components. The sample exhibiting a large l_m in Table 3 underwent the heat reaction at a high temperature, which is in agreement with the dependence of the accelerator amount trend. In particular, for the sample MG/E4_1.0, which has the lowest onset temperature and smallest l_m among the samples with the same accelerator amount, the thermal reaction between GMA of MG and the phenol novolac curing agent may suppress phase decomposition and result in a small l_m. Therefore, in these composites, the thermal reaction rate also affects the phase formation.

Generally, the amount of heat has a high correlation with the amount of covalent bonds formed during heat curing. The MH/E4_1.0 composite exhibits a lower amount of heat (142 J/g) than that of MA/E4_1.0 (163 J/g). Therefore, the epoxy thermosetting reactants for MH/E4_1.0 had a lower collision rate than that for MA/E4_1.0 and therefore formed fewer covalent bonds.

The shear storage modulus of MH/E4_1.0 at the curing temperature was 1,200 Pa, which is lower than that of MA/E4_1.0 (2,500 Pa) even though a lower modulus typically provides a high collision rate with highly mobile reactant molecules. Therefore, this lower

collision rate of the reactants for MH/E4_1.0 might be caused by chemical interactions via the hydroxyl group of MH.

The ^{1}H NMR FID curves measured by the solid echo and CPMG methods were well represented by Eqs. (1) and (2) ($R^2 > 0.98$) as shown in Figure 11, suggesting that the protons in the composites could be divided into one low-mobility and four high-mobility components. The low-mobility components exhibited small T_2 values (ca. 10^{-2} ms), whereas the high-mobility counterparts exhibited relatively large T_2 values (ca. 10^{-1} ms – 10^{0} ms).

The FID curves of the simple epoxy resin and acrylic polymer were measured using the solid echo and CPMG methods, respectively, and were divided into three components. The largest T_2 obtained for the epoxy resin alone and the smallest T_2 of the acrylic copolymer alone were very close, suggesting that these behaved as one component in the composites. Therefore, the FID curves of the composite were divided into five components. $T_2(1)$, $T_2(2)$, and $T_2(3)$ in Eq. (1) were attributed to the epoxy thermosetting resins, and $T_2(3)$, $T_2(4)$, and $T_2(5)$ in Eq. (2) were assigned to the acrylic polymer in the composites.

In addition, the linear combination of the fraction for each proton components in the simple epoxy and acrylic element simulates the complete phase-separated state. The fraction of each T_2 component (F_i(calc)) was derived using the following equation:

$$F_i(\text{calc}) = \begin{cases} f_i(\text{ep}) \times r_{ep} & (\text{for i} = 1, 2) \\ f_i(\text{ep}) \times r_{ep} + g_{i\text{-}2}(\text{ac}) \times r_{ac} & (\text{for i} = 3) \\ g_{i\text{-}2}(\text{ac}) \times r_{ac} & (\text{for i} = 4, 5) \end{cases} \quad (8)$$

where f_i(ep) is the fraction obtained for the epoxy thermosetting resin alone and $g_{i\text{-}2}$(ac) is the fraction measured for the acrylic copolymer alone. The index number i corresponds to the number of proton components in the composites, and r_{ep} and r_{ac} are the quantitative proton ratios calculated from the design values for the epoxy resin and acrylic copolymer. The MA/E4_1.0 composite exhibited r_{ep} and r_{ac} values of 0.674 and 0.326, respectively.

The FID curves of the composite were measured, and their fitting results were compared with the results of individual elements and their linear combinations as shown in Table 4 to consider the influence of mixing. Rows 1 and 3 list the T_2(i) and F_i values, respectively, that were derived from the FID curves of the composite. Row 2 lists the T_2(i) values for the epoxy thermosetting resin alone (left half) and acrylic copolymer alone (right half). Row 4 provides the F_i(calc) values calculated using Eq. (8). The MA/E4_1.0 composite exhibited a smaller F_1 value (49%; written in a bold-face in Table 4) than F_1(calc) (63%), which was due to the rigid cured epoxy resins. Therefore, F_3 (26%) surpasses the F_3(calc) values (12%). This result indicates that the amount of the lower mobility component assigned to the epoxy resin decreased because its mixing with the acrylic copolymer interfered with covalent bond formation during the curing process. The epoxy thermosetting resin did not react fully, and the protons were partly detected as the long-relaxation-time (T_2(3)) components along with the protons in the acrylic copolymer. However, these T_2(3) values (i.e., 0.098 ms) are smaller than 0.17 ms, which is the T_2(3) value of the simple acrylic copolymer. Therefore, the epoxy resins were sufficiently reactive to influence the acrylic polymer mobility.

Similarly to MA/E4_1.0, the MH/E2_1.0 composite, which contains two types of epoxide resin, exhibited a smaller F_1 than F_1(calc) and shorter T_2(3) than its individual

components. Although F_1 is the same as F_1(calc), the MG/E4_1.0 sample exhibited a larger F_2 than F_2(calc) and a shorter T_2(3 –5) than those of individual components, suggesting that the glycidyl group in MG reacts with the epoxy thermosetting system to form a covalent bond network. Therefore, the molecular mobility decreased overall.

For the MH/E4_1.0 sample, F_1 decreased, but T_2(3) remains the same as that of the acrylic copolymer alone, indicating that some epoxy resin remained in the acrylic polymer-rich phase and reacted poorly. Therefore, the protons in the epoxy resin may be detected as long-relaxation-time (T_2(3)) elements along with certain protons in acrylic polymer. However, in contrast to the components of MA/E4_1.0, the reactivity of this epoxy resin was too low to affect the acrylic polymer mobility. As a result, T_2(3) did not change from the T_2 value obtained for the acrylic polymer alone. Therefore, the protons in the acrylic polymer retained their mobility in the composite after curing. This decrease in reactivity appears as a reduced amount of heat in DSC (Figure 10).

The local surface elastic moduli are listed in Table 5. The methyl acrylate homopolymer (MA) and cured epoxy thermosetting system exhibited elastic moduli of 0.88 GPa and 2.9 GPa, respectively. Both the island and sea phases exhibited intermediate values in all of the samples.

In the MA/E4_1.0 and MH/E2_1.0 samples, these average values differ between the island and sea phases. In general, the number of covalent bonds formed by the epoxy resins influences the elastic modulus. Therefore, the state of the covalent bond network is considered to be different in each phase. However, the standard deviation is large. Therefore, the differences in the elastic moduli of each phase are not meaningful adequately. This large standard deviation is caused by two reasons. One is the sample

dimensions with a thickness in which the sea phase exists under the island phase. Another reason involves the incompleteness of the decompose state of the epoxy and acrylic element. This effect is recognizable because it was also detected as the low intensity of light scattering.

However, the MH/E4_1.0 and MG/E4_1.0 samples exhibited comparable elastic moduli and small standard deviations in both phases, implying that similar covalent bond networks were formed in both phases.

The tensile strengths at 250 °C are also listed in Table 5. All of the samples changing the acrylic component exhibited higher tensile strengths than MA/E4_1.0. In particular, the MG/E4_1.0 composite, which has an ambiguous border in the phase-separated structure, exhibited the highest value.

The SEM images of the edge of the cross-section corresponding to the fracture surface after the tensile test are shown in Figure 12. The insets show the surface morphologies at the same magnification, and the figures are the roughness (R_a) of the fracture surface measured by SPM.

The MA/E4_1.0 and MH/E2_1.0 composites exhibited cross-sections resembling their surface morphologies, indicating that the destruction propagates along the phase boundary. By contrast, the MG/E4_1.0 sample exhibited a flat fracture surface and an extremely small R_a value (5.6 nm). Therefore, the destruction may propagate through the island and sea phases.

The planar morphology of the fracture surface is smaller than the domain particle size (0.69 μm, Table 2) in the MH/E4_1.0 composite. This sample exhibited a lower R_a than MA/E4_1.0 despite their quasi-similar particle sizes. This result suggests that the

destruction partially propagates through both phases as proposed for MG/E4_1.0. When the destruction propagates through both phases, the fracture surface is smooth, and the tensile strength increases. This mechanism appears to be related to the elastic modulus differences between the phases.

In several previous studies that evaluated the phase separation phenomena and mechanical strength of epoxy composites [3, 5, 6, and 7], the sample had a co-continuous phase-separated structure provides an enormously high mechanical strength. However, the similarity of the network in both phases formed by the epoxy thermosetting resin system contributes to mechanical strength enhancement among the samples with the sea-island phase-separated structure. Based on the results of DSC and pulse ^{1}H NMR, the collision rate of the epoxy reactants is an important factor for network formation and depends on the molecular interactions via covalent and hydrogen bonds.

Conclusion

In this study, the phase structure and the mechanical properties of acrylic copolymer/epoxy thermosetting resin composites exhibiting phase-separated structures were evaluated. The SPM morphologies presented sea-island structures wherein the island domains had submicron diameters.

The influence of the epoxy thermosetting resin reactivity on the phase structure was investigated using composites containing different amounts of accelerator. The domain particle size decreased with increasing accelerator content. Thus, the diffusion of the reactants was limited, and the phase decomposition was suppressed by the viscosity increase due to resin polymerization, which results in the termination of structure formation. As a result, the structure of the sample with a high accelerator content would

be nearly fixed prior to sufficient progression of phase separation due to its fast reactivity.

The distribution of the domain particle diameter of the accelerator-rich sample closely approximated a normal Gaussian distribution. However, the domain particle diameter of the accelerator-poor sample exhibited a lognormal distribution. This lognormal distribution resulted from physical quantities obeying the law of proportionate effect. Therefore, small domains initially formed before accumulating and growing via a phase separation process.

There are peaks in the 1D intensity distribution profiles resulting from the 2D-FFT analysis of the SPM phase images. The samples containing small amounts of accelerator exhibited clearer peaks and longer correlation lengths, suggesting that the structural periodicity and domain size increased with decreasing amount of accelerator. These enhancements were also observed using light scattering measurements of the composites cured under various conditions. These results indicate that the phase-separated structures form via spinodal decomposition. In addition, the thermal reaction of the epoxy resin substantially affects structure formation and serves as a driving force.

The mechanisms governing the mechanical strength enhancement were evaluated by relating the phase structures and their mechanical properties using samples with different compositions. The samples that exhibited small fractions of island area showed similar elastic moduli for their sea and island phases as well as a low roughness values for their fracture surfaces. Considering that the number of covalent bonds strongly affects the elastic modulus, the epoxy thermosetting system may generate similar networks in both phases, and destruction may propagate through the phases.

When the fracture surface is smooth, the sample provides a high tensile strength. Therefore, the tensile strength increases when the destruction propagates through phases

because a considerably higher external force is required to break the boundary area.

Overall, the network structure changes with the composition, and the destruction propagates along or through the phase boundary area depending on the network states in both phases. Controlling these network structures in each phase, taking into account the interaction between the epoxy reactants and other components, is important and contributes to mechanical strength enhancement.

References

1) JEDEC Standard 22, Method A113F, "Preconditioning of plastic surface mount devices prior to reliability testing". Accessed on October 2008.
2) Y. Nakamura, M. Yamaguchi, A. Tanaka, and M. Okubo, *Polymer*, **34**, 3220-3224 (1993).
3) T. Iwakura, T. Inada, M. A. Kader, and T. Inoue, *e-Journal of Soft Materials*, **2**, 13-19 (2006).
4) S. P. Nunes, and T. Inoue, *Journal of Membrane Science*, **111**, 93-103 (1996).
5) H. Kishi, Y. Kunimitsu, J. Imade, S. Oshita, Y. Morishita, and M. Asada, *Polymer*, **52**, 760-768 (2011).
6) K.Yamanaka, Y. Takagi and T. Inoue, *Polymer*, **30**, 1839-1844 (1989).
7) K. Yamanaka and T. Inoue, *Polymer*, **30**, 662-667 (1989).
8) T. Ohnaga, W. Chen, and T. Inoue, *Polymer*, **35**, 3774-3781 (1994).
9) T. Shiraishi, H. Motobe, M. Ochi, Y. Nakanishi and I. Konishi, *Polymer*, **33**, 2975-2980 (1992).
10) K. Shimizu, H. Wang, G. Matsuba, Z. Wang, H. Kim, W. Peng and C. C. Han, *Polymer*, **48**, 4226-4234 (2007).

11) W. S. Rasband, ImageJ, N.I.H., Bethesda, Maryland, USA, (http://imagej.nih.gov/ij/), 1997-2012.

12) C.A. Schneider, W.S. Rasband and K.W. Eliceiri, NIH Image to ImageJ: 25 years of image analysis, *Nature Methods*, **9**, 671-675 (2012).

13) W. I. Lee, A. C. Loos and G. S. Spronger, *J. Composite Materials*, **16**, 510-520 (1982).

14) J. G. Powles, J. H. Strange, *Proc. Phys. Soc.*, **82**, 6-15 (1963).

15) S. Meiboom and D. Gill, *Rev. Sci. Instrum*., **29**, 688-691 (1958).

16) H. Tanaka and T. Nishi, *J. Chem. Phys.*, **82**, 4326-4331 (1985).

17) H. Tanaka and T. Nishi, *J. Chem. Phys.*, **85**, 6197-6209 (1986).

18) Y. Nakamura, Y. Nishida, H. Honda, S. Fujii and M. Sasaki, *J. Adhesion Sci. Technol.*, **25**, 2703-2716 (2011).

19) L.D. Landau and E.M. Lifshitz, "Theory of Elasticity (Volume 7 of Course of Theoretical Physics)" Pergamon, New York (1970).

20) S. Nagai and S. Fujinami, *Nihon Reoroji Gakkaishi*, **36**, 99-106 (2008).

21) S. C. Colbeck, *Acta metal.*, **35**, 1583-1588 (1987).

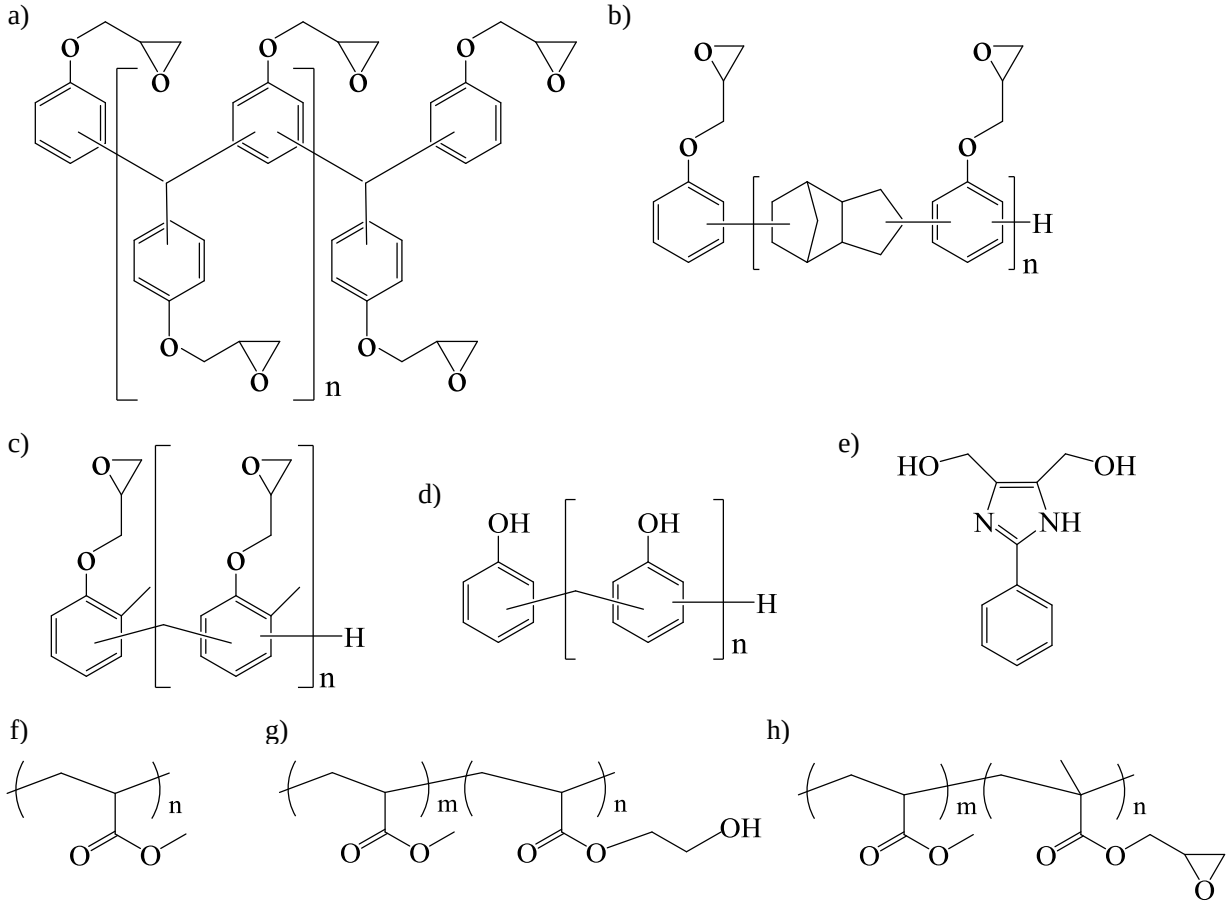

Figure 1. Epoxy thermosetting resin and acrylic polymer component for each sample
a) multifunctional epoxy resin, b) dicyclopentadiene epoxy resin,
c) *o*-cresol novolac epoxy resin, d) phenol novolac curing agent,
e) imidazole accelerator ([4-(Hydroxymethyl)-2-phenyl-1H-imidazol-5-yl]methanol),
f) methyl acrylate homo polymer (**MA**),
g) poly[(methyl acrylate) -*co*-(2-hydroxyethyle acrylate)] (m:n = 85:15 mol%) (**MH**), and
h) poly[(methyl acrylate) -*co*-(glycidyl methacrylate)] (m:n = 85:15 mol%) (**MG**).

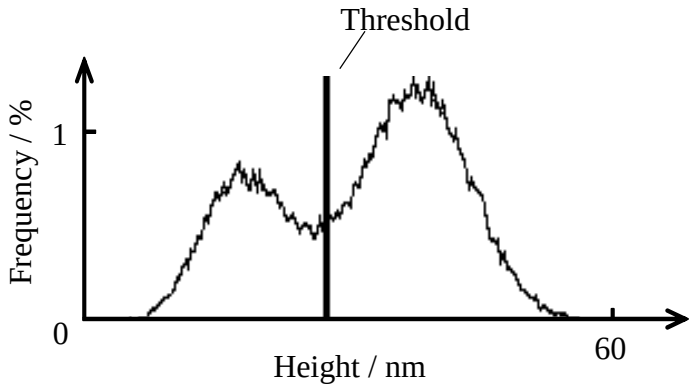

Figure 2. Height distribution of the MA/E4_1.0 surface after immersion treatment and threshold for conversion to binary image.

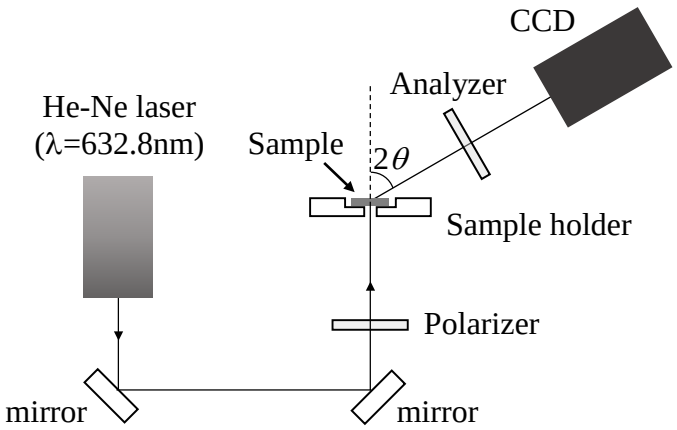

Figure 3. Optical system of light scattering apparatus.

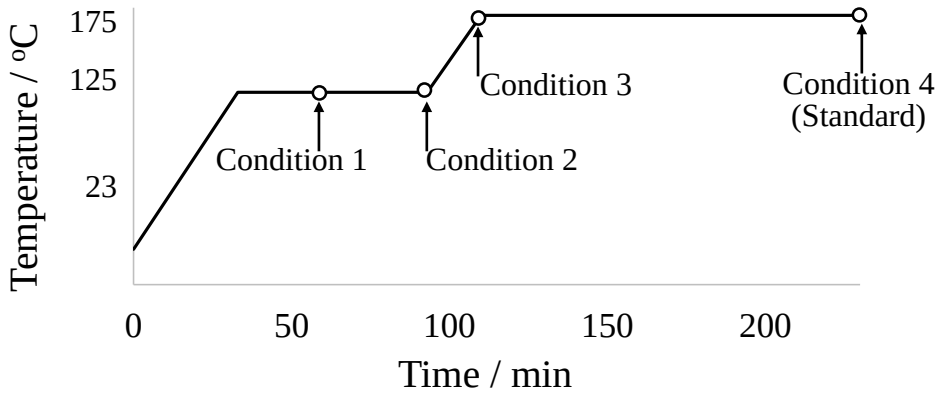

Figure 4. Curing condition profile of the sample for light scattering.

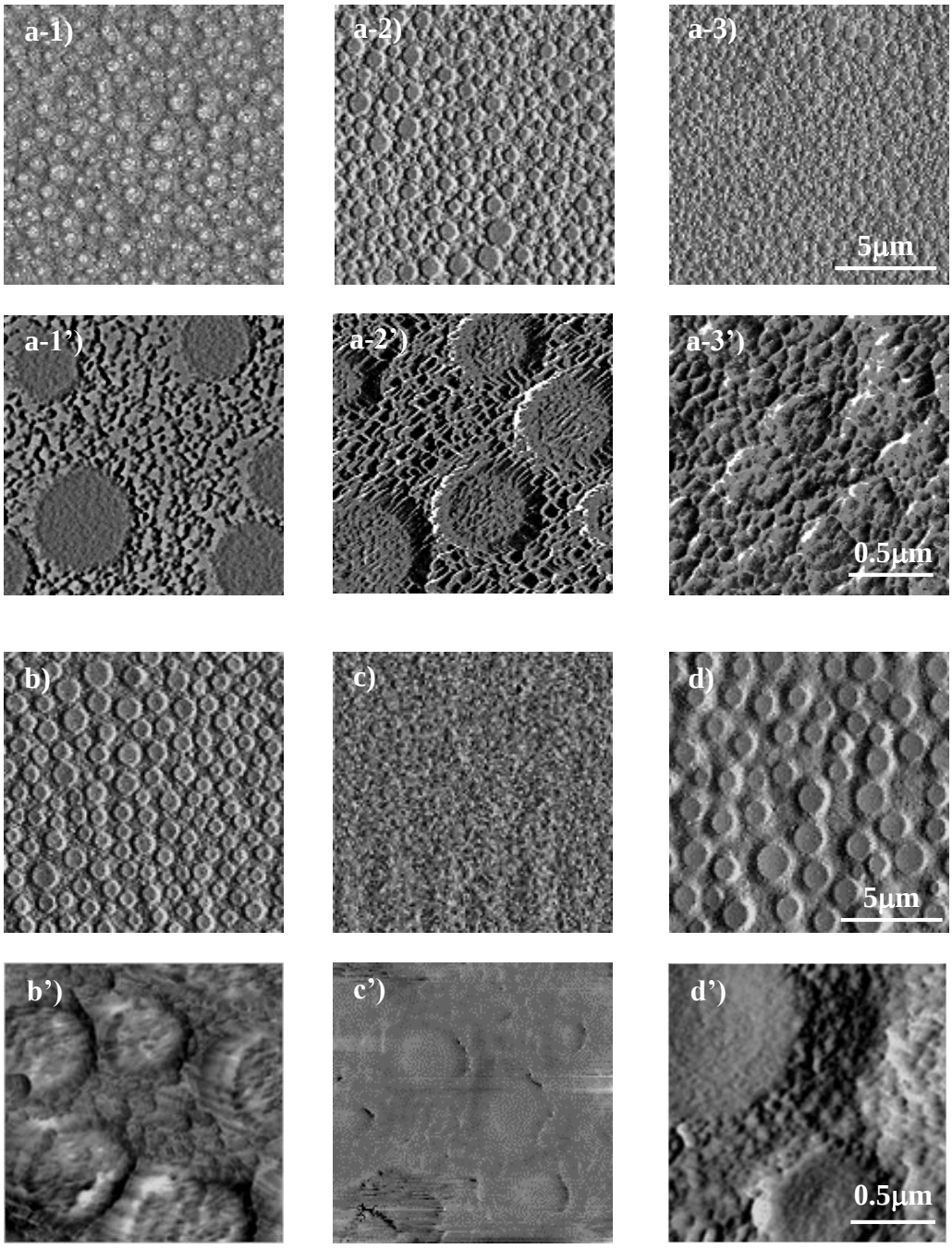

Figure 5. SPM phase image of a-1), a-1') MA/E4_0.25, a-2), a-2') MA/E4_1.0, and a-3), a-3') MA/E4_4.0, which have different amounts of the accelerator in the thermal curing systems and b), b') MH/E4_1.0, c), c') MG/E4_1.0, and d), d') MH/E2_1.0, which have different acrylic copolymer components and different epoxy thermosetting resin components.

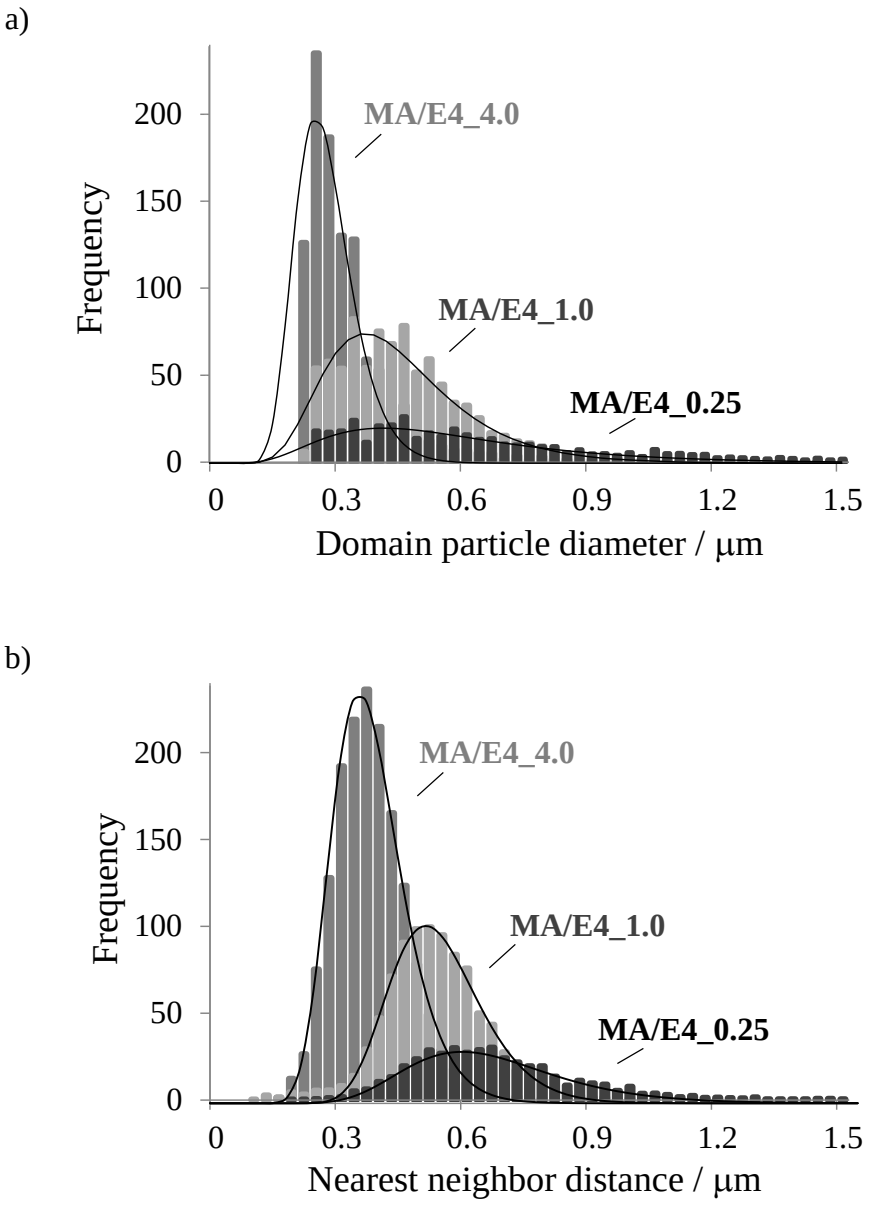

Figure 6. Distribution of a) domain particle diameter and b) nearest neighbor distance of the SPM topology images of the samples with different amounts of accelerator.

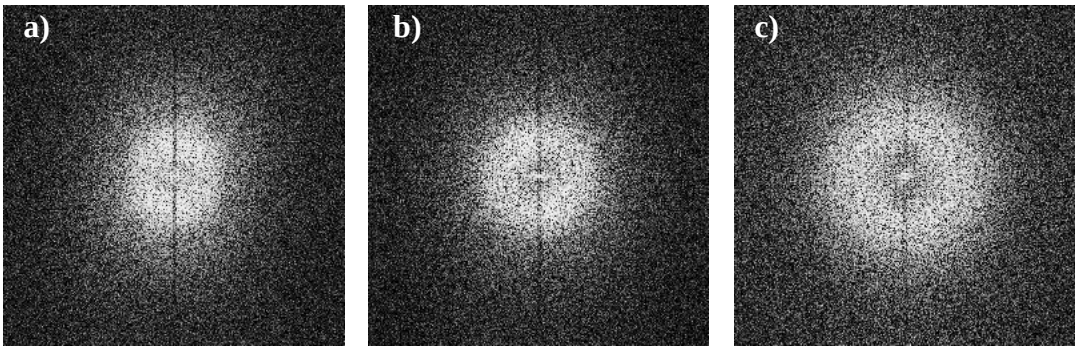

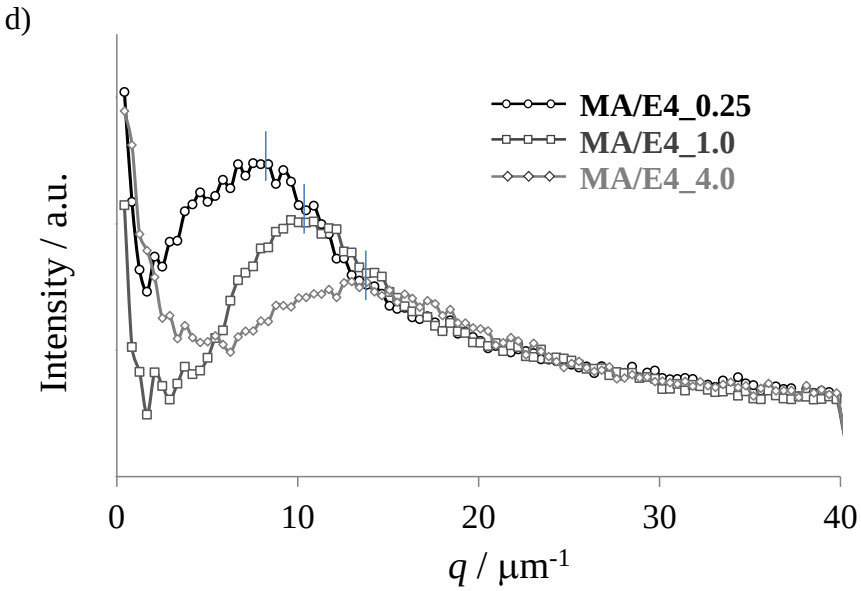

Figure 7. I Images after 2D-FFT with the SPM phase image of a) MA/E4_0.25, b) MA/E4_1.0 and c) MA/E4_4.0 as well as d) 1D intensity distribution profile.

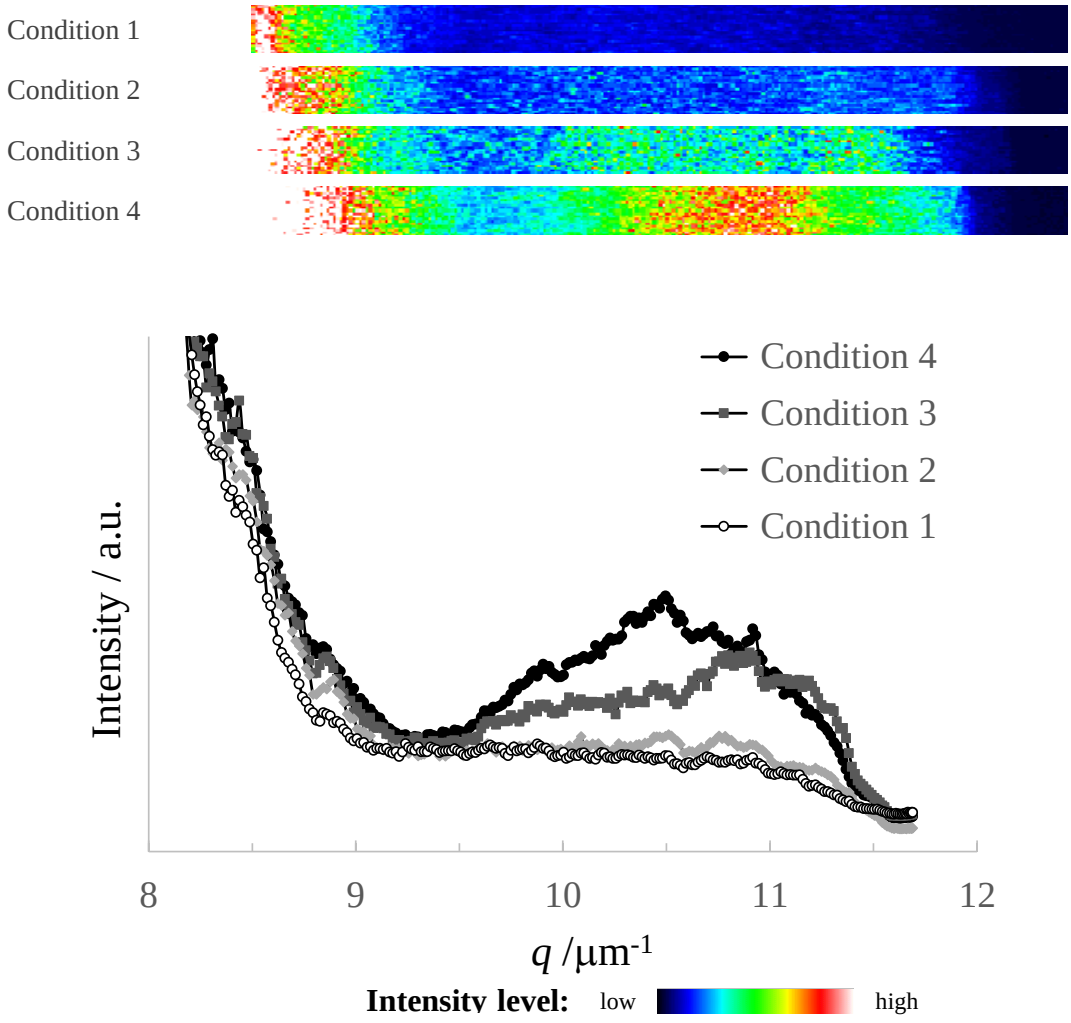

Figure 8. Light scattering pattern of cured MA/E4_1.0 and intensity profile under the various curing condition (Figure 4).

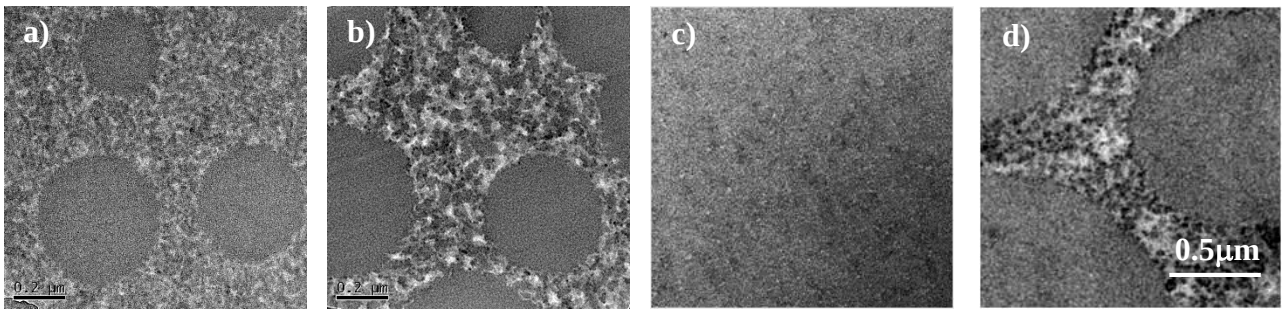

Figure 9. TEM image of the cross section for a) MA/E4_1.0, b) MH/E4_1.0, c) MG/E4_1.0, and d) MH/E2_1.0.

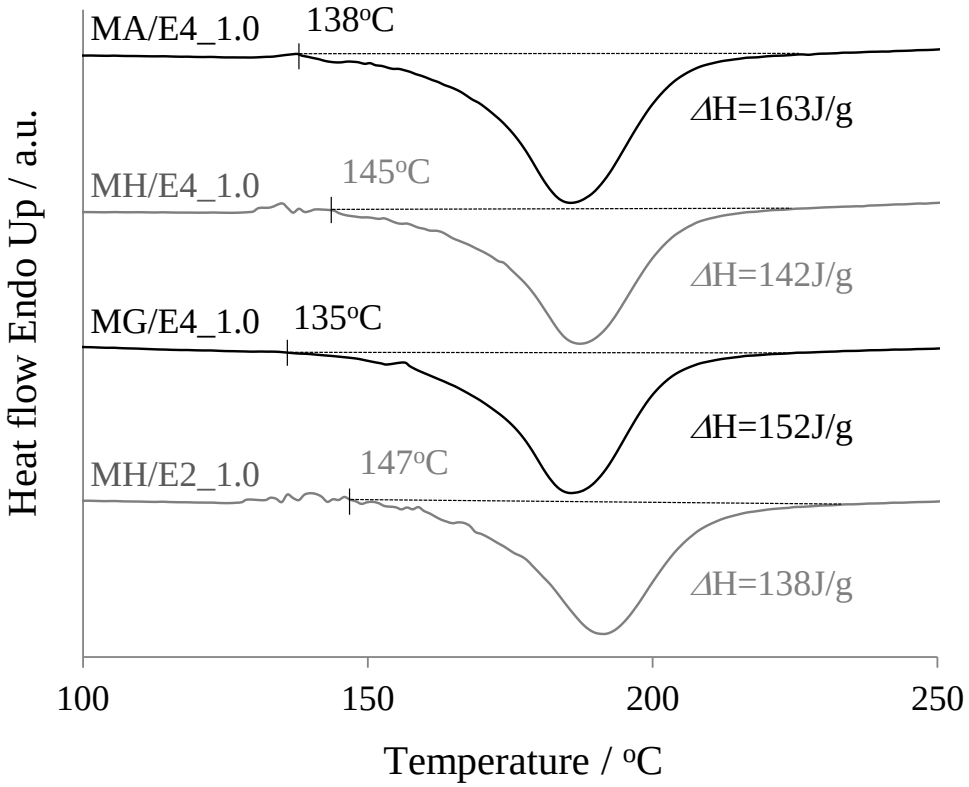

Figure 10. DSC thermograms. The onset temperature and amount of heat are shown in this figure.

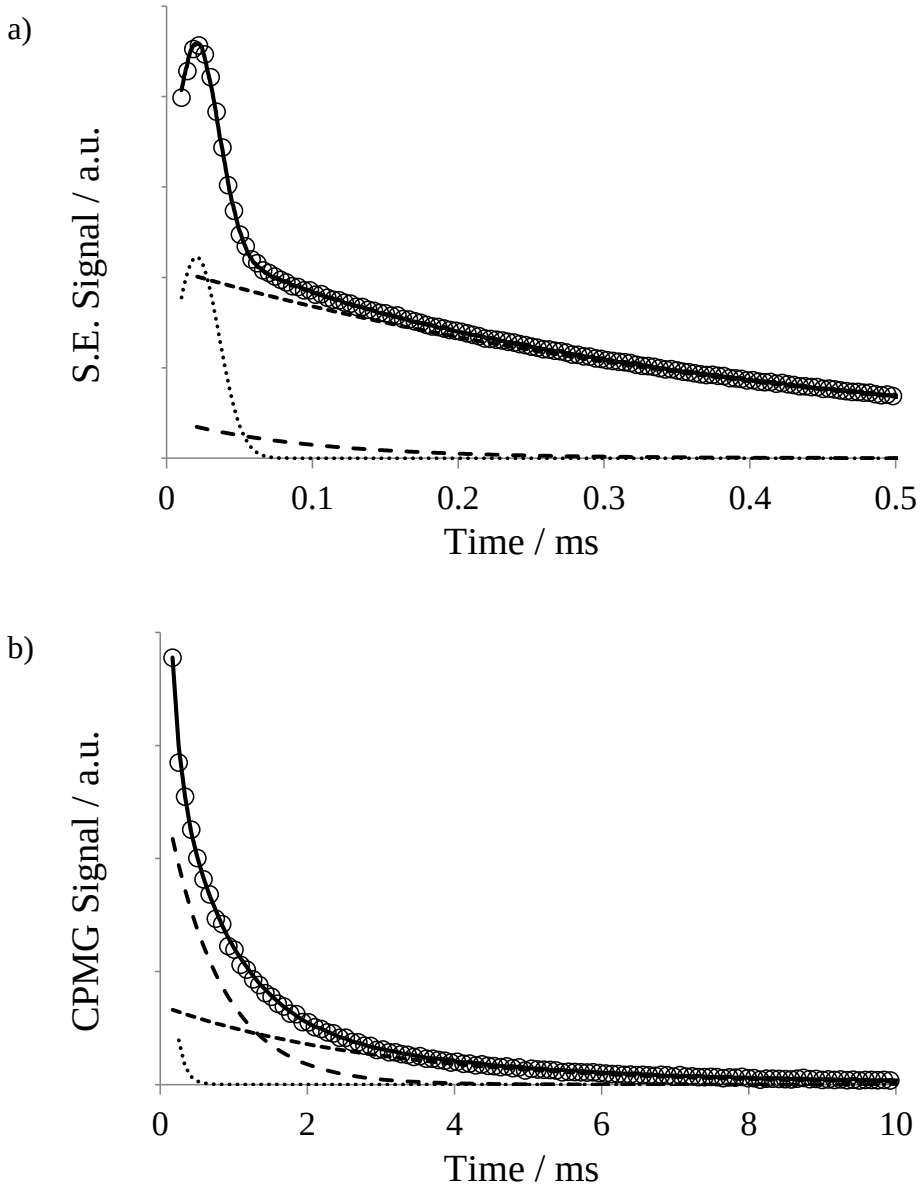

Figure 11. FID curve of ^{1}H pulse NMR measurement on a) the solid echo method and b) CPMG method with sample MA/E4_1.0. Open circle (○) shows observed data and rigid and dot lines are total fitting result and each curve element derived by formula (2) and (3).

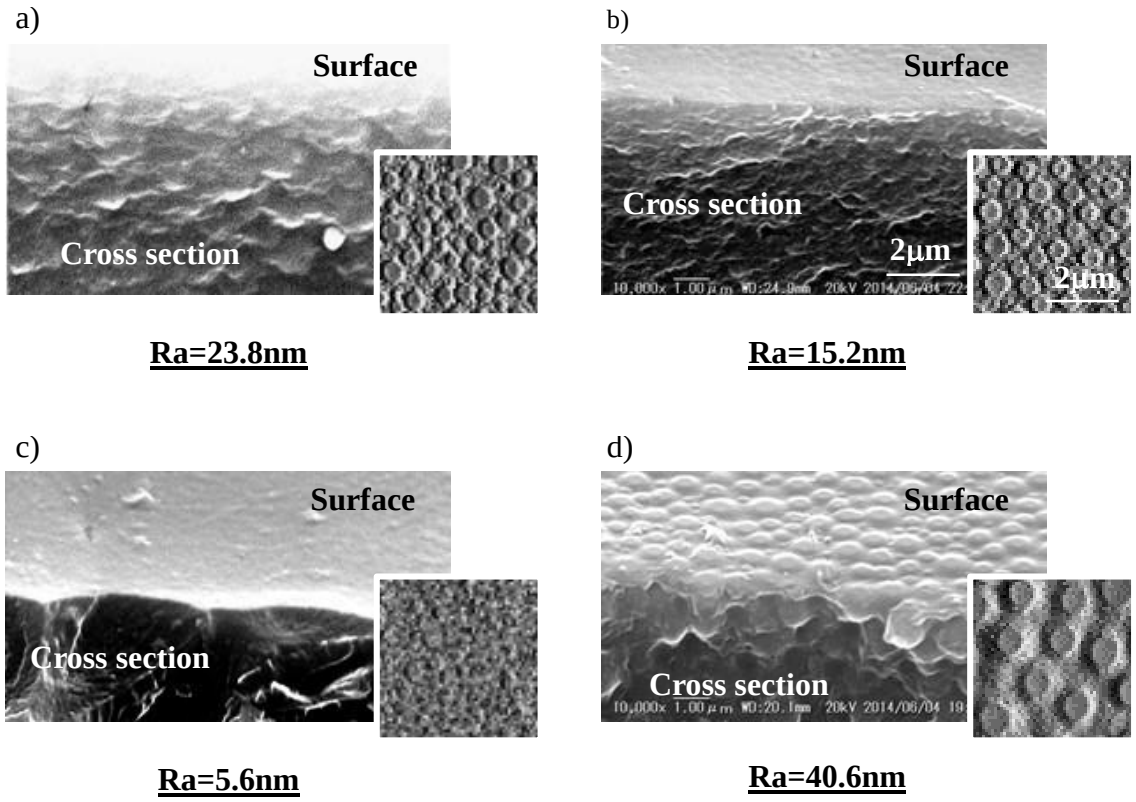

Figure 12. Edge of the cross-section (fracture surface) of the cured film after peel strength test (SEM image). **Inset**; SPM image (phase mode; same as Figure 5), **Number below**; Roughness of each cross-section.
a) MA/E4_1.0, b) MH/E4_1.0, c) MG/E4_1.0, and d) MH/E2_1.0.

Table 1 Composition of samples

Sample name	acrylic polymer*	epoxy thermo setting resin system	accelerator amount
MA/E4_1.0	MA	4types of epoxy resin**	Ctrl.***
MA/E4_0.25	MA	4types of epoxy resin	**×0.25**
MA/E4_4.0	MA	4types of epoxy resin	**×4.0**
MH/E4_1.0	MH	4types of epoxy resin	Ctrl.
MG/E4_1.0	MG	4types of epoxy resin	Ctrl.
MH/E2_1.0	MH	2types of epoxy resin	Ctrl.

* The ratio of the acrylic polymer and epoxy thermosetting resins are 30:70 in weight.
** Equivalent ratio of the hydroxyl group in curing agents to epoxied group was adjusted to 0.85.
*** 5.1 mmol for 1 mol of hydroxyl groups in the curing agents.

Table 3 q value at peak intensity ($\boldsymbol{q}_{\mathbf{peak}}$) on the 1D intensity profile and correlation length ($\boldsymbol{l}_{\boldsymbol{m}}$) derived from 2D-FFT analysis.

	$\boldsymbol{q}_{\mathbf{peak}}$ / μm^{-1}	$\boldsymbol{l}_{\mathbf{m}}$ / μm
MA/E4_0.25	8.4	0.75
MA/E4_1.0	10.9	0.58
MA/E4_4.0	13.8	0.45
MH/E4_1.0	8.0	0.79
MG/E4_1.0	13.0	0.48
MH/E2_1.0	4.2	1.50

Table 2 Fitting parameter with distribution analysis to the lognormal function, the mean value (***m***), the mode value (***p***) and the difference between them normalized by *p* ((***m-p)/p***)). And the total area fraction of island.

	Domain particle diameter / μm			Nearest neighbor distance / μm			Total area fraction of island / %
	m	*p*	(*m*-*p*) / *p*	*m*	*p*	(*m*-*p*) / *p*	
MA/E4_0.25	0.60	0.42	0.43	0.66	0.66	0.00	49.5
MA/E4_1.0	0.45	0.36	0.25	0.53	0.51	0.04	40.3
MA/E4_4.0	0.28	0.24	0.17	0.37	0.36	0.03	25.3
MH/E4_1.0	0.69	0.54	0.28	0.75	0.69	0.09	33.3
MG/E4_1.0	0.29	0.24	0.21	0.47	0.42	0.12	31.7
MH/E2_1.0	1.17	0.63	0.86	1.28	1.14	0.12	48.9

Table 4 T_2 and the fraction of each proton components measured by ^{1}H pulse NMR and the linear sum of each simple element.

		i=1	2	3	4	5
MA/E4_1.0	T_2(i) /ms	0.016	0.094	**0.098**	0.73	3.0
	T_2(i)*/ms	0.015	0.031	0.093 **0.17**	1.1	6.1
	F_i /%	**49**	7	26	14	4
	F_i(calc) /%	**63**	3	12 (10)**	19	3
MH/E4_1.0	T_2(i) /ms	0.016	0.084	**0.17**	1.0	6.3
	T_2(i)*/ms	0.015	0.031	0.093 **0.18**	1.0	5.3
	F_i /%	**47**	14	24	12	3
	F_i(calc) /%	**63**	3	12 (10)**	18	4
MG/E4_1.0	T_2(i) /ms	0.015	0.064	**0.11**	0.64	3.8
	T_2(i)*/ms	0.015	0.031	0.093 **0.25**	1.1	12
	F_i /%	**63**	**19**	14	3	1
	F_i(calc) /%	**63**	**3**	17 (15)**	14	3
MH/E2_1.0	T_2(i) /ms	0.014	0.079	**0.099**	0.67	2.8
	T_2(i)*/ms	0.014	0.036	0.10 **0.18**	1.0	5.3
	F_i /%	**47**	8	26	14	5
	F_i(calc) /%	**59**	6	12 (10)**	18	4

* T_2 value of the simple epoxy thermo setting resin (left half) and the simple acrylic copolymer (right half).

** The fraction of the proton component in the acrylic element ($g_{i\text{-}2}$(ac) × r_{ac} in equation (8)) whose index number (i) is 3 (in parentheses).

Table 5 Elastic modulus of local sea and island phase area on the sample surface and the tensile strength at 250ºC (standard deviations (SDs) are in parentheses).

	Elastic modulus of local area /GPa* (SD)		Tensile strength at 250ºC /MPa (SD)
	sea phase	island phase	
MA/E4_1.0	**1.96** (0.13)	**2.08** (0.19)	0.81 (0.09)
MH/E4_1.0	1.37 (0.05)	1.37 (0.05)	1.20 (0.14)
MG/E4_1.0	1.76 (0.10)	1.76 (0.07)	1.42 (0.12)
MH/E2_1.0	**1.91** (0.19)	**1.99** (0.17)	1.05 (0.12)

* The moduli of simple acrylic polymer and epoxy thermosetting resin are 0.88 GPa and 2.9 GPa, respectively.

Chapter 5

Phase-separated structure and adhesion properties of acrylic copolymer/epoxy thermosetting resin composite.

5-1. Introduction

Recently, polymeric materials have been introduced in several industrial products instead of inorganic compounds. However, it is difficult to simultaneously satisfy various requirements with single-polymer materials. Therefore the improvement of material properties through polymer blend technology is very useful and important. [1, 2]. Polymer blends comprising thermosetting resins generally used for an adhesive in the electronic components such as semiconductor IC package and printed circuit board. High adhesion durability and the insulating property are needed for them [3, 4]. In order to achieve the higher adhesion strength, epoxy thermosetting resin systems are used for the matrix resin [5, 6]. Some of these resin systems are immiscible with the thermoplastic resin components resulting in phase separation of micrometer scale. According to previous studies, this phase-separated structure is important for the adhesive strength [7 –10].

In Chapter 4, the phase-separated structure of acrylic copolymer/epoxy thermosetting resin composites were quantified by image analysis with morphological SPM images. The distribution of island domains diameter was represented as lognormal plots, indicating the small island domains are formed and accumulate. This phenomenon is observed in the late stage of phase separation via the spinodal decomposition. In addition, total area fraction of island domain was smaller than that of the design value, because a large amount of epoxy thermosetting resin remained in the acrylic copolymer phase. From the results of the tensile test, such composites showed the higher mechanical strength and the lower roughness of fracture surface. This is because the

destruction propagated through the phases rather than along boundaries and a considerably larger external force was needed to break the boundary area.

Consequently, the evaluation of the phase structure are very important for achieving better mechanical properties and the designing the advanced material of polymer blends with epoxy thermosetting resin.

In this chapter, in order to reveal a fracture mechanism and investigate the factors contributing to mechanical properties, the effects of phase-separated structure and the destruction test mode on mechanical strength were evaluated for the adhesives used in semiconductor assembles. These were mainly composed of acrylics copolymer and epoxy thermosetting resin and exhibit the phase separation structure in the size of μm order. In particular, the influence of the morphology aspects, the sizes of structure, and the interactions between acrylic co-polymer and epoxy thermosetting resin element on the mechanical strength was evaluated.

5-2. Experiment

5-2-1. Sample preparation

The molecular structures of epoxy thermosetting resins and acrylic copolymers used in this study are shown in Figure 1. As acrylic random copolymer, methyl acrylate homo polymer (**a** in Figure 1, M_w = 280,000, M_w / M_n = 2.9; **MA**), poly[(methyl acrylate) -*co*-(2-hydroxyethyle acrylate)] 95:5 (mol/ mol) (**b**, M_w = 510,000, M_w / M_n = 2.9; **Mh)** and 85:15 (**b**, M_w = 370,000, M_w / M_n = 4.2; **MH**), poly[(methyl acrylate) -*co*-(2-hydroxypropyl acrylate)] 85:15 (**c**, M_w =140,000, M_w / M_n = 3.8; **MHiP**), poly[(methyl acrylate) -*co*-(4-hydroxybutyl acrylate)] 85:15 (**d**, M_w = 190,000, M_w / M_n = 4.3; **MHB**),

poly[(methyl acrylate) -*co*-(benzyl acrylate)] 85:15 (**e**, M_w = 330,000, M_w / M_n = 3.3; **MBz**), poly[(methyl acrylate) -*co*- (2-hydroxyethyle acrylate) -*co*- (benzyl acrylate)] 70:15:15 (**f**, M_w = 59,000, M_w / M_n = 4.9; **MHBz**), and poly[(methyl acrylate) -*co*-(glycidyl metacrylate)] 85:15 (**g**, M_w = 270,000, M_w / M_n = 4.4; **MG**) were used. They were polymerized anionically and provided by Nippon Synthetic Chemical Industry Co., Ltd. (Osaka Japan).

In addition, poly[(methyl acrylate) -*co*-(2-hydroxyethyle acrylate) 95:5 prepared with **living radical** polymerization technique (**b**, TERPLUS N10506, Otsuka Chemical Co., Ltd., Osaka Japan; M_w =680,000, M_w / M_n =2.0; **MhL**) was also used.

The epoxy thermosetting system was prepared by mixing four types of epoxide compounds: the diglycidyl ether of bisphenol A epoxy resin (JER-828, Mitsubishi Chemical Corporation, Tokyo Japan), epoxy equivalent: 184 g/eq ~ 194 g/eq, viscosity: 12 Pa·s ~ 15 Pa·s (25 °C)), a multifunctional epoxy resin (**h** in Figure 1, EPPN-502H, Nippon Kayaku Co., Ltd., Tokyo Japan), epoxy equivalent: 158 g/eq ~ 178 g/eq, mp.: 60 °C ~ 72 °C), a dicyclopentadiene epoxy resin (**i**, HP-7200H, DIC Corporation, Tokyo Japan), epoxy equivalent: 274 g/eq ~ 286 g/eq, mp.: 88 °C ~ 98 °C), and an *o*-cresol novolac epoxy resin (**j**, EOCN-104S, Nippon Kayaku Co., Ltd., Tokyo Japan), epoxy equivalent: 218 g/eq, mp.: 92 °C). Phenol novolac (**k**, PAPS-PN4, Asahi Organic Chemicals Industry Co., Ltd., Tokyo Japan), hydroxyl equivalent: 104 g/eq, mp.: 111 °C) was used as a curing agent. 4,5-Dihydroxymethyl-2-phenylimidazole (**l**, 2PHZ-PW, Shikoku Chemicals Corp., Kagawa Japan), M_w = 188, mp.: 190 °C ~ 202 °C) was used as an accelerator.

The combination of **four types** and **two types** of epoxy resin were adopted. For four types mixture, a bisohenol A epoxy resin, a multifunctional epoxy resin, a

dicyclopentadiene epoxy resin, and an *o*-cresol novolac epoxy resin were mixed at the rate of 4:4:2:1 in epoxy equivalent amount. For two types mixture, a bisohenol A epoxy resin and an *o*-cresol novolac epoxy resin were combined at the rate of 3:8 in epoxy equivalent amount. The equivalent ratio of hydroxyl groups in curing agent to epoxide groups was adjusted to 0.85 and 5.1 mmol of accelerator was added for 1 mol of hydroxyl groups in curing agent. These compositions of epoxy thermosetting resin system are same as that of samples used in chapter 4.

The sample compositions are shown in Table 1. Twelve samples were prepared which have each acrylic copolymer and 2 or 4 types of epoxy resin systems. An acrylic copolymer and epoxy thermosetting resin system were mixed in a ratio of 3 pair 7. In addition to this, **silica filler** which has 3μm median diameter (EXCELICA UF-310, Tokuyama Corporation, Tokyo Japan), a drop of **silane coupling agent**, small amount of **thermoplastic polyester elastomer** and others were blended and solved to 2-butanone.

The film sample was made by casting and drying these solvent on a polyethylene terephthalate (PET) film which has release layer. The films has thickness of 40 μm and was called "uncured film". This uncured film sample was cured at 120 °C for 1 h and 175 °C for 2 h for observation and measuring.

In the sample name, the first character "f" means adhesive film, the latter character shows the combination of acrylic copolymer (Mh, MhL, MH, MHiP, MHB, MBz, MHBz, and MG) and the epoxy resin systems (E4; four types mixture, E2; two types mixture). Their sample name are **(a) f_MA/E4**, **(b) f_Mh/E4**, **(c) f_MhL/E4**, **(d) f_MH/E4**, **(e) f_MHiP/E4**, **(f) f_MHB/E4**, **(g) f_MBz/E4**, **(h) f_MHBz/E4**, and **(i) f_MG/E4**). In addition, the sample **(j) f_MH/E2** has MH as an acrylic copolymer and

two types epoxide resin mixture and has a 1.40 $\times 10^{-3}$ mol/ g of density of glycidyl group. It is a little smaller than that of (d) f_MH/E4 (1.47 $\times 10^{-3}$ mol/ g). And the sample **(k) f_MH/E4-TPE** has MH and 4 types of epoxy resin mixture without thermoplastic polyester elastomer. The sample **(l) f_MH/E4_C** has the same composition with (d) f_MH/E4 but cured on the different condition of 175 °C for 3 h.

The densities of functional group in acrylic polymer are also listed in Table 1.

5-2-2 Measurement and analysis

The morphology of the cured sample surface was examined by SPM images with two types of measuring area. 20 × 20 μm^2 and 125 $\times$125 μm^2 images were obtained using a SPA-300HV SPM equipment (Hitachi High-Tech Science Corporation, Tokyo Japan) and a SPM-9700 equipment (SHIMAZU, Kyoto Japan) in tapping mode, respectively. SI-DF40 cantilever was used for each measurement at a resonance frequency of c.a. 320 kHz.

In order to quantify the magnitude of phase structure, the SPM image was processed by the two dimensional fast-Fourier transform (2D-FFT) using Image-J software (NIH open source), and then the correlation length was derived from 1D intensity profile of 2D-FFT image [11, 12].

The distribution states of the compositions were observed by Raman mapping measurement with Microscopic laser Raman Nicolet Almega XR (Thermo Fisher Scientific K.K., Kanagawa Japan) using the 750 nm wavelength laser. The Raman

spectrum of (d) f_MH/E4 was measured in 20 ×20 μm^2 area at intervals of 2 μm. The area fractions of two peaks around 1610 cm^{-1} and 1730 cm^{-1} to the total scattered spectrum area were calculated at 121 points. These peaks are assigned to C=C stretching vibration in benzene ring and stretching vibration of carbonyl group, respectively. The mapping image of the area fraction value for former peak shows the distribution state of the epoxy thermosetting resin and that for latter peak shows the distribution state of the acrylic copolymer.

In order to evaluate the interaction between the acrylic and epoxy thermosetting components, the relaxation behavior was observed by DMA measurement on the heating condition, and the relaxation behavior of magnetization of proton was observed by ^{1}H pulsed NMR measurement on isothermal condition.

The tanδ peak temperature was derived by DMA measurement with DMA Q800 (TA Instruments, New Castle U.S.) at the heating rate of 3 °C /min in the temperature range of 0 °C –300 °C on the tension mode. The deformation amplitude was held at 10 μm and 10 Hz was selected as the frequency. The specimens were formed in the size of ca. 20 mm ×5.0 mm ×0.18 mm.

To derive the spin-spin relaxation time (T_2) and their fraction of proton component in cured adhesive samples, the relaxation process of magnetization was observed by ^{1}H pulse NMR equipment Minispec mq20 (Bruker BioSpin K.K., Kanagawa, Japan, ^{1}H at 20 MHz). The solid echo pulse sequence [90°$_x$ -τ- 90°$_y$] [13] was adopted for the fast decaying magnetization, and the spin echo pulse sequence Carr-Purcell-Meiboom-Gill (CPMG) method [90°$_x$ -τ- (180°$_y$ -2τ-)$_n$] [14] was adopted for the slowly one. The former

has the advantage of avoiding the dead time effect after the pulse and the latter can eliminate the effect of the inhomogeneity of magnetic field.

The equation (1) was fitted to the free induction decay (FID) signal measured by solid echo method. This equation is the linear sum of single Gaussian function and two exponential function. [15, 16 and 17]. The Gaussian component represents the relaxation process of low mobility proton elements in rigid structure, and exponential components represent the relaxation process of high mobility proton elements in flexible structure.

$$M(t)=M_1 \exp\{-1/2[t/T_2(1)]^2\}+ M_2 \exp[-t/T_2(2)]+ M_{3'} \exp[-t/T_2(3')] \qquad (1)$$

where the M_i is the magnetization intensity at t =0 for the i th component which has relaxation time $T_2(i)$. Dashed character in exponential component means "provisional value" for proton element which has longer relaxation time, because it is divided into three proton elements with CPMG method in detail.

Similarly, the FID signal measured by CPMG method was decomposed into the three exponential components. That is,

$$M(t)=M_3 \exp[-t/T_2(3)]+ M_4 \exp[-t/T_2(4)]+ M_5 \exp[-t/T_2(5)] \qquad (2)$$

The fraction of each component ($\boldsymbol{F}_i$) was calculated by equation below

$$\begin{cases} F_{\mathrm{i}} = \dfrac{M_{\mathrm{i}}}{\sum_{\mathrm{j}=1}^{3'} M_{\mathrm{j}}} & \text{(for i=1, 2)} \\ F_{\mathrm{i}} = \dfrac{M_{3'}}{\sum_{\mathrm{j}=1}^{3'} M_{\mathrm{j}}} \cdot \dfrac{M_{\mathrm{i}}}{\sum_{\mathrm{k}=3}^{5} M_{\mathrm{k}}} & \text{(for i=3, 4, 5)} \end{cases} \quad (3)$$

Measurements were carried out at 95 °C that is intermediated temperature of the glass transition temperature of the simple epoxy thermosetting resin system after curing (ca.150 °C) and that of the simple acrylic copolymer element (ca. 35 °C) used in this study.

As the mechanical properties, fracture toughness in mode I (K_{1C}) and shear strength were measured at 250 °C. The fracture toughness measurements was performed using Universal testing machine 5581 series (Instron, Massachusetts, U.S.) equipped with thermostatic chamber. The specimen has a 150 mm ×15 mm ×0.2 mm dimension and also has a 5 mm clack from the edge on the side at the center of longitudinal direction. The distance between the fulcrums was 100 mm and pulling rate was 30 mm/min.

The fracture surface after toughness test was observed by SEM VE-9800 (KEYENCE, Osaka Japan) and its roughness degree (R_a) in 2 ×2 μm^2 area was measured by SPM equipment SPA-300HV (Hitachi High-Tech Science Corporation, Tokyo Japan) at a cut off value 80μm to investigate a rupture mechanism in detail.

The die shear strength were measured at 250 °C by Bond tester dage400 (Nordson Advanced Technology Japan K.K., Tokyo Japan) at the shear rate of 30 mm/min. Test piece was made as a model of semiconductor devises shown in Figure 2. Two kinds

silicon die were prepared as the adherends. Each of them has polyimide coating and flat finishing (R_a < 5 nm) adhesive surface, respectively. Uncured film was sandwiched with them and cured at the same condition as cured film samples. The strength at break of bonding state against shear force was measured [18].

The fracture surface after die shear strength test was observed by SEM and the value of R_a on fracture surface were measured by 3D laser scanning microscope VK-9700 (KEYENCE, Osaka Japan) in the 96 ×72 μm^2 area at a cut off value 2.5 mm.

5-3 Results and Discussion

5-3-1 Morphological observation and analysis

The morphological structures of cured adhesive sample was observed by SPM as shown in Figure 3. Upper images in Figure 3 are the phase image of 125 ×125 μm^2 area, and the lower ones are zoomed images of them. The phase separation at the micrometer scale can be seen in all samples, but their morphology are different from each other. (d) f_MH/E4, (k) f_MH/E4-TPE and (h) f_MHBz/E4 using acrylic copolymer MH and MHBz display a co-continuous structure. Others exhibit a sea-island phase separation. Among them, the boundaries of (b) f_Mh/E4, (c) _MhL/E4, (f) f_MHB/E4, and (i) f_MG/E4 are ambiguous. So their morphological structure can be divided into three categories; “co-continuous phase-separated structure”, “sea-island phase-separated structure with ambiguous border”, and “sea-island phase-separated structure with clear border”. It is remarkable that (l) f_ MH/E4_C which has the same composition with (d) f_ MH/E4 of co-continuous structure exhibits the sea-island phase-separated structure with clear border.

The Raman mapping images of (d) f_MH/E4 in the range of 20 ×20 μm^2 are shown in Figure 4. The left image shows the epoxy element distribution state derived from the area fraction of benzene ring peak in the Raman spectrum and the right one shows the acrylic polymer distribution state derived from that of carbonyl group peak. Both peak were observed in spectra at all examined region, and in the region where the concentration of epoxy thermosetting resin is high, that of acrylic polymer is low. These images display the co-continuous shape similarly to the SPM image. It indicates that phase-separated structure is formed by epoxy rich and acryl rich phase.

The 2D-FFT images of each sample derived with SPM phase images are shown in Figure 5-1 (a) ~ (l). The distance from the image center represents the wavenumber absolute value (q), which is inversely proportional to the periodic length. Each image shows a white concentric annular area around its center indicating the presence of structural periodicity.

These 2D-FFT images were radially averaged to yield 1D intensity profiles (Figure 5 -2) and correlation lengths (l_m). In the each profile, the intensity decays exponentially toward high q value and has two peacks. The diffuse peak appears at high wavenumber region. The another at low wavenumber region has relatively small width. The peak wavenumber (q_{peak}) was dicided from the muximum of the modified intensity profile derived by subtracting the exponential function as the background from 1D profiles as shown in Figure 6. Through this processing, the q_{peak} values of (b)f_Mh/E4, (c)f_MhL/E4, (f) f_MHB/E4, and (g) f_MBz/E4 could be defined although the peacks were not apparent clearly at low wavenumber region in their intensity profiles.

Then, the correlation length (l_m) was calculated by following formula with q_{peak} and listed in Table 2.

$$l_m = 2\pi/q_{peak} \qquad (4)$$

The q_{peak} values at the lower wavenumber region is different from each other. In chapter 4, the l_m value for the sea-island phase-separated structure corresponds to the nearest neighbor distance between the centers of island domains. By this method, even for the co-continuous phase-separated structure which has not defined particle domain, the sizes of structure could be also quantified as the l_m value which is the structural periodicity information.

Comparing the l_m value with the morophology image in Figure 3, for the sample (b) f_Mh/E4 and (j) f_MH/E2, the largest l_m are due to the connected structure of a few spherical islands. For the sample (g) f_MBz/E4 which has the third largest l_m, the island domains are small but the nearest neighbor distance between the centers of them are long.

For the sample (e) f_MHiP/E4, (f) f_MHB/E4, and (i) f_MG/E4 which has smaller l_m, the island shapes are almost spherical and unconnected but the domain sizes and the nearest neighbor distance between the centers of them are different each other. The sample (l) f_MH/E4_C has small island domain and large connected domain, so distribution of the domain size is wide, although the nearest neighbor distance between the centers of island are small. It was also found that the sample (a) f_MA/E4 has the ring shape band on the peripheral area of islands and its width seems to be represented as smaller correlation length. For the sample (c) f_MhL/E4, island dmains are

interconnected, but the coalescing domain is composed of a few islands and standed alone with small size.

As to the sample has the co-continuous structure, the l_m values exhibite the summation of average thickness of both phases and become longer in the order of (h) f_MHBz/E4, (k) f_MH/E4-TPE, and (d) f_MH/E4.

5-3-2 Network states of epoxy thermosetting resin system

In order to evaluate the interaction between acrylic and epoxy thermosetting elements which mainly compose the phases, the temperature dependence of storage modulus and tanδ were measured by DMA as shown in Figure 7 (the results of (a) f_MA/E4, (d) f_MH/E4, (i) f_MG/E4, and (j) f_MH/E2 are represented) and the storage modulus at 250 °C and tanδ peak temperatures are listed in Table 2. There are two tanδ peaks for each cured sample except for the (i) f_MG/E4. The peak exists around 30 °C attributed to the relaxation process of molecular motion for acrylic polymer. And another exists around 200 °C corresponds to that for epoxy thermosetting resin. Generally, for a highly miscible blend with two materials, the temperature dependence of tanδ has only a single peak between the glass transition temperatures of two components. For (i) f_MG/E4, there is a single tanδ peak at 166 °C and the storage modulus at 250 °C is high. It indicates that a good deal of epoxy thermosetting element is miscible with acrylic polymer element and forms the covalent bond network with the glycidyl group in MG during the thermal curing.

For (d) f_MH/E4, (h) f_MHBz/E4, and (k) f_MH/E4-TPE which have co-continuous phase-separated structure, the tanδ peak temperature around 30 °C is higher than those

of others and storage moduli are high, indicating that the acrylic polymer elements are partially miscible with epoxy thermosetting element and its mobility is influenced by rigid epoxy elements.

For others which form sea-island phase-separated structure the tanδ peak temperatures around 30 °C are a little lower than that of simple acrylic polymer such as MA of 30 °C, Mh of 35 °C, MhL of 34 °C, and MH of 32 °C. Considering their lower storage moduli at high temperature, it will be caused by low molecular weight component, which must be the unreacted epoxy thermosetting resins. From these fact, the rigid covalent bond network formed by epoxy thermosetting resins seems to be not formed enough to affect the mobility of acrylic component.

Concerning the tanδ peak at higher temperature around 200 °C, no significant difference is found except for the (i) f_ MG/E4.

In order to investigate the network formation states of epoxy thermosetting resins, the FID curves were obtained by ^{1}H pulse NMR measurement for the (a) f_MA/E4 and (j) f_MH/E2 which have a "sea-island phase-separated structure with clear border", (b) f_Mh/E4 and (i) f_MG/E4 which have a "sea-island phase-separated structure with ambiguous border", and (d) f_MH/E4 and (h) f_MHBz/E4 which have a "co-continuous phase-separated structure".

They were well represented with formula (1) and (2), i.e., R^2 factors were above 0.98 in every fitting result. T_2(i) and F_i values are listed in Table 3.

The proton element with the shortest T_2 (T_2(1)) is attributed to that of epoxy thermosetting resin component. Because the shortest T_2 values of 0.015 ms and 0.014 ms for simple epoxy thermosetting resin systems are almost same as that of each

composite samples.

The F_1 value of (i) f_MG/E4 is largest. Considering the results of DMA, glycidyl groups in acrylic polymer MG react with phenol novolac curing agent and appear to form the covalent bond network. As a results, the fraction of the proton component which has lowest molecular mobility become large.

Except for (i) f_MG/E4, the F_1 values of the adhesives which has co-continuous structure are larger than that of others. The existence of two separated peaks of the tanδ at DMA measurement indicates that the epoxy resin does not react with acrylic element. But the large F_1 value at ^{1}H pulse NMR measurement indicates that the epoxy thermosetting resin react within them considerably.

This tendency are observed for the samples have sea-island phase-separated structure with ambiguous border. They have a little lager F_1 value and slightly larger storage moduli than the clear border samples.

5-3-3 Mechanical strength property on mode I

The cross section after fracture toughness test for (a) f_MA/E4, (d) f_MH/E4, (i) f_MG/E4, and (j) f_MH/E2 were observed by SEM as shown in Figure 8. The insets in Figure 8 are the SPM image of the cured sample surface shown in Figure 3 at the same magnification with the cross section images. Although these cured samples have little difference in composition with a part of acrylic element, their planar morphology of the fracture surface are quite different. Comparing these SEM and SPM images, the shapes of fracture surface are similar to the surface morphologies.

To discuss about asperities of them quantitatively, the roughness (R_a) of fracture surface were measured by SPM and its dependence on the structural correlation length was derived as shown in Figure 9. The R_a values depend on the correlation length; the samples which have long correlation length (l_m) tend to provide the large R_a value. It implies that the destruction propagates along the boundary of each phases. Thus, the sample has larger l_m makes the rougher fracture surface. The samples which have the co-continuous phase-separated structure shows the large R_a relatively, but the deference from others is small. In other words, the R_a values of fracture surface are not influenced by the phase separated aspects.

In addition, the R_a value is a little dispersed. Because the value of l_m is summation of the size of island and the thickness of sea phase, and the destruction proceed along the domains boundaries area. Thus, when the samples have the same l_m but the different island size, the fracture surface are formed in a different way.

The relation between the fracture toughness on mode I (K_{1C}) and the structural correlation length is also shown in Figure 9. The value of K_{1C} seems to not depend on the value of l_m but the adhesive samples which have co-continuous phase-separated structure may provide the rather high value.

To verify the significance of l_m and morphology aspect as a factor contributing to K_{1C}, these results were analyzed with *F*-test. The *F*-test is used to assess whether the expected values of factors are significant or not by comparing the *F* value to F^i_j(x %). *F* value is calculated from the variances of pre-defined group and population. The F^i_j(x %) is the level of significance, which means “the possibility of conclusion to be significantly different is wrong in x %” at the degree of freedom for the factor variation (i) and the residual degrees of freedom (j). The i value is calculated by subtracting 1 from the

number of factor variation and the j value is calculated by subtracting the i and the degree of freedom for the population from the total number of data. Generally the degree of freedom for the population is equal to 1. When the F value is larger than F^{i}_{j}(x %), the expected values of a factor are significant above (100-x) % for the population.

The F value of the K_{1C} for (d) f_MH/E4, (h) f_ MHBz/E4 and (k) f_MH/E4-TPE, which display the co-continuous structure, and the F value of the K_{1C} for (b) f_Mh/E4, (c) f_ MhL/E4, (f) f_MHB/E4 and (i) f_MG/E4, which display sea-island structure with ambiguous border, are 2.8 and 0.5, respectively. They are below the F^{2}_{23}(5 %) of 3.4 and F^{3}_{22}(5 %) of 3.1.

Therefore these samples, which have the different l_m value each other, exhibit little influence on the K_{1C} value with the level of significance above 5 %. However the influence of morphological aspects on K_{1C}, where the number of factor is 3 for phase separation structure category, is meaningful in level of significance less than 1 % because the F value of K_{1C} for morphological aspects of 18.7 greatly exceeds the F^{2}_{70}(1 %) of 4.9.

From these results, the destruction propagates dominantly along the phase boundary area, but the increase of the fracture surface area, which is influenced a great deal by the structure size of l_m, does not affect K_{1C}. The samples with co-continuous phase structure, in which the covalent bond formed by epoxy element affects the acrylic polymer mobility, have a tendency to provide the higher strength. It appears that the interaction between acrylic polymer and epoxy thermosetting resin has an influence on K_{1C} at the fracture toughness test on mode I.

5-3-4 Mechanical strength property on mode II

At the shear strength test, the adhesive state was broken on the cohesive failure mode for all samples. The fracture surface after the shear strength test of (a) f_MA/E4 and (d) f_MH/E4 were observed by optical microscope and SEM as shown in Figure 10.

The left figures show the all area of the adhesive surface observed by optical microscope and the center figures are loading side for external force and the right figures are opposite side of them observed by SEM.

For (a) f_MA/E4 the fracture surface at the loading side is very smooth, but it is rough at the opposite side. On the other hand, for (d) f_MH/E4 the fracture surface is rough on both sides similarly.

Tadepalli et al. investigated the toughness of Cu–Cu thermo compression bonds using a bonded chevron specimen, whose sharp chevron tip of adhesive interface serves as a stress-concentration point, and it is effective means for characterizing the interface toughness in mode II [19, 20 and 21]. They reported that when the shear stress was applied to this specimen, a crack initiates at the chevron notch after the elastic loading and it propagates along the bonded interface and initially results in stable crack propagation. At some crack length, the propagation becomes unstable and catastrophic failure occurs which coincides with the point of maximum loading.

In our method, the specimen does not have the stress concentration point like the notch but cohesive destruction was caused completely and the load-displacement curve was similar to the results of chevron test as shown in Figure 11. Thus, this destruction process can be regarded as fracture propagation in mode II. The smooth fracture surface at the loading side of specimen with (a) f_MA/E4 seems to represent the area in which the

crack grow stably. In the load-displacement curve of Figure 11, this area is exhibited with the region between (a) and (b). And the rough surface at the opposite side appears to indicate the catastrophic failure area after maximum loading, which is exhibited with the region between (b) and (c) in Figure 11. Therefore, the shape of fracture surface at loading side greatly influences the maximum shear force.

The roughness (R_a) of fracture surface at loading side after the shear strength test was measured by 3D laser scanning microscope and the dependence on the structural correlation length was acquired as shown in Figure 12. The roughness of fracture surface after the shear test are higher than that after the fracture test on mode I. Especially, for (d) f_MH/E4 and (k) f_MH/E4-TPE, which have co-continuous structure and large correlation length provide rougher destruction surface. The destruction seems to progress along the phase boundary that exist in succession bulk.

For the samples have sea-island phase-separated structure, the destruction also seems to progress along the boundary area but partly proceeds the sea phase because of their discontinuous phase structure. And among them, the R_a for samples has sea-island structure with ambiguous border are slightly smaller. It indicates that the destruction propagates through the both phases because of border ambiguousness. It is also remarkable that the R_a value strongly depends on the morphology aspects. And the R_a value has tendency to become larger with the correlation length in each phase-separated aspect category.

The dependence of the shear strength on the structural correlation length is also shown in Figure 12. For the samples which have co-continuous structure, the shear strength becomes higher depending on l_m value, and also the roughness of fracture surface are larger with shear strength. At this time, the effect of an increase in the fracture surface

area appears to develop effectively.

On the other hands, among the samples have sea-island phase-separated structure, the sample has ambiguous border exhibits the higher strength than the sample has clear border. However, their roughness of fracture surface is smaller, thus the less increasing effect of fracture surface area can expect to develop.

From the large F_1 value at ^{1}H pulse NMR measurement, the network state in island domain formed by epoxy thermosetting resins is rigid enough to affects the mobility of acrylic element. Therefore the structural difference of two phases composed of each elements seems to be ambiguous at the boundary area on its morphology, and the interaction between them appears to be rather large. Thus, much external force will be needed when the propagation proceed this area.

5-4. Conclusion

Considering the fracture mechanism and parameters contributing to mechanical strength, we evaluated the phase structure and mechanical properties with adhesive film mainly composed of acrylic copolymer and epoxy thermosetting resin. The phase structure of cured adhesive samples was examined by 2D-FFT analysis of SPM images, providing the correlation length as quantitatively structural information about the periodicity.

Morphologies and correlation length altered with the composition and curing condition. The morphology aspects could be divided into three categories. One is a “co-continuous phase-separated structure” and next one is “sea-island phase-separated structure with ambiguous border” and another one is “sea-island phase-separated structure with clear

border".

The fracture toughness (K_{1C}) and the shear strength were measured as the mechanical properties. Referring to the fracture surface of both strength test, the shape of fracture surface after K_{1C} measuring was similar to the morphologies and its roughness depended on the correlation length. Therefore, the fracture appeared to propagate along the phase separated boundary. However, its surface roughness has a little dependence on the morphology aspects, which are categorized in three groups. On the other hand, the roughness after shear strength test depend on their morphology aspects a great deal. Especially the sample which has co-continuous structure shows rougher destruction surface. The destruction seems to progress along the phase interface that exist throughout bulk in succession. In addition to this the roughness of fracture surface tends to become larger with increasing the correlation length in each structure category.

Referring the strength of both test, the value of K_{1C} does not depend on the morphology aspects and the value of l_m. It appears that the interaction between acrylic polymer and epoxy thermosetting resin influences on K_{1C} value. In fact, the samples, in which the covalent bond is formed enough to affect the acrylic polymer mobility, have a tendency to provide a higher strength. Contrary to this, the morphology aspect is greatly dominant on the shear strength. The sample displaying the co-continuous structure provides a larger strength depending on the l_m value. An increasing effect of fracture surface area appears to develop at destruction proceeding process of these samples.

Summarizing the above, the l_m has a dominant influence on the roughness of fracture surface at the both strength tests, but the dependence of the strength on l_m alters with the destruction mode. The K_{1C} is not affected by morphology aspects and the l_m value.

However, the increasing effect of fracture surface area on the strength develops effectively on the share strength test, in which the external force added to the parallel to destruction proceeding direction.

References

1) H. Kishi, Y. Kunimitsu, J. Imade, S. Oshita, Y. Morishita and M. Asada, *Polymer*, **52**, 760 (2011).

2) M. Ochi and S. Shimaoka, *Polymer*, **40**, 1305 (1999).

3) JEDEC Standard 22, Method A113F, "PRECONDITIONING OF PLASTIC SURFACE MOUNT DEVICES PRIOR TO RELIABILITY TESTING.

4) I. Ichikawa, K. Enomoto and K. Uchida, *J. Adhesion Soc. Japan*, **40**, 51 (2004).

5) Y. Ebe, H. Senoo, T. Sugino and O. Yamazaki, *J. Adhesion Soc. Japan*, **40**, 379 (2004).

6) Y. Ebe, H. Senoo, T. Sugino and O. Yamazaki, *J. Adhesion Soc. Japan*, **41**, 289 (2005).

7) K.Yamanaka and T. Inoue, *Polymer*, **30**, 662 (1989).

8) K.Yamanaka, Y. Takagi and T. Inoue, *Polymer*, **30**, 1839 (1989).

9) S. Inada, K. Hatakeyama and T. Matsuzaki, *J. Network Polym. Japan*, **25**, 13 (2004).

10) S. Inada, T. Iwakura, K. Hatakeyama and T. Matsuzaki, *J. Network Polym. Japan*, **26**, 18 (2005).

11) K. Shimizu, H. Wang, G. Matsuba, Z. Wang, H. Kim, W. Peng and C. C. Han, *Polymer*, **48**, 4226 (2007).

12) W. S. Rasband, ImageJ, N.I.H., Bethesda, Maryland, USA, (http://imagej.nih.gov/ij/), 1997-2012.

13) J. G. Powles, J. H. Strange, *Proc. Phys. Soc.*, **82**, 6 (1983).

14) S. Meiboom and D. Gill, *Rev. Sci. Instrum*.. **29**, 688 (1958).

15) H. Tanaka and T. Nishi, *J. Chem. Phys.*, **82**, 4326 (1985).

16) H. Tanaka and T. Nishi, *J. Chem. Phys.*, **85**, 6197 (1986).

17) Y. Nakamura, Y. Nishida, H. Honda, S. Fujii and M. Sasaki, *J. Adhesion Sci. Technol.*, **25**, 2703 (2011).

18) MIL-STD (Military Standard) -883G, METHOD 2019.7

19) R. Tadepalli, K. T. Turner and C. V. Thompson, *Acta Materialia*, **56**, 438 (2008).

20) R. Tadepalli, K. T. Turner and C. V. Thompson, *Journal of the Mechanics and Physics of Solids*, **56**, 707 (2008).

21) R. Tadepalli and K. T. Turner, *Engineering Fracture Mechanics*, **75**, 1310 (2008).

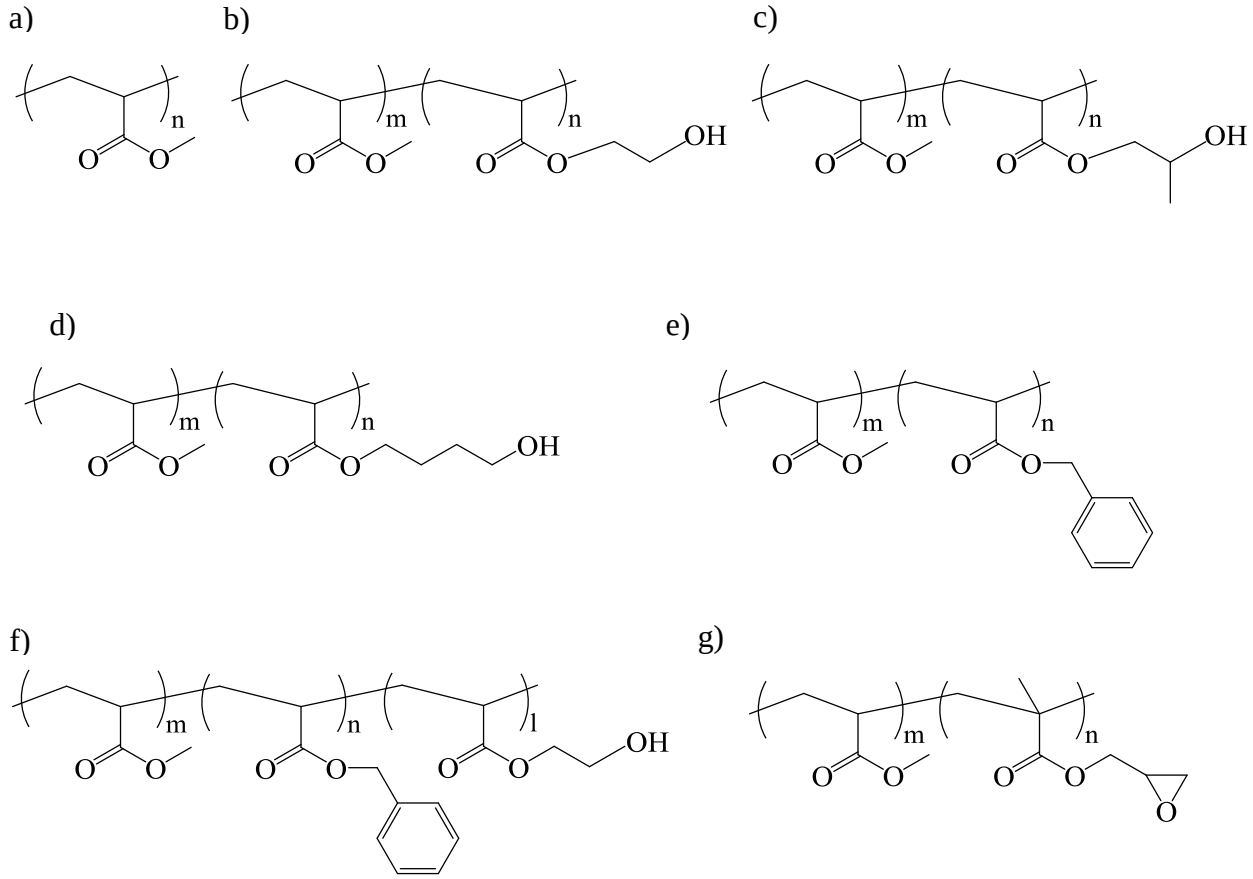

Figure 1-1. Acrylic polymer component for each sample.
a) methyl acrylate homo polymer (M_w= 280,000) (**MA**)
b) poly[(methyl acrylate) -*co*-(2-hydroxyethyle acrylate)] (m:n = 95: 5 mol% (M_w= 510,000)) (**Mh**)
(m:n = 95: 5 mol% (M_w= 680,000)) (**MhL**)
(m:n = 85:15 mol% (M_w= 370,000)) (**MH**)
c) poly[(methyl acrylate) -*co*-(2-hydroxypropyl acrylate)] (m:n = 85:15 mol% (M_w=140,000)) (**MHiP**)
d) poly[(methyl acrylate) -*co*-(4-hydroxybutyl acrylate)] (m:n = 85:15 mol% (M_w= 190,000)) (**MHB**)
e) poly[(methyl acrylate) -*co*-(benzyl acrylate)] (m:n = 85:15 mol% (M_w= 330,000)) (**MBz**)
f) poly[(methyl acrylate) -*co*- (2-hydroxyethyle acrylate) -*co*- (benzyl acrylate)]
(m:n:l = 70:15:15 mol% (Mw= 59,000, Mw/Mn= 4.9)) (**MHBz**)
g) poly[(methyl acrylate) -*co*-(glycidyl metacrylate)] (m:n = 85:15 mol% (M_w= 270,000)) (**MG**)

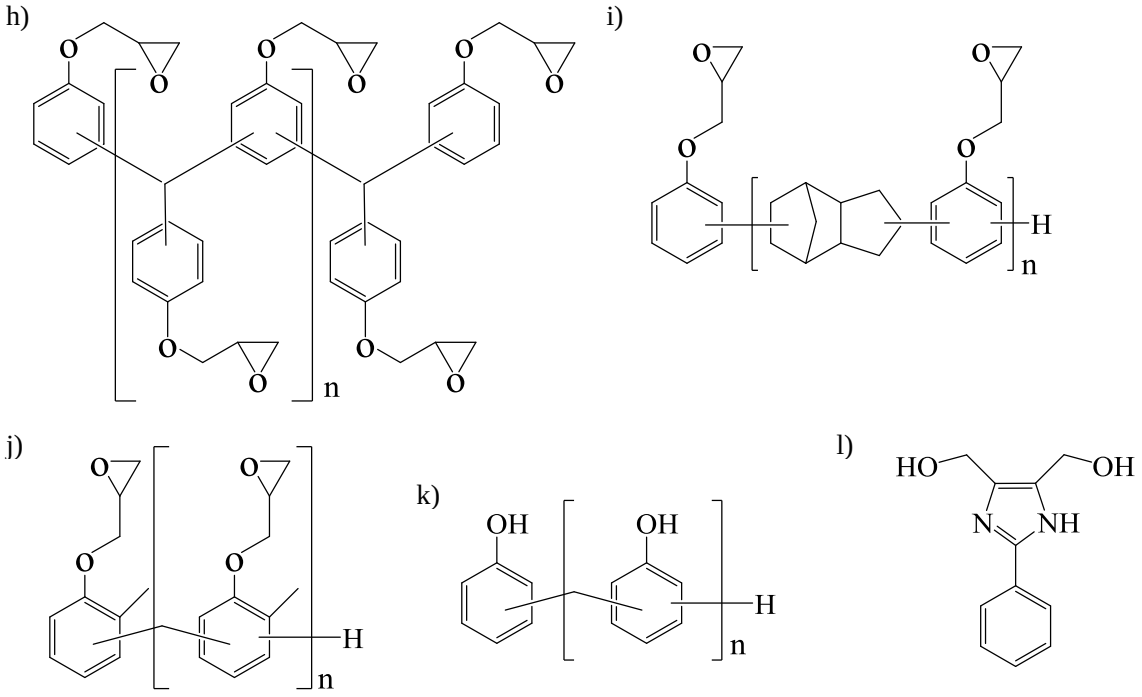

Figure 1-2. Epoxy thermo setting resin component for each sample.
h) multifunctional epoxy resin,
i) dicyclopentadiene epoxy resin,
j) *o*-cresol novolac epoxy resin,
k) phenol novolac curing agent
l) imidazole accelerator (4,5-Bis(hydroxymethyl)-2-phenyl-1H-imidazole)

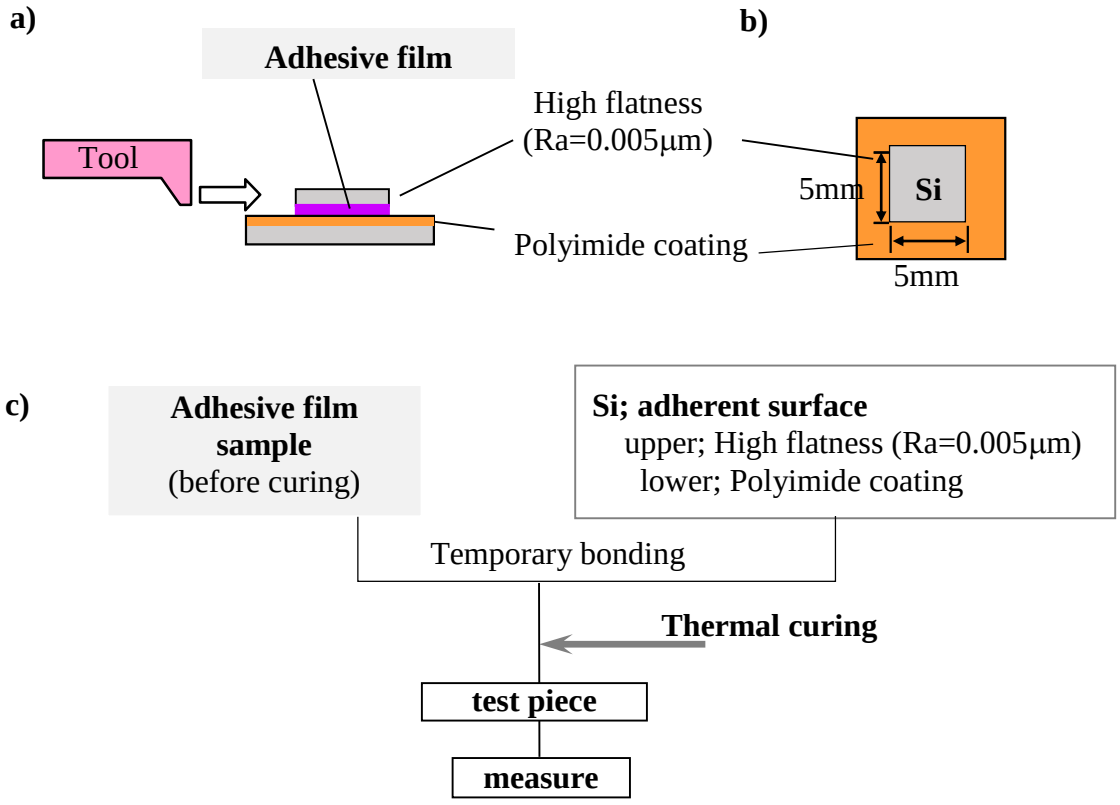

Figure 2. Measuring method of shear strength. a), b) test piece, c) measuring flow.

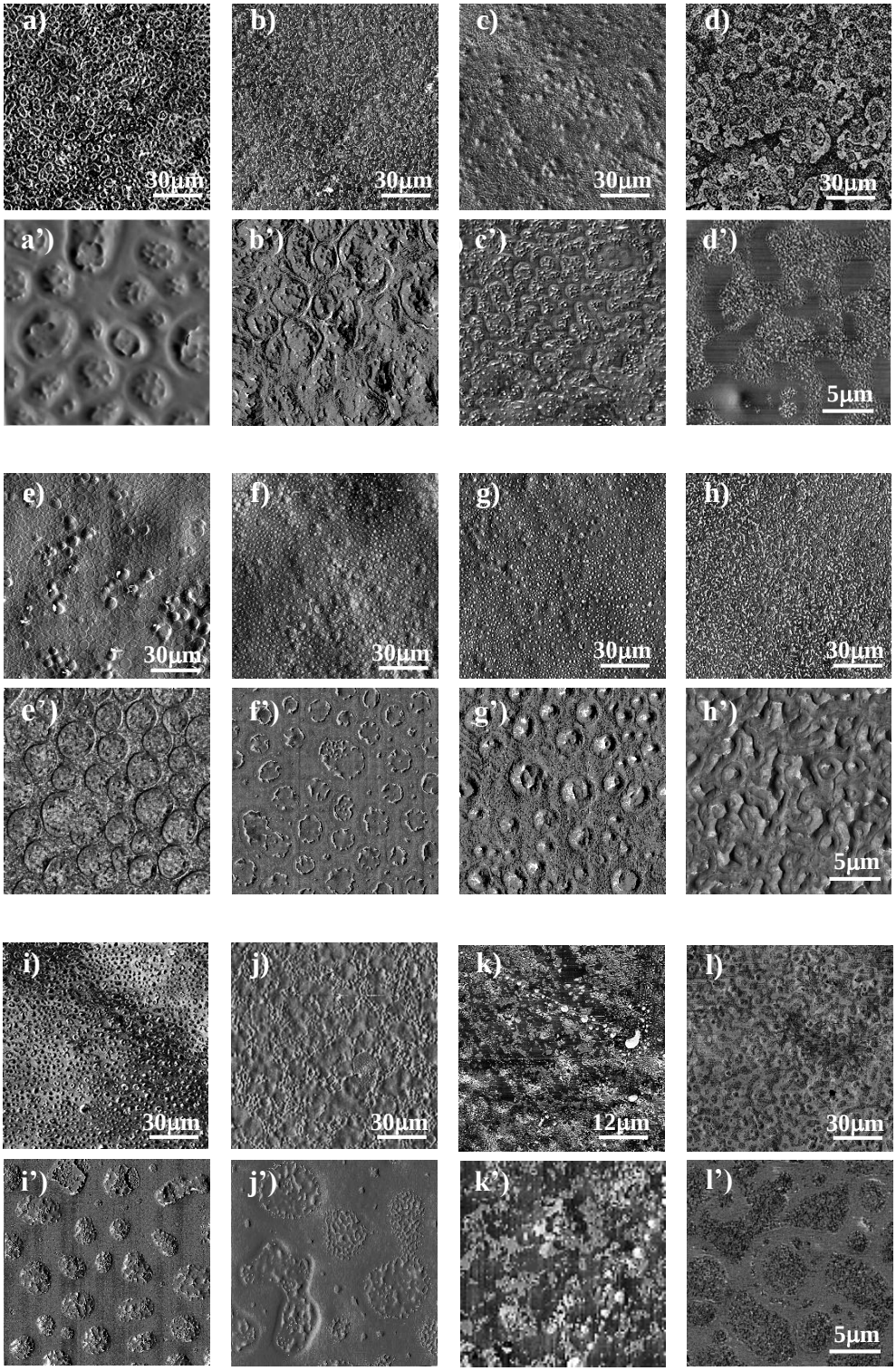

Figure 3. SPM phase image of 125μm square for (a) f_MA/E4, (b) f_Mh/E4, (c) f_MhL/E4, (d) f_MH/E4, (e) f_MHiP/E4, (f) f_MHB/E4, (g) f_MBz/E4, (h) f_MHBz/E4, (i) f_MG/B4, (j) f_MH/E2, (k) f_MH/E4-TPE*, and (l) f_MH/E4_C and the image of 20μm square of each accompanied the letter with apostrophe.

*the magnification of upper image for (k) f_MH/E4-TPE is different from others.

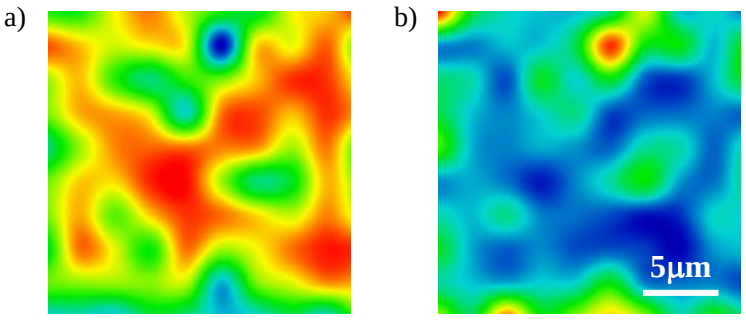

Figure 4. Raman mapping image of (d) f_MH/E4 (20µm square)
a) Distribution of the high intensity region of the benzene ring peak attributed to the epoxy thermosetting system and b) the high intensity region of carbonyl peak of spectrums attributed to the acrylate polymer element.

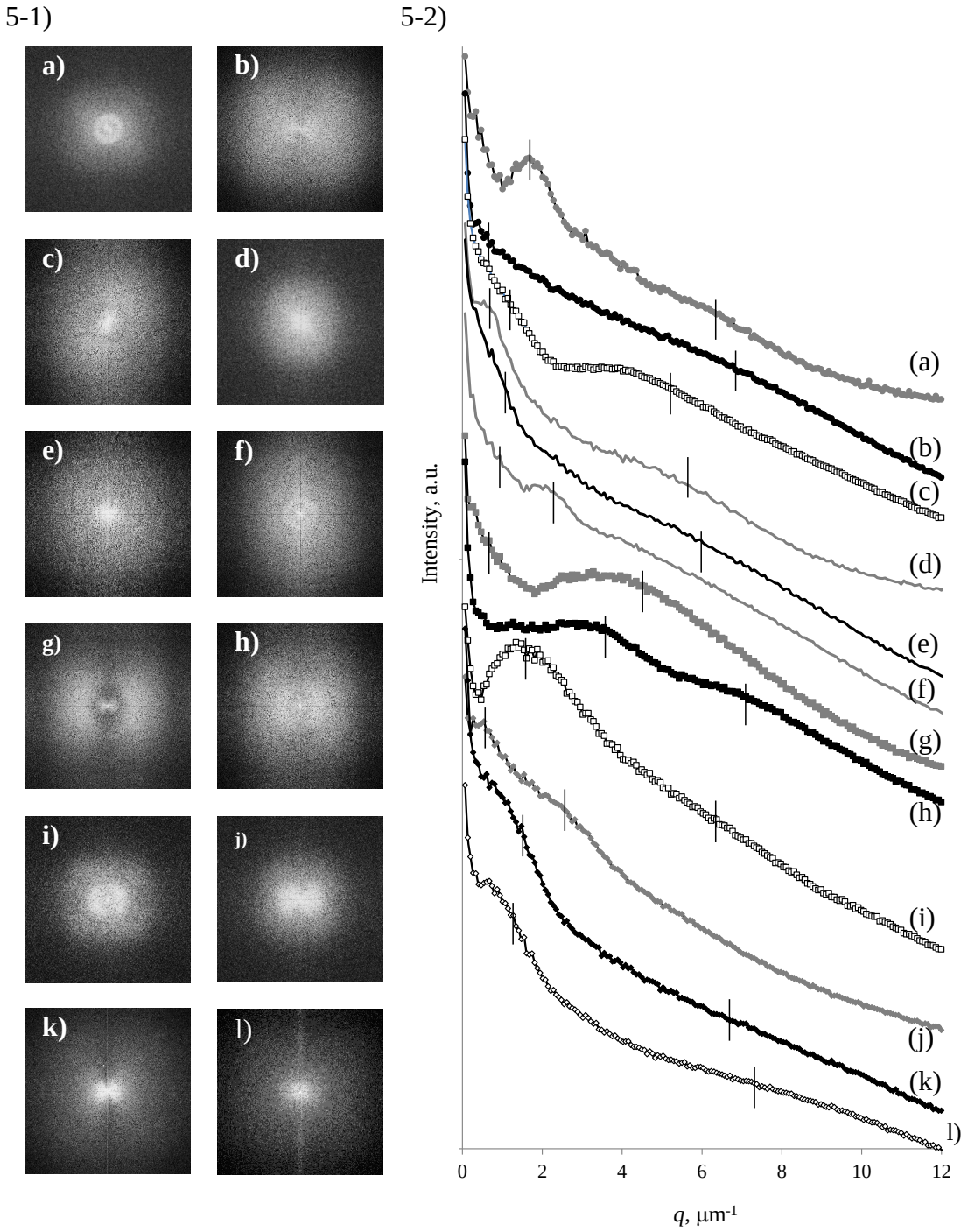

Figure 5. 2D-FFT analysis results with SPM phase images.
5-1) 2D-FFT images of composite samples (a) ~ (l) in the *q* range from -12.9μm^{-1} to12.9 μm^{-1} on horizontal and vertical axis.
5-2) The 1D intensity profile derived from 2D-FFT image.
(a) f_MA/E4, (b) f_Mh/E4, (c) f_MhL/E4, (d) f_MH/E4, (e) f_MHiP/E4, (f) f_MHB/E4, (g) f_MBz/E4, (h) f_MHBz/E4, (i) f_MG/B4, (j) f_MH/E2, (k) f_MH/E4-TPE, and (l) f_MH/E4_C

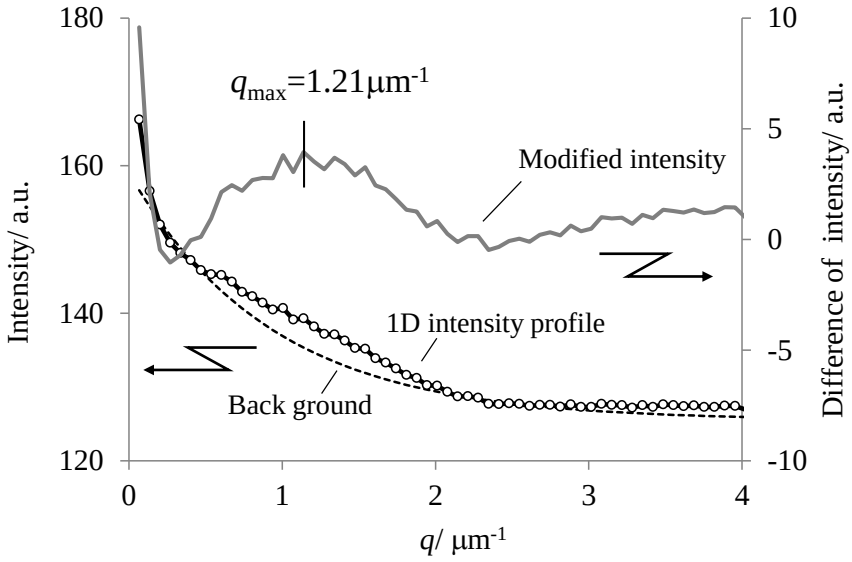

Figure 6. The modified intensity profile derived by subtracting the exponential function as the background from 1D profiles of 2D-FFT image for (c) f_MhL/E4.

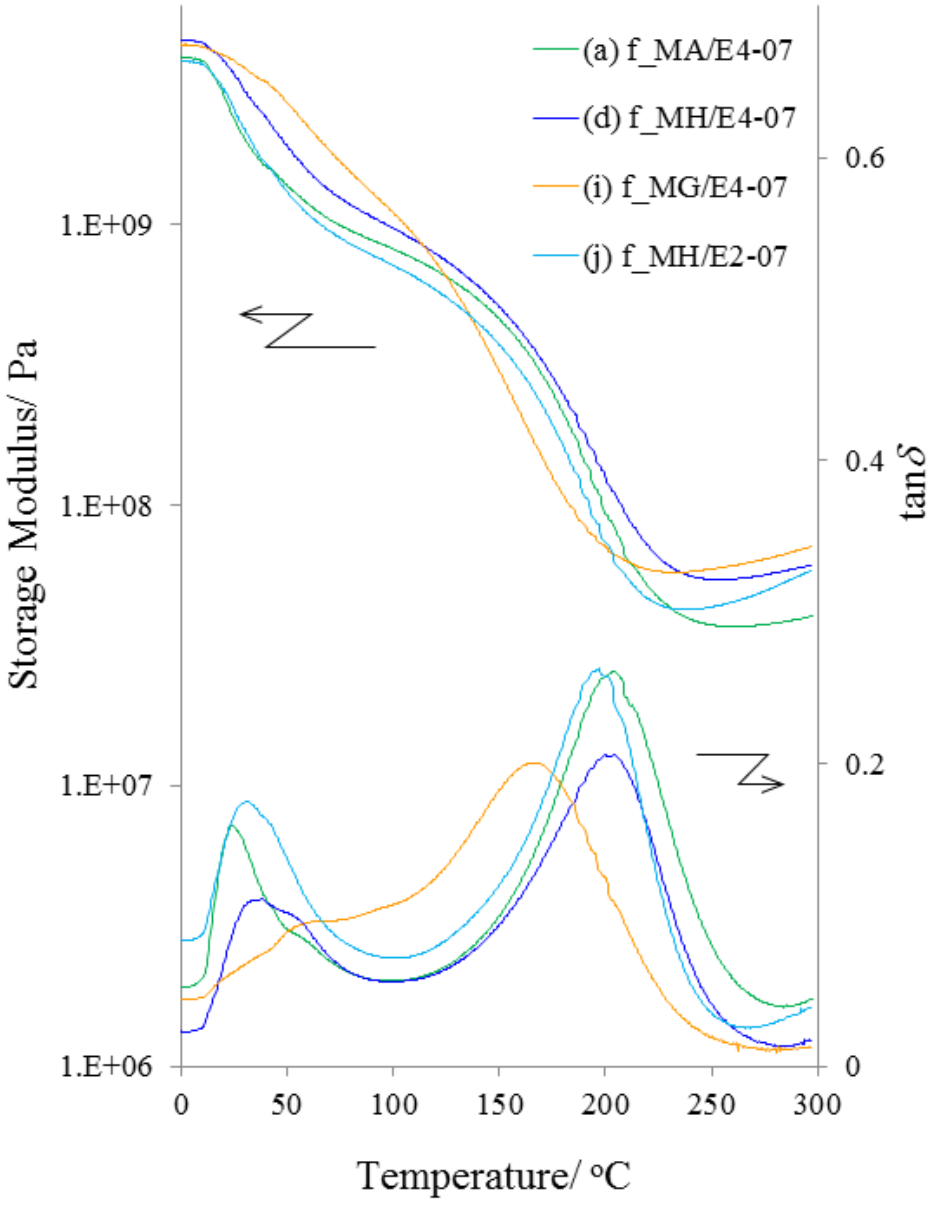

Figure 7. The temperature dependence of storage modulus and tanδ for (a) f_MA/E4, (d) f_MH/E4, (i) f_MG/E4, and (j) f_MH/E2 measured by DMA.

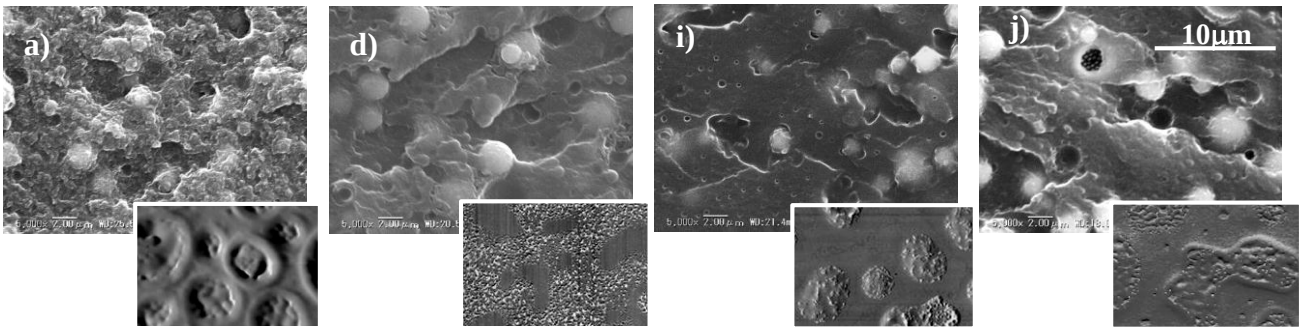

Figure 8. Cross section after fracture toughness test at 250°C observed by SEM.
(a) f_MA/E4, (d) f_MH/E4, (i) f_MG/B4, (j) f_MH/E2
(The insets are SPM image shown in Figure 3 in the same magnification)

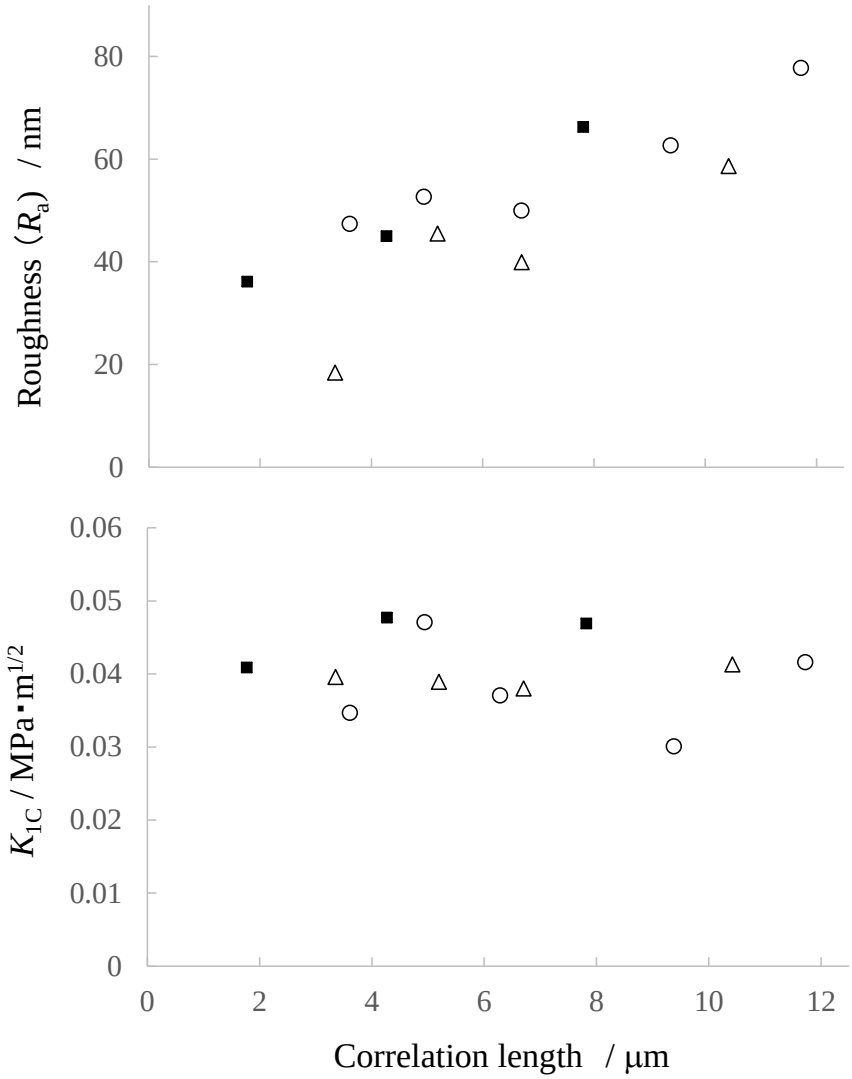

Figure 9. The dependence of the roughness (R_a: upper) and the fracture toughness (K_{1C}: lower) on the structural correlation length.

The open circle symbols (○) show the results of the samples which have the sea-island phase separated structure with clear border, the open triangle symbols (△) show the results of the samples which have the sea-island phase separated structure with ambiguous border, and the closed square symbols (■) show the results of the samples which have the co-continuous phase separated structure.

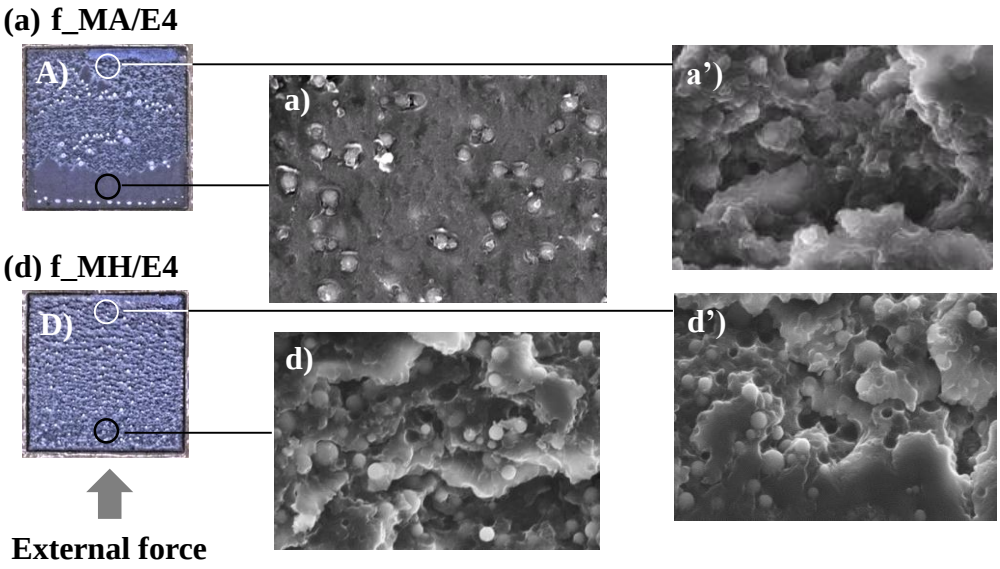

Figure 10. Fracture surface of adhesive sample which adhere to the upper die after shear strength test for the sample (a) f_MA/E4 (upper) and (d) f_MH/E4 (lower). All adhesive area after breaking observed by optical microscope (left figure with capital letter), the loading side of external force (center figure with small letter) and the opposite side of it (right figure with small letter and apostrophe) observed by SEM.

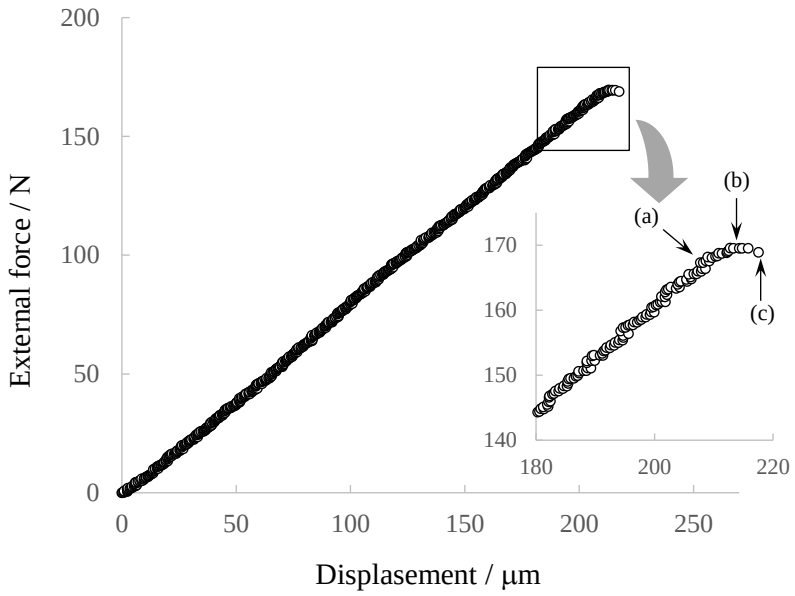

Figure 11. Load – displacement curve of die shear test for the sample of (a) f_MA/E4
Inset show the zoomed figure at the breaking area.
The point marked "(a)" is the crack initiation point, the point marked "(b)" is the maximum loading point, and the point marked "(c)" is the destruction completion point.

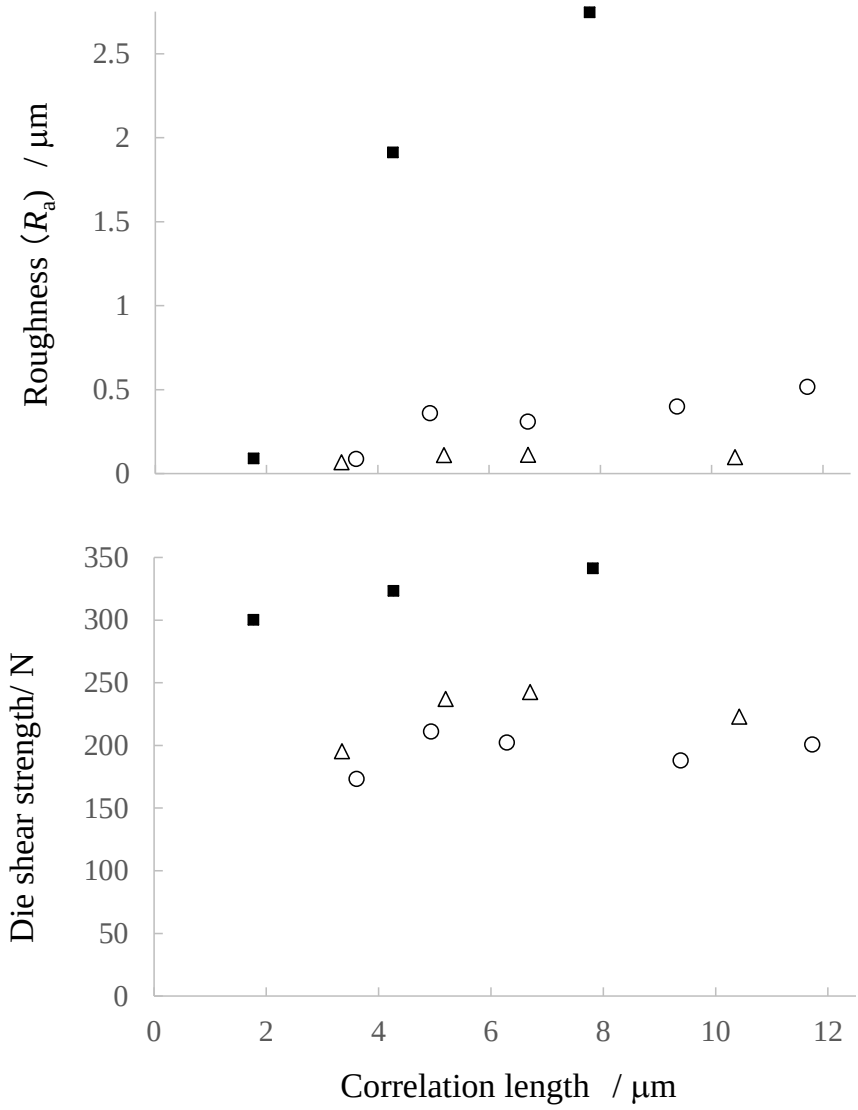

Figure 12. The dependence of the roughness (R_a: upper) of the fracture surface at the force loading side and the die shear strength (lower) on the structural correlation length.

The open circle symbols (○) show the results of the samples which have the sea-island phase separated structure with clear border, the open triangle symbols (△) show the results of the samples which have the sea-island phase separated structure with ambiguous border, and the closed square symbols (■) show the results of the samples which have the co-continuous phase separated structure.

Table 1 Samples Composition

Sample name	**acrylic polymer** [1] **(monomer species / mol fraction and** its **abbreviation)**		**Density of functional group of Ac element (mol/g)**
(a) f_MA/E4 [2]	methyl acrylate /100	**MA**	-
(b) f_Mh/E4	methyl acrylate, 2-hydroxyethyle acrylate / 95:5	**Mh**	OH: 1.1×10^{-4}
(c) f_MhL/E4	methyl acrylate, 2-hydroxyethyle acrylate / 95:5	**MhL** [3]	OH: 1.1×10^{-4}
(d) f_MH/E4	methyl acrylate, 2-hydroxyethyle acrylate / 85:15	**MH**	OH: 3.1×10^{-4}
(e) f_MHiP/E4	methyl acrylate, 2-hydroxypropyl acrylate / 85: 15	**MHiP**	OH: 3.1×10^{-4}
(f) f_MHB/E4	methyl acrylate, 4-hydroxybutyl acrylate / 85:15	**MHB**	OH: 3.0×10^{-4}
(g) f_MBz/E4	methyl acrylate, benzyl acrylate / 85:15	**MBz**	Ph: 2.9×10^{-4}
(h) f_MHBz/E4	methyl acrylate, 2-hydroxyethyle acrylate, benzyl acrylate / 70:15:15	**MHBz**	Ph: 2.8×10^{-4} OH: 2.8×10^{-4}
(i) f_MG/E4	methyl acrylate, glycidyl metacrylate / 85:15	**MG**	Glycidyl: 3.0×10^{-4}
(j) f_MH/E2 [4]	methyl acrylate, 2-hydroxyethyle acrylate / 85:15	**MH**	OH: 3.1×10^{-4}
(k) f_MH/E4 _TPE[5]	methyl acrylate, 2-hydroxyethyle acrylate / 85:15	**MH**	OH: 3.4×10^{-4}
(l) f_MH/E4 _C[6]	methyl acrylate, 2-hydroxyethyle acrylate / 85:15	**MH**	OH: 3.1×10^{-4}

1) The ratio of acrylic polymer and epoxy thermo setting resins are 30:70 in weight.
2) Equivalence ratio of hydroxyl group in curing agents to epoxied group was adjusted to 0.85 and 5.1mmol accelerator was included for 1mol of hydroxyl group of curing agents. The glycidyl group equivalent is 1.40×10^{-3} mol/ g.
3) Polymerized by **living radical technic**.
4) **2 types** of epoxy compounds whose glycidyl group equivalent is 1.40×10^{-3} mol/ g.
5) Not contain the **thermoplastic polyester elastomer**.
6) Cured at **175 ºC for 3 hours**. (Others are cured at 125 ºC for 1 hour and 175 ºC for 2 hours)

Table 2 Morphology aspect and q value at peak intensity ($\boldsymbol{q}_{\mathbf{peak}}$)on the 1D intensity profile derived from 2D-FFT analysis and correlation length ($\boldsymbol{l}_{\boldsymbol{m}}$) at the lower q region and DMA tanδ peak temperature at lower temperature region and higher temperature region which attributed to the glass transition temperature (T_g) of acrylic polymer and cured epoxy therm setting resin, respectively.

	Morphology aspect	2D-FFT analysis		DMA tanδ peak temp. /^{o}C**	Storage modulus /MPa***
		$\boldsymbol{q}_{\mathbf{peak}}$ /μm^{-1}	$\boldsymbol{l}_{\mathbf{m}}$/μm		
(a) f_MA/E4	sea-island	1.9	**3.6**	24 / 204	37.3
(b) f_Mh/E4	sea-island*	0.60	**10.4**	28 / 205	38.9
(c) f_MhL/E4	sea-island*	1.2	**5.2**	32 / 208	40.7
(d) f_MH/E4	co-continuous	0.80	**7.8**	39 / 203	54.2
(e) f_MHiP/E4	sea-island	1.0	**6.3**	27 / 209	36.7
(f) f_MHB/E4	sea-island*	0.94	**6.7**	28 / 207	51.6
(g) f_MBz/E4	sea-island	0.67	**9.4**	27 / 209	34.4
(h) f_MHBz/E4	co-continuous	3.6	**1.8**	36 / 206	55.4
(i) f_MG/E4	sea-island*	1.9	**3.4**	- / 166	59.2
(j) f_MH/E2	sea-island	0.54	**11.7**	30 / 197	32.0
(k) f_MH/E4-TPE	co-continuous	1.5	**4.3**	33 / 209	75.2
(l) f_MH/E4_C	sea-island	1.3	**4.9**	34 / 210	51.3

* sea-island phase separated structure with ambiguous border

** the figure represent the tanδ peak at low temp. /high temp. region

*** storage modulus at 250^{o}C

Table 3 T_2 and the fraction of each proton components measured by ^{1}H pulse NMR

		i=1	2	3	4	5	Remarks (morphology)
(a) f_MA/E4	T_2(i)* /ms	0.015	0.031	0.21	1.4	8.5	sea-island
	F_i */%	**48**	7	24	17	4	
(b) f_Mh/E4	T_2(i) /ms	0.014	0.057	0.16	1.0	7.7	sea-island**
	F_i /%	**51**	11	22	14	3	
(d) f_MH/E4	T_2(i) /ms	0.015	0.047	0.15	0.97	8.3	co-continuous
	F_i /%	**53**	12	23	10	2	
(h) f_MHBz/E4	T_2(i) /ms	0.015	0.072	0.16	1.1	8.1	co-continuous
	F_i /%	**56**	13	20	9	2	
(i) f_MG/E4	T_2(i) /ms	0.015	0.063	0.14	0.95	9.6	sea-island**
	F_i /%	**66**	13	15	4	2	
(j) f_MH/E2	T_2(i)* /ms	0.013	0.058	0.15	1.0	7.1	sea-island
	F_i */%	**49**	11	23	14	3	

* T_2 /ms, (F /%) of simple epoxy element (4 types): **0.015 (93.2)**, 0.031 (4.4), 0.093 (2.4)
(2 types): **0.014 (87.9)**, 0.036 (9.1), 0.10 (3.0)

** sea-island phase separated structure with ambiguous border

Chapter 6

Conclusion.

Biphenyl type epoxide resins, lately applied to the molding compound for IC package and the printed wiring board material and provide the high adhesive reliability, do not have the carbon bridge between aromatic rings. It is known that the internal stress generated on the adhesive interface between cured epoxy thermosetting resins and metal adherend can be decreased by introducing biphenyl structure into the epoxy matrix network, because these molecules are easily arranged and interact intermolecularly. **In Chapter 2,** in order to investigate the effects of mesogenic moieties like the biphenyl type on the mechanical property, the mean intermolecular distance of cured epoxy thermosetting resins using these biphenyl compound were derived and their mechanical properties were evaluated. Introducing the biphenyl moieties effected on the structure of epoxy resin network resulting the decrease of mean intermolecular distance, and caused the low elastic modulus and low thermal expansion coincidentally. Both are required for adhesive materials to the metal adherend used at high temperature, because an internal stress generated on the adhesive interface is decreased.

These results were applied to the epoxy molding compound for the semiconductor package. Ultimately, the package exhibiting the high reliability was provided with the molding compound had biphenyl moieties in the epoxy matrix network.

In addition, phase structural aspects was influenced by using these biphenyl compound. **In Chapter 3** in order to evaluate the effects of the phase structure on the adhesion property, the epoxy thermosetting resins using [1,1’-Biphenyl]-4,4’-diol (BP) as a curing agent were prepared. The resin system formed poly-domain structure and its aspect was affected by mixing and kneading process. In addition to this, the mechanical properties altered with the domain structure. From the appearance of the polarization microscope and the halo pattern in the scattering profile of X-ray, there is no difference of the structure

in the domain except for its size. From results of Raman spectrum analysis, the domains seem to be composed of BP rich and poor phases. As to the results of the mechanical properties, thermal expansion was suppressed and adhesive properties were enhanced with the samples having small domain size.

Considering these facts, the thermal expansion of BP rich phase seems to be smaller than that of BP poor phase, and the interphase has relatively small expansion formed in boundary area of phases. The amount of interphase are increased with smaller domain particles, and the linear expansions for bulk samples appear to be suppressed.

In Chapter 4, the phase separation behavior and properties were evaluated. Especially, the effects of thermal curing reactivity on phase-separated structures of acrylic copolymer/epoxy thermosetting resin composites were investigated with the samples containing various accelerator amounts. These composites exhibited a sea–island structure, for which the island size decreased as increasing the amount of accelerator. The island diameter distribution was represented by a lognormal plot. Thus, island formation was explained by the law of proportionate effect. As observed during the last stage of phase separation via spinodal decomposition, fine island domains were generated before growing and coalescing.

The effects of material composition on the phase structures and mechanical properties were also examined. The morphologies changed depending on the components, specifically the total island area fraction. As to the mechanical properties, the tensile strength and the shape of fracture surface were different from each samples. A small fraction of island area resulted in the lower fracture surface roughness and the higher mechanical strength. This indicated that, for the sample provided the stronger strength,

many epoxy components remained in the acrylic copolymer-rich sea phases. At this time the destruction propagated through phase boundaries, because the network formation states of sea and island phases were not significantly different from each other. External force seemed to be required for the destruction propagating through phases.

Then these acrylic copolymer/epoxy thermosetting resin composites were applied for adhesive material, and the influence of phase separated structure aspects on the adhesion properties were investigated in **Chapter 5**. The effects of the phase structure on the mechanical strength of adhesives were investegated. The phase structure of cured adhesive samples was examined by 2D-FFT analyses of SPM images, providing quantitatively structural information about the periodicity and the correlation length. Mechanical strength tests were conducted on mode I and II. At mode I test, the destruction propagates in perpendicular direction against external force, whereas at mode II test the destruction propagates in parallel direction against external force.

Morphologies and the correlation length changed with the composition. During the fracture toughness test on mode I, the fracture surface aspects were similar to the surface morphologies and the roughness of fracture surface depended on the correlation length. The sample having larger correlation length provided the rougher fracture surface. This indicated that the fracture propagated along the phase-separated boundary. But the correlation length exhibited little influence on the strength. During the shear test on mode II, the roughness of fracture surface and the strength were influenced by the morphology aspects. The samples with co-continuous structure provided the rougher fracture surface and the larger share strength depending on the correlation length. Thus, much larger external force was expended to form the large specific surface area of the fracture surface at the strength test on mode II with the co-continuous phase-separated composites.

In present study, the influence of primary and higher order structure on the adhesive properties for epoxy composite adhesion materials were most interest, which aims to propose a fracture mechanism of adhesive state and enhance an adhesive strength.

The effects of the molecular structure on the morphological feature and the adhesive property of epoxy resin composition introducing mesogenic framework were investigated in **Chapter 2 and 3**. The effects of the phase structure on mechanical properties of the epoxy composites with acrylic polymer were investigated in **Chapter 4 and 5.**

The importance of the deductive evaluation process with quantitative analysis of the molecular configuration and conformation for the designing of epoxy resin composites were exhibited adequately in present study.

Research works

Publications

[1] I. Ichikawa, K. Enomoto and K. Uchida, "Electron Structure and Orientation of Epoxy Resin Network Chains and its Application for Molding Compound for IC Package", *J. Adhesion Soc. Japan,* **40**, 51 (2004). (Chapter 2)

[2] I. Ichikawa and K. Uchida, "The new molding compound material for semiconductor addressing the lead-free solder", *Adhesion Technology, Japan,* **24**, 73 (2004). (Chapter 2)

[3] I. Ichikawa, T. Sugizaki, K. Uchida, "Morphology and properties of liquid crystalline epoxy composite matrices introducing mesogenic structure into the network", *J. Adhesion Soc. Japan,* **46**, 240 (2010). (Chapter 3)

[4] I. Ichikawa, T. Sugizaki, S. Akasaka and S. Asai, "Quantitative analysis of phase separation structure and mechanical properties of acrylic copolymer/epoxy thermo setting resin composite*", Polym. J.*, [in press]. (Chapter 4)

[5] I. Ichikawa, H. Suzuki, T. Sugizaki, S. Asai, "Analysis of the Curing Reaction of the Epoxy Resin Composition by Pulsed ^{1}H-NMR and Adhesive Properties"*J. Jpn. Soc. Colour Mater.,* **88**, 125 (2015). (Chapter 5)

[6] I. Ichikawa, K. Yanagimoto, M. Furudate, M. Kashio and T. Sugizaki, "Electron Structure of Silane Coupling Agent and Stability of Adhesive Function in Its Application for Epoxy Adhesive", *J. Adhesion Soc. Japan,* **47**, 335 (2011). (Chapter 4, 5)

Patent

[1] Japanese Patent No. 3842258 (Chapter 2, 3)

[2] Japanese Patent No. 5566141 (Chapter 2)

[3] Japanese Patent No. 5426831 (Chapter 4, 5)

[4] Japanese Patent No. 5602669 (Chapter 5)

Presentation

[1] I. Ichikawa, K. Uchida, "Analysis of Adhesive Surface between Molding Compound and Metal for Semiconductor Package and its Application", ***40th Annual Meeting of the Adhesion Society of Japan*** *(2002).* (Chapter 2, 3)

[2] I. Ichikawa, K. Enomoto, K. Uchida, "Electron Structure and Orientation of Epoxy Resin Network Chains and its Application for Molding Compound", ***41th Annual Meeting of the Adhesion Society of Japan*** *(2003).* (Chapter 2)

[3] I. Ichikawa, K. Enomoto and K. Uchida, "Morphology and Properties of Liquid Crystalline Epoxy Composites and its Application for Molding Compound for IC Package" ***53th Network Polymer Symposium Japan*** *(2003).* (Chapter 3)

[4] I. Ichikawa, K. Uchida, A. Kishi, Y. Taniguchi, "Estimation of Epoxy Resin Network Orientation by XRD and their Property", ***42th Annual Meeting of the Adhesion Society of Japan (2003)***. (Chapter 2)

[5] I. Ichikawa, K. Yanagimoto, M. Furudate, M. Kashio, T. Sugizaki, "Electron Structure of Silane Coupling Agent and Stability of Adhesive Function in Its Application for Epoxy Adhesive", ***49th Annual Meeting of the Adhesion Society of Japan*** *(2011).* (Chapter 4, 5)

[6] I. Ichikawa, S. Akasaka and S. Asai, "Phase Separation Structure and Mechanical Properties of Acrylics Copolymer/Epoxy Thermosetting Resin Composites", *the 2014* ***Annual Meeting of the Society of Fiber Science and Technology Japan*****.** (Chapter 4)

[7] I. Ichikawa, T. Sugizaki, S. Akasaka and S. Asai, Quantitative analysis of phase separation structure and mechanical properties of acrylics copolymer/epoxy thermo setting resin compositions, ***International Symposium on Fiber Science and Technology 2014***. (Chapter 4).

[8] I. Ichikawa, T. Sugizaki, S. Akasaka, S. Asai, Phase separation structure and adhesion properties of acrylics copolymer/epoxy thermo setting resin compositions, ***5th World Congress on Adhesion and Related Phenomena 2014***. (Chapter 5).

Acknowledgements

The present thesis is based on the studies carried out by the author under the guidance of his supervisors, Associate Prof. Shigeo Asai and Assistant Prof. Shuichi Akasaka, Department of Chemistry and Materials, Tokyo Institute of Technology, from Oct. 2012 to Jun. 2015. The author wishes to express his sincere gratitude to them for their continuing guidance and encouragement through this work.

The author wishes to express his thanks to Dr. Thoshio Sugizaki and Dr. Masaru Hoshi for their valuable suggestions and comments relating to the preparation of the thesis,

Special thanks also to Dr. Tomoko Shirahase and students of Asai Lab. Tokyo Institute of Technology for their valuable suggestions and comments relating to present study.

The author gratefully indebted to Dr. Kazuyoshi Ebe for giving him this precious opportunity to study.

Finally the author gratefully indebted to Lintec Corporation during three years doctor course study and wish to contribute to repay this obligation.